

Important Notice

This copy may be used only for the purposes of research and private study, and any use of the copy for a purpose other than research or private study may require the authorization of the copyright owner of the work in question. Responsibility regarding questions of copyright that may arise in the use of this copy is assumed by the recipient.

UNIVERSITY OF CALGARY

Exploring Maya Ruins in Belize, Central America
using Ground-Penetrating Radar (GPR)

by

Julie Ann Aitken

A THESIS

SUBMITTED TO THE FACULTY OF GRADUATE STUDIES
IN PARTIAL FULFILMENT OF THE REQUIREMENTS FOR THE
DEGREE OF MASTER OF SCIENCE

DEPARTMENT OF GEOSCIENCE

CALGARY, ALBERTA

SEPTEMBER, 2008

© Julie Aitken 2008

UNIVERSITY OF CALGARY
FACULTY OF GRADUATE STUDIES

The undersigned certify that they have read, and recommend to the Faculty of Graduate Studies for acceptance, a thesis entitled " Exploring Maya Ruins in Belize, Central America using Ground-Penetrating Radar (GPR)" submitted by JULIE ANN AITKEN in partial fulfilment of the requirements of the degree of MASTER OF SCIENCE.

Supervisor, Dr. Robert R. Stewart, Department of Geoscience

Dr. John Bancroft, Department of Geoscience

Dr. Kathryn Reese-Taylor, Department of Archaeology

Date

Abstract

A number of GPR surveys have been conducted by the University of Calgary at the Maya archaeological sites of Maax Na and La Milpa in Belize, Central America. Undertaken from 2001 to 2008, our research has focussed on enhancing the quality of the GPR images, highlighting anomalous features, and mapping near-surface stratigraphy and topography across the Maya plazas. Significant differences in radar velocities between field seasons are attributed to varying climatic conditions (rainfall) and can be explained through fluid substitution using the Wyllie Time Average Equation. Variations in velocities, depth of penetration and resolution have a significant effect on the interpretation of events on a GPR record. Based on the analysis of more than 40 2-D lines and four 3-D surveys, the best anomalies have been identified and catalogued, and will serve as a possible basis for future excavation. GPR surveys show considerable promise for subsurface imaging at Maya sites.

Acknowledgements

I would like to extend my thanks to all the students, staff and faculty who I have had the pleasure to work along side over the past few years, especially Peter Manning and Kevin Hall. Their support, expertise and encouragement have all contributed to an enjoyable experience in the Department of Geoscience. I would like to acknowledge Drs. J.M. Maillol and John Bancroft for imparting to me their knowledge and enthusiasm for the subject of geophysics. I am eternally grateful to my supervisor, Dr. Robert Stewart, for suggesting that I pursue a Masters in Geophysics and for trusting me with the task of working on an archaeological ruin in Belize. I am indeed privileged to be involved in the sacred Maya sites of Maax Na and La Milpa with two wonderful archaeologists, Drs. Leslie Shaw of Bowdoin College, Maine and Eleanor King of Howard University, Washington, D.C., and anthropologist, Dr. Claire Allum. I would also like to acknowledge the permit holder for the overall Programme for Belize Archaeology Project, Dr. Fred Valdez Jr., and the Belizean Institute of Archaeology. Lastly to my incredible family who have been my biggest supporters and without whom I could not have embarked on this new path in my life. To my daughter Jenny, my hero, whom I have proudly watched grow up more independent during my time at the university, and to my husband Bill Cameron, who is and will continue to be part of the adventure.

Table of Contents

Approval Page.....	ii
Abstract.....	iii
Acknowledgements.....	iv
Table of Contents.....	v
List of Tables.....	viii
List of Figures and Illustrations.....	ix
List of Symbols, Abbreviations and Nomenclature.....	xv
Epigraph.....	xvi
CHAPTER ONE: INTRODUCTION.....	1
1.1 Motivation.....	1
1.2 Study Area of Maax Na and La Milpa.....	3
1.3 Geological and Lithological Framework in Area of Maax Na and La Milpa.....	5
1.4 The Maya Civilization.....	9
1.5 Urban Design and Architecture of Maya Cities.....	9
1.6 Building Methods and Materials.....	12
1.7 The Site of Maax Na.....	12
1.8 The Site of La Milpa.....	14
CHAPTER TWO: GROUND-PENETRATING RADAR THEORY.....	17
2.1 What is GPR?.....	17
2.2 Electromagnetic Theory and Wave Properties.....	18
2.3 Physical Laws and Properties Affecting GPR.....	18
CHAPTER THREE: GPR ACQUISITION AND SURVEYS.....	25
3.1 Survey equipment.....	25
3.2 Survey design.....	29
3.3 Elevation and coordinate map using the Total Station Surveying Tool.....	32
CHAPTER FOUR: RADAR VELOCITY AND MODELLING.....	34
4.1 Rock Properties affecting GPR.....	34
4.2 Comparison of radar velocity measurements in the field.....	34
4.3 Water content and its effect on radar velocities.....	36
4.4 Modelling of GPR data.....	37
4.5 Radar velocity measurement in lab.....	44
CHAPTER FIVE: PROCESSING.....	46
5.1 Processing Steps.....	46
5.2 ReflexW Processing Flow and Examples.....	46
5.2.1 Data manipulation.....	48
5.2.2 Trace Interpolation.....	48
5.2.3 Bulk Shift.....	49
5.2.4 Normal Move-out.....	50
5.2.5 Muting.....	51
5.2.6 Dewow Filter.....	51

5.2.7 Gain Function	52
5.2.8 Filtering	54
5.2.9 Migration	54
5.2.10 Q-Filter	56
5.3 Common Mid-point Survey (CMP).....	58
5.4 Merging and Interpolation of 3-D Grids.....	59
CHAPTER SIX: INTERPRETATION.....	61
6.1 Interpreting GPR lines	61
6.2 2-D lines crossing plaza.....	63
6.3 2-D lines across altar.....	67
6.4 The Caves at Maax Na.....	72
6.5 2003 3-D grid and excavated pit.....	74
6.6 Schematic of second pit and correlation with GPR data	76
6.7 Mapping of bedrock based on the GPR interpretation	77
6.8 Rebar experiment.....	79
6.9 Interpretation of CMP Analysis.....	81
6.10 Interpretation of the Total Station Survey Data.....	82
CHAPTER SEVEN: THE MAYA RUIN SITE OF LA MILPA	87
7.1 GPR 3-D template over known cave	87
7.2 Pulse EKKO line and CMP across cave feature.....	95
CHAPTER EIGHT: CONCLUSIONS	98
8.1 Benefit to archaeology	98
8.2 Recommended acquisition procedure and processing flow.....	98
CHAPTER NINE: FUTURE WORK.....	101
9.1 Recommendations.....	101
REFERENCES	103
APPENDIX A: A GEOLOGICAL AND GEOPHYSICAL OVERVIEW OF NORTHERN BELIZE AND ITS EXPLORATION POTENTIAL	110
A.1. Introduction.....	110
A.2. Regional and Stratigraphic Setting	112
A.3. Tectonics.....	112
A.4. The Stratigraphy and Paleogeography of the Corozal Basin	113
A.4.1. Santa Rosa Group	114
A.4.2. Hillbank Formation.....	114
A.4.3. Yalbac Formation	115
A.4.4. Barton Creek Group.....	115
A.5. Geophysics.....	116
A.5.1. Gravity and Magnetics.....	116
A.5.2. Seismic.....	118
A.5.3. Play types.....	118
A.6. Conclusions.....	119

APPENDIX B: CATALOGUE OF GPR LINES	125
B.1. 2002 GPR Data:	126
B.2. 2003 GPR Data:	129
B.3. 2004 GPR data:	131
B.4. 2008 GPR data:	140
APPENDIX C: ANALYSIS AND OPTIMIZATION OF GROUND PENETRATING RADAR ACQUISITION PARAMETERS	148
C.1. Introduction	148
C.2. Survey Site	149
C.3. GPR Survey	150
C.4. Processing of the GPR data	151
C.5. GPS Survey	152
C.6. Septic Field	153
C.7. Results	154
C.8. Conclusions	159
C.9. Acknowledgements	159

List of Tables

Table 2.1 Important EM properties of near-surface materials reproduced from (Davis and Annan, 1989), (Daniels, 1996), and (Leckebusch, 2003).	21
Table 3.1 Acquisition parameters for the 2002-2008 field seasons.....	28
Table 4.1 Velocity Information observed during the different field seasons.	35
Table 6.1 Catalogue of anomalies observed at Maax Na.....	67

List of Figures and Illustrations

Figure 1.1 Map of Belize within Central America (www.cyberschoolbus.un.org).....	3
Figure 1.2 Map outlining the extent of the Rio Bravo Conservation and Management area in Northern Belize (www.belizereport.com).....	4
Figure 1.3 Lush vegetation in plaza at Maax Na (left), with typical Belizean wildlife on right (photo courtesy of R. Stewart, and www.parkerlab.bio.uci.edu).....	5
Figure 1.4 Transect through Northern Belize (from www.northernbelize.com).....	7
Figure 1.5 Geological overview of Belize (reproduced from Campbell et al., 1997).	8
Figure 1.6. Urban design of city of Copan (National Geographic, 1989).	10
Figure 1.7 Maya pyramids rebuilt over existing ones (Fasquelle and Fash, 1991).	10
Figure 1.8 The monumental centre of Maax Na; GPR surveys were conducted at Plaza A (PfBAP, 2004).	14
Figure 1.9 Layout of Plaza A at the Maya site of La Milpa (www.travelbelize.org).....	15
Figure 2.1 A schematic of how GPR works (adapted from www.cflhd.gov).....	17
Figure 3.1 Noggin 250 MHz Smart-cart unit (left); photo courtesy of R. Stewart, and the Pulse EKKO 100 MHz unit (right) (www.eescience.uteledo.edu).....	25
Figure 3.2 Antenna placement and footprint of the Noggin 250 MHz unit (reproduced from Sensors and Software Inc.).....	26
Figure 3.4 A schematic of GPR data collection (www.rtblark.com).....	26
Figure 3.4 Curve fitting to point diffractors to determine radar velocity.	27
Figure 3.5 Orientation of GPR survey lines and grids at Maax Na plaza during multiple field seasons (reproduced from E. King, 2004, pers. comm.).....	30
Figure 3.6 Topographic map of Maax Na incorporating total station survey data of GPR lines and archaeological turning points.....	32
Figure 3.7 Ceremonial centre of Maax Na; note reservoir to the southwest of North Plaza (King, 2005, pers. comm.).....	33
Figure 4.1 Schematic representation of the pit (reproduced from E. King).	38
Figure 4.2 Radargram generation using a pseudo-dielectric permittivity and conductivity log.	41

Figure 4.3 Comparison of 2002 data (wet) with GPR radargram.....	42
Figure 4.4 Comparison of 2003 data (dry) with GPR radargram.	42
Figure 4.5 Time comparison between the 2002 and 2003 GPR data.....	43
Figure 4.6 Depth comparison between 2002 and 2003 GPR data.	44
Figure 5.1 ReflexW processing flow applied to the GPR data.	47
Figure 5.2 A GPR section showing skipped or repeated traces.....	49
Figure 5.3 A GPR section with the skipped traces deleted or zeroed out.....	49
Figure 5.4 A GPR section showing the application of INFILL DATA to correct for the skipped traces.....	49
Figure 5.5 Example of a GPR record with and without a dewow filter.....	51
Figure 5.6 Comparison between a raw record and one with energy decay applied.....	53
Figure 5.7 Different migration algorithms applied to the GPR data.....	56
Figure 5.8 Comparison of Q-filter values.....	57
Figure 5.9 Comparison before and after a Q-filter and spatial filter.	58
Figure 5.10 Raw CMP profile acquired at La Milpa.	59
Figure 5.11 Acquisition layout of 3-D grid at Maax Na.....	60
Figure 6.1 Comparison of GPR data acquired the same day in opposite directions.....	63
Figure 6.2 Interpretation of Line 4 across the Plaza A at Maax Na.....	64
Figure 6.3 Line 6 showing the effect of surface debris on data quality of GPR lines.	65
Figure 6.4 Altar near ball court at Maax Na (photo courtesy of R. Stewart).....	68
Figure 6.5 An X-cut, Y-cut and time slice from a 3-D across the altar at Maax Na.	69
Figure 6.6 Time slice of 3-D across the altar.....	69
Figure 6.7 3-D GPR Line 4 across the altar.....	70
Figure 6.8 3-D GPR line across altar showing diffraction.....	71
Figure 6.9 Maya pottery (www.parkerlab.bio.uci.edu), and Dr. Claire Allum in a cave at Maax Na (photo courtesy of R. Stewart).	72

Figure 6.10 GPR Line adjacent to caves at Maax Na.	73
Figure 6.11 An X-cut, Y-cut and time slice of the 2003 3-D acquired at Maax Na.	74
Figure 6.12 Dr. King explaining the plaza layering (photo courtesy of R. Stewart).	75
Figure 6.13 Schematic of excavated pit, GPR record and radargram.....	76
Figure 6.14 GPR Line showing anticlinal feature which was excavated.	76
Figure 6.15 Schematic of the excavated pit (reproduced from the work of E. King, pers. comm., 2005).....	77
Figure 6.16 3-D line showing the pick values for the base of the plaza layering.	78
Figure 6.17 Mapped surface of the top of the bedrock.	78
Figure 6.18 Diffraction from rebar line at Maax Na (Note repeated traces at left).	79
Figure 6.19 Difference in diffraction tails with survey direction.	80
Figure 6.20 CMP analysis of data from Maax Na.	82
Figure 6.21 Charting of the elevation coordinates for 2008 N-S GPR Line.....	83
Figure 6.22 Charting of the elevation coordinates for 2008 E-W GPR Line.	83
Figure 6.23 Charting of the elevation coordinates for 2004 N-S GPR Line 2.....	83
Figure 6.24 Charting of the elevation coordinates for 2004 Northern E-W GPR Line....	84
Figure 6.25 Charting of the elevation coordinates of the 2004 southern E-W Line.....	84
Figure 6.26 Elevation contour map and likely flow direction of rainwater.....	85
Figure 7.1 Location of La Milpa in northern Belize (MARL).....	87
Figure 7.2 Topographic map of Plaza A at La Milpa, outlining the 3-D GPR survey across chultune (reproduced from Tourtellot et al. 1993).....	88
Figure 7.3 La Milpa plaza with 3-D grid and cave (photos courtesy of B. Cameron).	89
Figure 7.4 GPR Response from a limestone cavity (reproduced from Annan, 2003).	90
Figure 7.5 Anomalous event observed on y-line 60 at La Milpa.....	91
Figure 7.6 Photograph of the top of the cave at La Milpa (courtesy of B. Cameron).	92
Figure 7.7 3-D image of cave feature below the plaza surface.....	93

Figure 7.8 Timeslice outlining circular feature of cave in lower right.	93
Figure 7.9 Time slice of 3-D at 82.4ns, outlining two caves below La Milpa plaza.	94
Figure 7.10 Map of picked cave horizon at La Milpa.....	95
Figure 7.11 Pulse EKKO line acquired across the cave at La Milpa.....	95
Figure 7.12 CMP analysis of Line 16 at La Milpa.	97
Figure A.1 Location of Maya study sites in Northern Belize (MARL).....	120
Figure A.2 Extension of Yucatan Platform and associated faults (World Oil, 2008). ...	120
Figure A.3 Tectonic Map of Belize with location of cross-section A-B (Geology and Petroleum Office, 1995).....	121
Figure A.4 Geological cross-section of western Belize (Geology and Petroleum Office, 1995).	121
Figure A.5 The stratigraphic column of the Corozal Basin (Geology and Petroleum Office, 1995).	122
Figure A.6 Seismic Base Map of Belize (Geology and Petroleum Office, 1995).	123
Figure A.7 Possible play concepts in northern Belize(Geology and Petroleum Office, 1995).	124
Figure B.1 Schematic of GPR line locations across Plaza A in 2002 and 2003 (not to scale).	125
Figure B.2 E-W Project 2: Line 1 across north plaza.	126
Figure B.3 S-N Project 2: Line 2 across north plaza.	126
Figure B.4 E-W line: Project 2: Line 3 across north plaza.	127
Figure B.5 W-E Project 3: Line 1 across north plaza (reverse direction to Project 2 Line 1).....	127
Figure B.6 N-S Project 3: Line 2 across plaza (reverse direction to Project 2 Line 2)...	128
Figure B.7 W-E Project 3 Line 3 across north plaza (reverse direction to Project 2 Line 3).....	128
Figure B.8 W-E Project 1: Line 1 across plaza.....	129
Figure B.9 E-W Project 1: Line 2 across plaza (reverse of Line 1).....	130

Figure B.10 Schematic outlining the layout of GPR lines acquired in 2004.....	130
Figure B.11 Project 5: Line 1 across plaza.	131
Figure B.12 Project 5: Line 2 across plaza.....	132
Figure B.13 Project 5: Line 3 across north plaza.....	132
Figure B.14 Project 5: Line 4 across north plaza.....	133
Figure B.15 Project 5: Line 5 across north plaza.....	133
Figure B.16 Project 5: Line 6 across north plaza.....	133
Figure B.17 Project 5: Line 7 across north plaza.....	134
Figure B.18 Project 5: Line 8 across north plaza.....	134
Figure B.19 Project 5: Line 9 across north plaza.....	134
Figure B.20 Project 5: Line 10 across north plaza.....	135
Figure B.21 Project 5: Line 11 across north plaza.....	135
Figure B.22 Project 5: Line 12 across north plaza.....	135
Figure B.23 Project 5: Line 13 across north plaza.....	135
Figure B.24 Project 5: Line 14 across north plaza.....	136
Figure B.25 Project 6: Line 0 across plaza.	136
Figure B.26 Project 6: Line 1 across western part of north plaza; reverse to Line 0.....	137
Figure B.27 Project 6: Line 2 across plaza.	138
Figure B.28 Project 6: Line 3 across north plaza.....	139
Figure B.29 Project 6: Line 4 across north plaza.....	139
Figure B.30 Project 6: Line 5 across north plaza.....	140
Figure B.31 Line 0 acquired east to west across eastern part of north plaza.....	140
Figure B.32 Line 1 acquired west to east across eastern part of north plaza.....	141
Figure B.33 Line 2 acquired north to south across eastern part of north plaza.	142
Figure B.34 Line 3 oriented south to north across eastern part of north plaza.	143

Figure B.35 Line 4 oriented north-south across western part of north plaza.....	144
Figure B.36 Line 5 oriented south to north across western part of north plaza.....	144
Figure B.37 Line 6 oriented west to east across western part of north plaza.	145
Figure B.38 Line 7 oriented east to west across western part of north plaza.	145
Figure B.39 Line 8 oriented west to east across ramp of north structure.	146
Figure B.40 Line 10 acquired across ramp - repeat of Line 8 due to skipped traces.....	146
Figure B.41 Line 9 oriented east to west along ramp; reverse direction to Lines 8/10. .	146
Figure B.42 Line 11 acquired north to south perpendicular to ramp; no topographic correction applied.....	147
Figure B.43 Line 12: second line acquired north to south perpendicular to terrace; no topographic correction has been applied.....	147
Figure C.1 Different acquisition directions.	151
Figure C.2 GPS Survey topographic map.....	153
Figure C.3 A likely septic field configuration at site (courtesy of A1 Sewage Services).....	153
Figure C.4 Profile line Y132 showing the location of sewer pipes.	154
Figure C.5 Time slice of X grid forward pattern.	155
Figure C.6 Time slice of X grid reverse pattern.	155
Figure C.7 Time slice of X grid forward-reverse set-up.....	155
Figure C.8. Time slice of X grid forward pattern.	156
Figure C.9 Time slice of Y grid forward pattern.	157
Figure C.10 Time slice of X grid reverse pattern decimated every second line.	158

List of Symbols, Abbreviations and Nomenclature

α	attenuation
σ	electrical conductivity
ϵ	permittivity
ϵ_0	permittivity of free space (8.85×10^{-12} farad/m)
ϵ_r	relative permittivity or dielectric constant
μ	magnetic permeability
μ_0	magnetic permeability of free space (1.26×10^{-6} henry/m)
μ	relative magnetic permeability
2-D	two dimensional
3-D	three dimensional
AGC	automatic gain control
c	speed of light in a vacuum (3.0×10^8 m/s)
CMP	common mid-point
EM	electro-magnetic
f-k	frequency-wavenumber
GPR	ground-penetrating radar
MHz	megahertz (10^6 Hz)
NMO	normal move-out
ns	nanosecond (10^{-9} s)
radar	radio detection and ranging
V	velocity
m/ns	metres per nanosecond
m	metres
V_A	actual velocity
V_F	fluid velocity
V_M	matrix velocity
ϕ	porosity
s	distance
t	time
P	loss factor
ω	angular frequency
R	coefficient of reflectivity at an interface
ϵ_{r1}	relative dielectric permittivity of overlying material
ϵ_{r2}	relative dielectric permittivity of underlying material
RDP	relative dielectric permittivity
λ	wavelength
f	frequency
CREWES	Consortium for Research in Elastic Wave Exploration Seismology

Epigraph

Carpe Diem

Chapter One: INTRODUCTION

This thesis explores the use of Ground-Penetrating Radar (GPR) at two Maya archaeological sites in Belize, Central America. The main objectives of this investigation were to: conduct GPR reconnaissance across a Maya plaza at Maax Na, process and interpret the data, highlight any observed geophysical anomalies, and template a known subterranean cave, or chultun, at La Milpa. The final goal was to catalogue and prioritize the best anomalies noted in the near-surface at these sites as a possible basis for excavation in the future.

1.1 Motivation

GPR surveys have been conducted by the University of Calgary at several Maya sites in Belize, Central America since 2001 (Aitken and Stewart, 2002). Archaeological excavations tend to be expensive because of the slow meticulous work required and the sheer manpower involved. In contrast, GPR is a geophysical method that is non-invasive and non-destructive. It also provides a snapshot of the subsurface to pin-point a feature of interest and thus offers the potential to focus the excavation activity effectively and efficiently. GPR data acquisition has the potential to improve the archaeological return from excavation sites (Moldoveanu et al., 2002).

Ground penetrating radar involves the propagation of pulses of electromagnetic energy into the ground. Because of its sensitivity to conductive or resistive boundaries in the subsurface, GPR can be successfully used to locate void spaces and regions of disturbance (Henley et al., 2002). In terms of an archaeological context, the transmitted pulse travels through the lithologic layers of the earth, scattering and reflecting from stratigraphic boundaries, walls, house floors, pits or rubble (Goldberg, 2001).

Near-surface geophysical techniques, particularly GPR, have been traditionally employed in archaeological investigation (Leckebusch, 2003). In the past, non-geophysicists have routinely conducted these surveys across areas of interest and relied on the raw, real time displays from the GPR unit to flag or map anomalous features. For large, continuous and areally extensive features, showing sufficient contrast in electromagnetic physical properties, this type of methodology is sufficient to target or map out such features. Smaller features however are more difficult to delineate.

A goal of the research at the University of Calgary is to apply our geophysical expertise to acquire more detailed analysis of this smaller type of feature in the form of crisper and more coherent images of the subsurface through improved acquisition parameters and enhanced processing flows. Pre-existing modeling software, and interpretation methodology employed in seismic exploration, has been applied to the GPR surveys. GPR computer mapping and 3-D visualization techniques were implemented to identify and resolve surfaces of ancient habitation, and aid the archaeologists in their attempt to reconstruct the history of the Maya civilization at this site. This collaborative effort between the fields of geophysics and archaeology holds great promise as GPR technology continues to evolve. Continued research and numerous theses and papers outlining the application and success of GPR at different Maya archaeological sites will pave the way to more interest, use and acceptance by archaeologists as a reconnaissance tool. These include the mapping of Maya buried structures in Ceren, El Salvador (Conyers, 1995), the successful application of GPR at the Maya site of Kaminaljulu, Guatemala (Valdes and Kaplan, 2000), and the integration of GPR data with Maya archaeological data at Los Naranjos, Honduras (Tchakirides et al., 2006). This investigative methodology has

additional relevance to Earth Science in its potential use in environmental and geotechnical applications (Daniels, 2000), including hydrological permafrost studies by Moorman and Michel (2000) and Nieto (2005).

1.2 Study Area of Maax Na and La Milpa

The country of Belize is situated between the equator and the Tropic of Cancer at the northern latitude of (15° to 19° N). Formerly British Honduras, it gained independence from Britain in 1981 and is bounded by Mexico to the north, Guatemala to the south and west, and the Caribbean Sea to the east (Figure 1.1). Belize is considered to have a sub-tropical climate, with a wide range of rainfall, humidity, and temperatures throughout the country.



Figure 1.1 Map of Belize within Central America (www.cyberschoolbus.un.org)

Maax Na and La Milpa are two of 800-plus Maya archaeological sites situated in Belize alone. Located in The Rio Bravo Conservation and Management area that covers 260,000 acres of lush, broadleaf forest, both sites are parts of a larger region under the auspices of

The Programme for Belize Conservation Area (PfBCA). The Conservation Area was created in 1988 with funding from the Belizean Government and is dedicated to the preservation of the archaeological ruin sites and the indigenous wildlife within its boundaries (Figure 1.2).



Figure 1.2 Map outlining the extent of the Rio Bravo Conservation and Management area in Northern Belize (www.belizereport.com).

A diversity of plant life including tall mahoganies, mangroves, ferns, vines, and flowers create a dense rainforest, with large twisted roots and leaves littering the ground surface. Over the different field seasons the environments we encountered have varied from parched with little vegetation growth and an absence of insects, to ones of lush greenery, and an overwhelming richness of wildlife (Figure 1.3).



Figure 1.3 Lush vegetation in plaza at Maax Na (left), with typical Belizean wildlife on right (photo courtesy of R. Stewart, and www.parkerlab.bio.uci.edu).

Maax Na (“Spider Monkey House” in local Mayan) was discovered in 1995 by a group of archaeological surveyors from the University of Texas on a quest to locate other Maya sites in the area (Allum, 2004). Subsequent excavations and mapping have revealed hundreds of intact structures within and around the site centre, now considered to be ceremonial in nature (King, pers. comm., 2004). To date, a number of geophysical surveys conducted by the University of Calgary at Maax Na and La Milpa have provided good quality images of the near surface indicating the existence of caves, a looter’s trench and other important archaeological features. These ancient landmarks provide archaeologists with the necessary cultural footprints to assist in unravelling and reconstructing the history of the Maya.

1.3 Geological and Lithological Framework in Area of Maax Na and La Milpa

An overview of the geology and geophysics of northern Belize was undertaken to

become familiar with the geology in and around several Maya ruin sites in northern Belize including Maax Na and La Milpa. A close examination of the lithological information and regional geological setting was required to understand what resources and materials were available to the Maya, and the location and placement of the monuments and cities of the Maya civilization.

The present geological configuration of Belize involves a long history of plate tectonics, faulting, major transgressions, regressions, and erosion. Maax Na and La Milpa are located in the Corozal basin of Northern Belize, one of three geological provinces, that form the Belize mainland (Campbell, et al., 1997). The Corozal basin consists of a thick sequence of marine carbonates, primarily limestone, interspersed with lime-rich muds (marls) and capped by alluvial sands deposited from the Cretaceous period to the Pleistocene. This basin is an extension of the Yucatan Peninsula and is stratigraphically part of the North Peten Basin of Guatemala (Aitken and Stewart, 2002).

The topography of the area consists of a series of escarpments formed by successive cycles of faulting, slumping and weathering, and is oriented in a southwest-northeast direction. This alignment has influenced the drainage pattern of the rivers and streams in the Three Rivers region, appropriately named after the Rio Azul, the Rio Bravo and the Booth's Rivers (Figure 1.4).

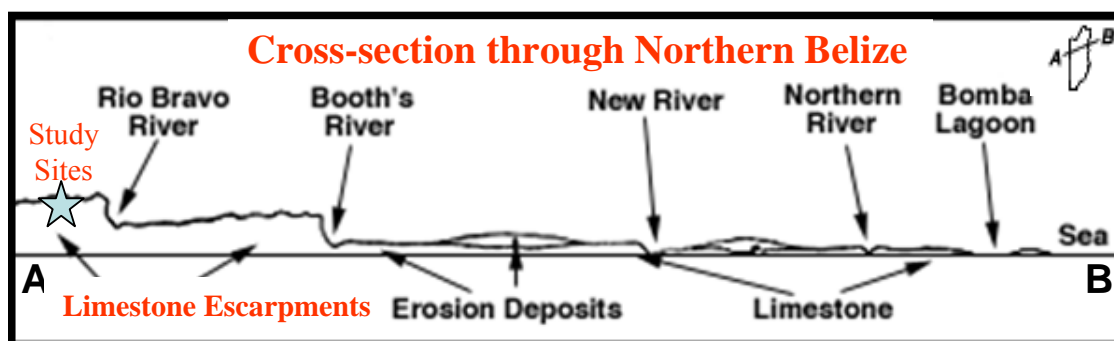


Figure 1.4 Transect through Northern Belize (from www.northernbelize.com).

The study sites of Maax Na and La Milpa are situated west of the La Lucha Escarpment. Geomorphically, the study area is a central pediplain, a broad, low-relief erosional surface with gentle topography, and linear-trending lakes of karstic origin (Moldoveanu et al., 2002). The region is also characterized by thousands of natural caves and caverns below the surface caused by limestone dissolution. The geologic sequence and paleogeography of the region in the near surface consists of the Santa Rosa Group, the Hillbank Formation, and the Yalzac Formation. The limestone quarries extensively exploited by the Maya originated from these formations. Figure 1.5 outlines the main outcropping formations and geologic rock type that characterize the different regions of Belize. The locations of Maax Na and La Milpa are primarily dominated by Mesozoic carbonates. A more detailed report on the geology of Belize is offered in Appendix A.

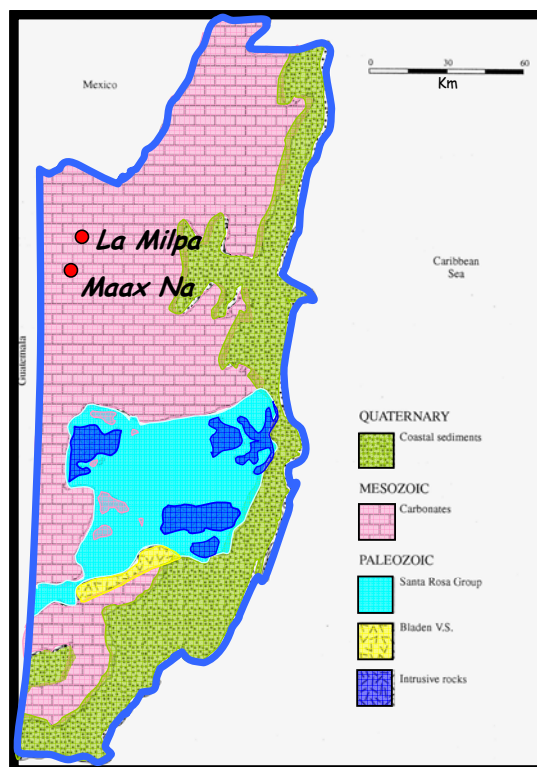


Figure 1.5 Geological overview of Belize (reproduced from Campbell et al., 1997).

Northern Belize supports a number of different ecosystems. Lowland broadleaf forests cover the limestone escarpments of Rio Bravo, where rich, lime soils derived from the erosion of the Maya Mountains have developed. To the east, more nutrient-poor soils are common, giving rise to pine trees and savanna grasses. Fresh-water wetlands and swamps known as “bajos” exist in areas of low topographic relief especially along rivers, while mangrove forests blanket the north-east and coastal regions.

The stratigraphy of the near-surface sediment of the Maax Na plaza consists of a fertile brown soil matrix and humus, underlain by multiple man-made layers of limestone plaster, and detrital, stacked above the limestone bedrock. This tiered arrangement has been verified by two archaeological pits excavated at the plaza, and will be discussed later in the thesis.

1.4 The Maya Civilization

The Maya are considered to be one of the greatest Mesoamerican civilizations with expertise in mathematics, astronomy and engineering. Their culture flourished in Central America for over a millennium. Culminating during the Classic Period (A.D. 300-900), their ceremonial complexes have stone temples, palaces, ballcourts and stone stlae (Demareist, 2006). It was a time of industrious construction in which immense structures were built within and atop the topographically highest points in the region (Miller, 1999). Kings erected massive temples and palaces to reinforce their legitimacy and power, and as tribute to their gods. Important historical dates festooned the palaces and other stone monuments. Their architecture not only made use of the corbel arch but certain temples were positioned so that the precise observations of the equinox, solstice and other astronomic events could be made by sighting planets and stars along defined positions on special buildings (Awe, 2007). Large plazas surrounded these structures and served as the loci for religious ceremonies and royal processions.

1.5 Urban Design and Architecture of Maya Cities

Figure 1.6 is an artistic representation of the ceremonial centre of the great Maya city of Copan highlighting the great plaza and surrounding temple pyramids. Although Maax Na and La Milpa are at a much smaller scale to Copan, they are similar to many Maya sites throughout Central America. Maya site planning varied from one location to another, as differing natural features were integrated into the design. Some sense of order is evident however in that elevated structures such as temples, palaces and large plazas were typically located in the civic centre and surrounded by residential compounds. At times, causeways, known as "sacbeob", connected various parts of the settlement. These ancient

roadways were also constructed of limestone and paved with natural white lime cement called "sascab".



Figure 1.6. Urban design of city of Copan (National Geographic, 1989).

The Maya rarely demolished existing structures, choosing to expand through accretion as temples, palaces, and entire complexes were rebuilt over and over again through the centuries (Coe, 1999). Buildings were often placed upon or abutted to older structures as depicted in Figure 1.7.



Figure 1.7 Maya pyramids rebuilt over existing ones (Fasquelle and Fash, 1991).

In terms of architecture, the Maya are most noted for their stepped and ornate structures from the Pre-Classic period through to the Post-Classic period (400 B.C. – 1200 A.D.). Temples were buildings elevated on high pyramidal platforms with restricted interior spaces and large free-standing facades called roof combs (Sharer, 1994). Palaces were single-storied, multi-room buildings situated on low platforms that served administrative and residential functions (Coe, 1999).

The plaza areas were extensive, and built to accommodate the Maya crowds who gathered for sacred rites and processions. Classic Maya cities commonly have a north plaza dedicated to ritual events surrounded by religious buildings built on high platforms and pyramids (Allum, 2004). Other plazas throughout the city were used as public market areas, venues for public ceremonies or were exclusive to elite residences (Allum, 2004). Each new phase in construction of the pyramids and temples often required refurbishing of the plaza surface, resulting in a multitude of layers capped by a hard lime-based plaster. According to archaeologist Leslie Shaw, an excavated pit at Maax Na “found layer upon layer of plaster floor and limestone rubble, evidence of a very constructed landscape” (Allum, 2004).

The Maya ingeniously developed various methods to store rainwater in strategically placed reservoirs. One method of reservoir construction was to dig down to bedrock with tools often made of chert and obsidian, and sculpt the soft, friable limestone into large concave features. At Maax Na, these excavated depressions, at the periphery of the plazas, were then lined with wet clay and allowed to dry in the heat, forming reservoirs (Shaw, pers. comm., 2004). The plazas were intentionally designed to tilt slightly in the direction of the reservoirs to collect and store precipitation during the rainy season. This

inclination was observed in our case at Maax Na by topographic mapping of the plaza using the Total Station survey instrument.

1.6 Building Methods and Materials

The Maya were resourceful builders, using available construction materials including soil, natural limestone cobbles and boulders, large crudely chiseled limestone blocks, and stucco (Wilson and Wilson, 1990). Tons of recycled rubble and quarried limestone were used to construct the pyramids and plazas. The abundant soft-limestone beds were easily manipulated and cut into blocks or reduced by burning to produce lime for plaster (Sharer, 1994). The resultant white plaster proved to be impermeable and very durable and was used to top plaza surfaces and as a top coat to temples and pyramids, which were then brightly painted. The plaster also served to cover any imperfections in workmanship. The Maya did not have access to metal tools, yet their work shows great skill and creativity.

1.7 The Site of Maax Na

The identification of Maax Na as a monumental centre was first documented in 1995 when an archaeological reconnaissance team for the Programme for Belize Archaeology Project (PFBAP), directed by Dr. Fred Valdez Jr. of the University of Texas at Austin (Valdez, 1997), surveyed the area. The Maax Na Archaeology Project, co-directed by Drs. Leslie Shaw (Bowdoin College) and Eleanor King (Howard University), initiated investigations in 1996 with emphasis on site mapping and exploration. Site mapping remains ongoing. Based on the initial work, the site appears to have been occupied from the Late Preclassic Period (250 B.C.–A.D. 250), to the Late Classic Period (600-800 A.D.) A major construction episode took place during the Early Classic (250-600 A.D.).

Maax Na is one of five major sites within the boundaries of the PfBAP conservation area, and with this high site density, each site must have had to balance its economy in reference to the volatile political world that surrounded it (PfBAP Report, 2005).

The monumental center at Maax Na is located on a hilltop at 180 m above sea level and includes three plazas (Plaza A, Plaza B and Plaza C) connected by a wide causeway.

Maax Na's site centre is unique in that the large distances between buildings in Plaza A imply it was deliberately built on a grand scale (Figure 1.8). A free-standing stela (stone column) with no discernable markings was discovered at the southern end of the causeway, possibly to represent the commencement of sacred versus secular space as is found in the Maya city of Copan (PfBAP, 2005). Plaza B contains a single large pyramid atop a natural hill and stands approximately 24.6 m above the plaza surface. A set of steps carved out of the hill created a base for the pyramid structure. Early excavations at the plaza have revealed layers of buried stonework, each of which served as a pavement surface at different stages of Maax Na's construction and development.

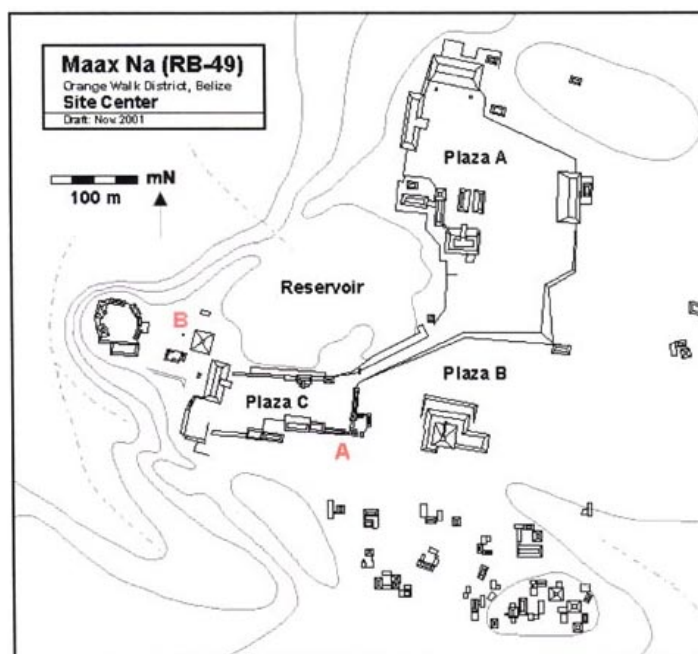


Figure 1.8 The monumental centre of Maax Na; GPR surveys were conducted at Plaza A (PfBAP, 2004).

Due to the proximity of the Rio Azul/Rio Hondo drainage basin and Thompson's Creek, a large reservoir filled the area to the west of the causeway. We can imagine that the reservoir would have contributed both aesthetically and functionally to the community (PfBAP report, 2005). The residential zones in the vicinity of Maax Na suggest an economic focus on agricultural products. Areas east of the site centre appear to have had only limited settlement due to the location of the escarpment and bajo.

1.8 The Site of La Milpa

La Milpa is also part of the Programme for Belize, within the Rio Bravo Conservation area and adjacent to the La Milpa field station (Figure 1.2).

This site was initially discovered in 1938 by Sir Eric Thompson, and additional mapping of the main plaza was undertaken in the 1970's by David H. Pendergast and H. Stanley Loten (Tourtellot III et al., 1993). More extensive excavation work did not begin until

1992, under the guidance of Dr. Norman Hammond from Boston University. La Milpa is considered to be the third largest ancient Maya city in Belize after Caracol and Lamanai, covering over 75 square kilometres. It was founded in 400 BC, and flourished at several times during its history. The recent discovery of a royal burial site has raised the profile of La Milpa. The undisturbed tomb of the Maya King, “Bird Jaguar”, or his successor, believed to have ruled around 450 AD, was highlighted by a magnificent jade necklace adorning the remains (www.belizereport.com).

Termed the Northern Group, Plaza A is approximately 18 km² in areal extent and the largest constructed in the Classic period in Belize. Figure 1.9 outlines the layout of the plaza we investigated at the archaeological site of La Milpa.

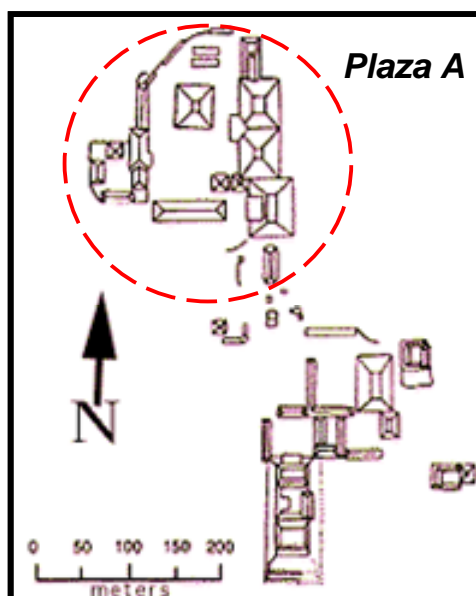


Figure 1.9 Layout of Plaza A at the Maya site of La Milpa (www.travelbelize.org).

Plaza A is surrounded by four pyramids over 24 metres high, postulated to have housed elite residences and administrative offices. The plaza also contains two ball courts, and two chultunes under the plaza floor. Chultunes are bottle-shaped underground storage

chambers often used to collect rainwater, but in this locale were most likely used as storage pits. Although the pyramids and temples are hidden away beneath grassy hills and sub-tropical rainforest, the plaza has been mostly stripped of vegetation, making it an ideal location for GPR reconnaissance.

Chapter Two: GROUND-PENETRATING RADAR THEORY

2.1 What is GPR?

The term ‘ground-penetrating radar’ (GPR) refers to a technique designed primarily to detect “the location of objects or interfaces buried beneath the earth’s surface or located within a visually opaque structure” (Daniels, 2004). GPR uses electromagnetic (EM) radiation in the microwave band (UHF and VHF), and generally operates in the frequency range of 10 -1000 MHz. A high-frequency electromagnetic (EM) energy pulse is transmitted into the ground and is partially reflected back to the surface because of changes in bulk electrical properties (Bristow and Jol, 2006). The resultant GPR trace is simply a recording of the electric field from the subsurface as a function of time (Figure 2.1).

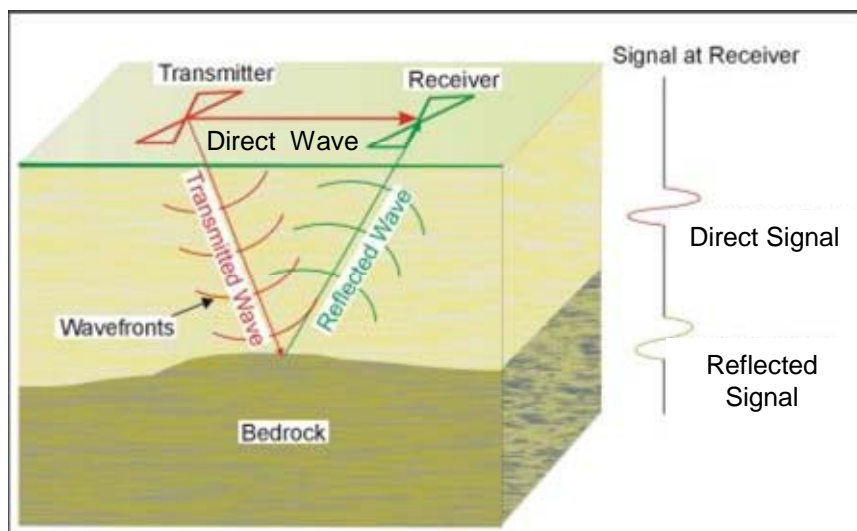


Figure 2.1 A schematic of how GPR works (adapted from www.cflhd.gov).

From this series of reflections, we can infer information about the near-surface. Signal recognition is fairly straightforward because the arrivals recorded by the receiver look

very similar to the original emitted signal (Annan, 2003). The basic unit of electromagnetic wave travel time is the nanosecond (ns), where $1 \text{ ns} = 10^{-9} \text{ s}$.

The success of GPR surveys is site dependent. The composition of near-surface materials and local or temporary conditions, such as the clay content of soils and the saturation level of the material, all play key roles in obtaining interpretable images of the earth. The saturation level results in considerable changes in dielectric permittivity which translates into varying velocities as evidenced in the surveys undertaken during the dry and wet field seasons encountered at Maax Na.

2.2 Electromagnetic Theory and Wave Properties

An important aim of geophysical surveying is to measure electromagnetic properties, and to deduce information about the composition and distribution of near surface materials based on contrasts within these physical properties. GPR is a geophysical tool employing electromagnetic waves. Understanding the behaviour of electrical and magnetic fields, and the properties of matter is a necessary first step in resolving a correct and meaningful interpretation (Olehoft, 2000).

2.3 Physical Laws and Properties Affecting GPR

Maxwell's Equations are a combination of electrical and magnetic property laws based on discoveries by scientists including Faraday, Gauss and Ampere. These equations describe electromagnetic phenomena. The principles and development of ground-penetrating radar are based on these laws. Charles (2007) offers a thorough explanation of Maxwell's equations.

The events or reflections on a GPR record are caused by impedance differences in one or more of the three physical properties that affect radar, namely dielectric permittivity,

magnetic susceptibility, and electrical conductivity. The interactions between the electrical field and charged particles (specifically electrons) are dependent on the electrical properties of the material. Electrical properties control how electromagnetic waves travel through a material. The dielectric permittivity primarily controls the wave velocity while conductivity determines the amplitude or attenuation of the signal.

Conduction is due to the movement of charge carriers. Energy is lost from the electrical field and converted to heat. Electrical polarization, or dielectric permittivity, is the displacement and separation of charges due to an applied electromagnetic field, and results in the redistribution of subatomic particles and molecules to new equilibrium positions. This mechanism conversely stores energy. The dielectric permittivity of a medium can vary with saturation, composition, type of pore fluid, material texture, and temperature (Hubbard, 1997).

Magnetic polarization (permeability or susceptibility) is created by the rotation and motion of electrons in atomic orbits, resulting in energy dissipation and storage (Olhoeft, 2000). The magnetic properties of most geologic material, barring those rocks that contain high concentrations of magnetic minerals, are considered to be similar to those of a vacuum. Therefore, it is relatively common to make the assumption that the magnetic permeability is equal to one.

The velocity of radar waves in a medium is given by the following formula (Reynolds, 1997):

$$, \quad (2.1)$$

Error! Objects cannot be created from editing field codes.

Where $c = 0.3$ m/ns (speed of light in air), ϵ_r - relative dielectric constant,

μ_r - magnetic permeability, P - the loss factor where $P = \sigma/\omega\epsilon$,

$\epsilon = \epsilon_r\epsilon_0$ ($\epsilon_0 = 8.854 \times 10^{-12}$ F/m which is the permittivity of free space),

σ - conductivity, and $\omega = 2\pi f$, where f is frequency.

The conditions at Maax Na appear to be favourable to GPR surveying as there seems to be little clay content and an absence of saturated saline fluids. At high frequencies and in conditions conducive to GPR (i.e. a non-magnetic medium, with $\mu_r = 1$, that contains low-loss materials, $P \sim 0$), electrical properties tend to be the dominant factor controlling GPR responses (Annan, 2003), giving the approximate radar velocity as:

$$V = \frac{c}{\sqrt{\epsilon_r}}, \quad (2.2)$$

Error! Objects cannot be created from editing field codes.

Where V = velocity of the radar pulse, ϵ_r = relative dielectric constant

and c = speed of light in air (0.3 m/ns).

Table 2 lists the dielectric permittivity, electrical conductivity, radar velocity and attenuation ranges for common rock and near-surface materials.

Table 2.1 Important EM properties of near-surface materials reproduced from (Davis and Annan, 1989), (Daniels, 1996), and (Leckebusch, 2003).

Material	Relative Dielectric Constant (ϵ_r)	Radar Velocity (v ; m/ns)	Electrical Conductivity (σ ; mS/m)	Attenuation (α ; dB/m)
Air	1	0.3	0	0
Distilled water	80	0.033	0.01	2×10^{-3}
Tap water	80	0.033	0.5	0.1
Salt water	80	0.033	3×10^3	600
Sand (dry)	5	0.130	0.01	0.01
Sand (saturated)	20-30	0.060	0.10-1.00	0.03-0.30
Silts	5-30	0.070	1-100	1-100
Shales	5-15	0.090	1-100	1-100
Clays	5-40	0.060	2-1000	1-300
Humid soil	30	0.055		
Cultivated soil	15	0.078		
Rocky soil	7	0.113		
Sandy soil (dry)	2.6	0.190	1.4	1
Sandy soil (saturated)	25	0.060	69	23
Clayey soil (dry)	2.5	0.190	2.7	3
Clayey soil (saturated)	19	0.070	500	200
Sandstone (saturated)	6	0.100		
Limestone (dry)	4-8	0.106 - 0.150	0.50 - 2	0.40-1.00
Limestone (saturated)				
Basalt (saturated)	8	0.106		
Granite (dry)	5	0.134	0.01 - 1	0.01-1.00

Conversely, this formula may be written as:

$$\epsilon_r = \frac{\epsilon}{\epsilon_0} \quad (2.3)$$

Error! Objects cannot be created from editing field codes.

As noted above, the relative dielectric permittivity (RDP) of a material is its capacity to store and allow the motion of charges within an imposed electromagnetic field. It is dimensionless. RDP is calculated as the ratio of a material's electrical permittivity to the electrical permittivity of a vacuum, which has an RDP of 1 (Conyers and Goodman, 1997).

Amplitudes of the reflections generated on a GPR profile, are the direct result of the differences between the relative dielectric permittivity of a material within the subsurface. The magnitude of the reflection generated at the interface can be shown as (Conyers and Goodman, 1997):

$$R = \frac{\epsilon_{r1} - \epsilon_{r2}}{\epsilon_{r1} + \epsilon_{r2}} \quad (2.4)$$

Error! Objects cannot be created from editing field codes.

where R = coefficient of reflectivity at an interface

ϵ_{r1} = RDP of overlying material

ϵ_{r2} = RDP of underlying material.

Significant reflections are generated when changes in the dielectric permittivity between two materials occur over a small distance. When the RDP changes gradually with depth, only minute differences in reflectivity will occur, resulting in the absence of a reflector or at best a weak response (Conyers and Goodman, 1997).

The depth of penetration of the data can be calculated using the following formula:

$$s = v * t \quad (2.5)$$

where v = average radar velocity in m/ns,

s = distance or depth to target in metres,

t = two way time of the latest coherent signal in nanoseconds.

For example, based on the above equation, and using an average velocity of 0.072 m/ns and the maximum two-way travel time of coherent data of 50 ns (as taken from the GPR sections collected at the plaza), the total depth of the GPR survey was 1.8 m.

The vertical resolution of a GPR survey, or the ability to identify the top and bottom of a layer or object, is dependent upon the frequency of the transmitting antenna and its

associated wavelength. As the thickness of a layer or diameter of an object approaches or decreases to less than a wavelength, the top and bottom of the object can no longer be resolved but can still be detected, appearing as a point-source return or diffraction (Moorman and Michel, 2000). Lower frequency antennas will allow for deeper penetration whereas higher frequency antennas can provide excellent resolution of the near-surface.

The dominant wavelength in the GPR pulse can be calculated using the following formula:

$$\lambda = \frac{v}{f}, \quad (2.6)$$

where λ = wavelength in m

v = average radar velocity in m/ns

f = dominant frequency

If we assume a vertical resolution of $\lambda/4$, then using a frequency of 250 MHz, and an average velocity of 0.072 m/ns, the wavelength is 0.288 m, and the resolution is 0.072 m.

In drier conditions, the velocity increases to 0.122 m/ns. The calculated wavelength is therefore 0.488 m, with a decreased resolution of 0.122 m.

Archaeologists can identify very thin layers below the surface of the plaza. According to the detailed analysis of a two by one metre excavated pit by onsite archaeologist, Dr.

Eleanor King, the layers vary from 0.07 to 0.30 m in thickness. This represents the limits of GPR resolution in this particular location, but it still may be possible to identify and differentiate the plaza strata. Plaza construction consisted of rubble and cobble layering,

with plaster intervals. Rubble zones, such as these, may provide permeable horizontal pathways and create major conduits for fluid flow (Hubbard, et al, 1997). The electromagnetic properties of common earth materials can vary significantly and seemingly randomly over small distances. Large property changes in dielectric permittivity may be created by water saturation for example. Chapter 4 contains further discussion and GPR modelling of the plaza at Maax Na.

During our field work in 2004, permission was granted by the archaeologists to obtain samples of the limestone cobble which form the plaza layering. Lab tests to quantify the physical properties especially the dielectric permittivity based on these rock samples are currently being conducted.

Chapter Three: GPR ACQUISITION AND SURVEYS

3.1 Survey equipment

The GPR surveys were conducted between 2002 and 2008 at the sites of Maax Na and La Milpa using several systems from Sensors and Software Inc., including the NOGGIN and Pulse EKKO units as shown in Figure 3.1.



Figure 3.1 Noggin 250 MHz Smart-cart unit (left); photo courtesy of R. Stewart, and the Pulse EKKO 100 MHz unit (right) (www.eescience.uteledo.edu).

The Noggin unit incorporates a frequency antenna of 250 MHz and an associated bandwidth of 125-375 MHz. The transmitter and receiver antennas are each 0.114 m long, 0.016 m thick, and housed in a shielded yellow case. The antennas inside the unit are parallel but are usually oriented perpendicular to the survey line (Greg Johnson, personal comm., 2006). This allows for better 2D imaging as the radiation energy largely stays in the path of the survey line as demonstrated by the oval shape of the antenna footprint, and off-line reflections are minimized (Figure 3.2).

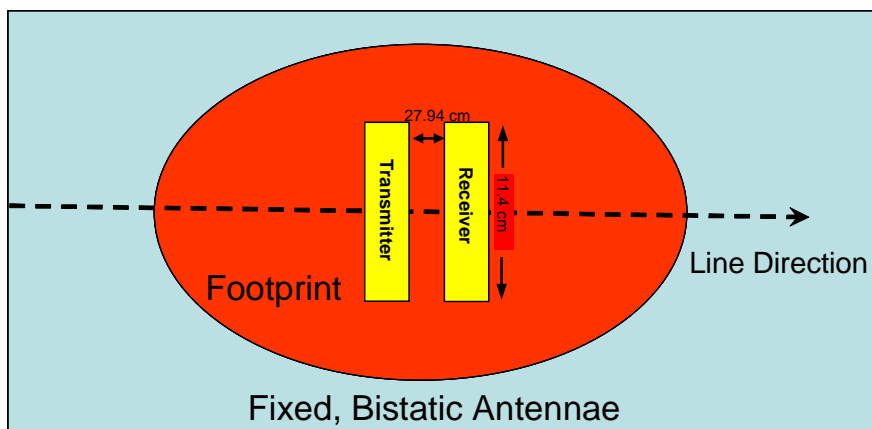


Figure 3.2 Antenna placement and footprint of the Noggin 250 MHz unit (reproduced from Sensors and Software Inc.).

One advantage of this instrumentation is that the antennas are attached to a “lawnmower-type” cart which is lightweight, efficient and simple to operate. A digital video logger (DVL), mounted on the cart, enables one to control the antennas and survey acquisition, observe real time data on a display screen, and store the data into internal memory or an external Flash card. An odometer mounted on one of the wheels controls the speed and frequency of trace collection. Figure 3.3.outlines how the GPR data is collected.

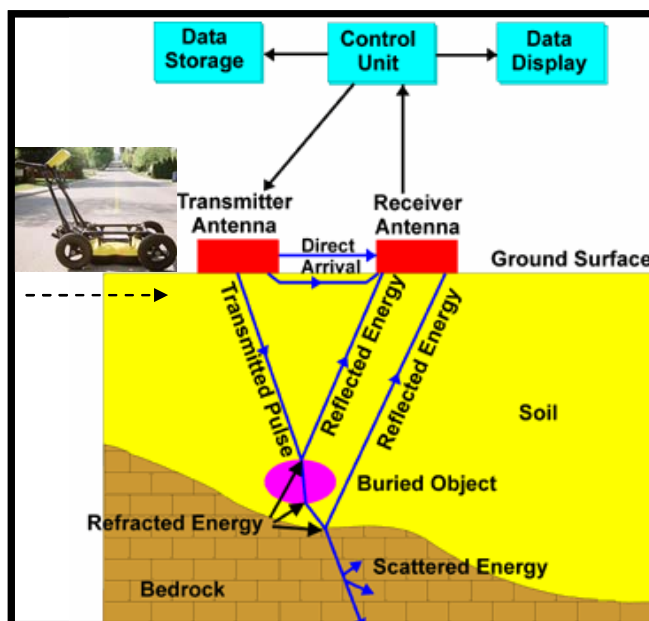


Figure 3.3 A schematic of GPR data collection (www.rtlark.com).

The one disadvantage of this setup is that a common mid-point (CMP) velocity survey cannot be conducted because the Noggin is a bistatic and monolithic system in which the transmitter and receiver antennas are housed in the same unit at a fixed separation interval of 0.28 m. As a result, velocities are measured by fitting hyperbolic curves to point diffractors in the near-surface as demonstrated in Figure 3.4. Note that radar velocities typically decrease with depth.

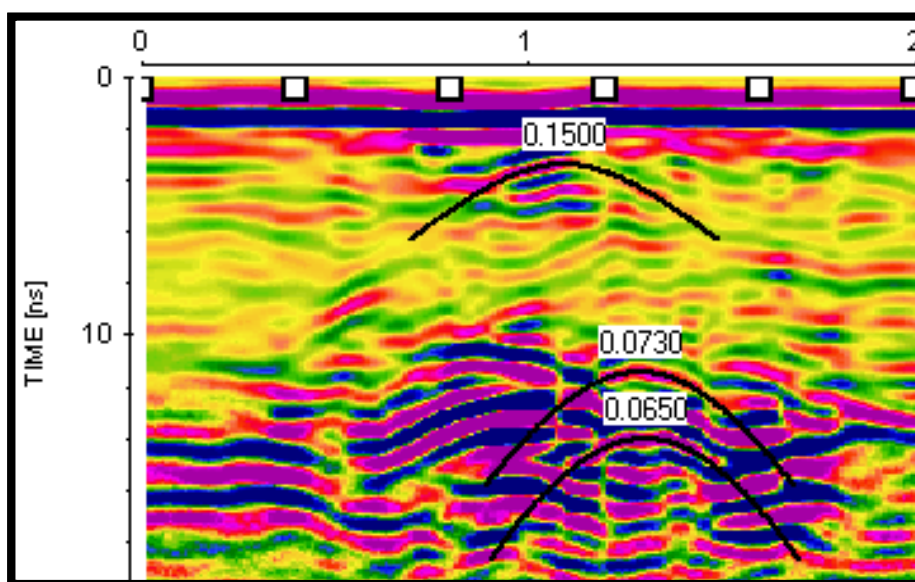


Figure 3.4 Curve fitting to point diffractors to determine radar velocity.

Field acquisition parameters for the 2-D lines included trace spacing at 0.05 m with temporal spacing set at 0.4 ns. The pseudo 3-D surveys were acquired in a forward reverse set-up in which every second line was shot in the opposite direction for expediency. The area of the 3-D GPR grids varied in size from 25 to 49 m². Line spacing was 0.5 m, with spatial and temporal spacing similar to the 2-D lines. A listing of the acquisition parameters is outlined in Table 3.1.

Table 3.1 Acquisition parameters for the 2002-2008 field seasons.

GPR Acquisition Parameters							
Noggin	Frequency 250 MHz			Antenna Separation 0.28 m			
GPR Data	# Traces	Stn interval (m)	Line Length (m)	# samples	Sample rate (ns)	Total time (m)	Direction
2002 2-D							
Project 2							
Line 1	990	0.05	49.45	196	0.4	78.4	E-W
Line 2	1874	0.05	93.65	196	0.4	78.4	S-N
Line 3	786	0.05	39.25	196	0.4	78.4	E-W
Project 3 (reverse of 2)							
Line 1	964	0.05	48.15	196	0.4	78.4	W-E
Line 2	1878	0.05	93.85	196	0.4	78.4	N-S
Line 3	770	0.05	38.45	196	0.4	78.4	W-E
Project 5							
Line 1	421	0.05	21	508	0.4	78.4	S-N
Line 2	415	0.05	20.7	508	0.4	78.4	N-S
Line 3	200	0.05	9.95	508	0.4	78.4	E-W
2003 2-D							
Rebar Line	44	0.05	2.2	196	0.4	78.4	S-N
Line 1	1360	0.05	68.25	196	0.4	78.4	W-E
Line 3	1349	0.05	67.4	196	0.4	78.4	E-W
3-D Grid 5/6							
Line interval	0.5						
X-lines	155	0.05	7	196	0.4	78.4	W-E
Y-lines	155	0.05	7	196	0.4	78.4	S-N
3-D Grid 7/8							
Line interval	0.5						
X-lines (11 lines)	100	0.05	5	196	0.4	78.4	W-E
Y-lines (11 lines)	100	0.05	5	196	0.4	78.4	S-N
2004 2-D							
Project 5(Altar)							
Line 0	345	0.05	17.2	248	0.4	99.2	E-W
Line 1/2	2480/2463	0.05	123.95/123.1	248	0.4	99.2	E-W/W-E
Line 3/4	256/258	0.05	12.75/13.35	248	0.4	99.2	N-S/S-N
Line 5/6	262/268	0.05	13.05/13.35	248	0.4	99.2	E-W/W-E
Line 7/8	111/119	0.05	5.5/5.9	248	0.4	99.2	E-W/W-E
Line 9/10	992/989	0.05	49.55/49.94	248	0.4	99.2	E-W/W-E
Line 11/12	1179/2000	0.05	58.9/59.95	248	0.4	99.2	N-S/S-N
Line 13/14	772/772	0.05	38.55/38.55	248	0.4	99.2	S-N/N-S
Project 6							
Line 0/1	2450/2466	0.05	122.4/123.25	248	0.4	99.2	W-E/E-W
Line 2/3	1955/1954	0.05	97.7/97.65	248	0.4	99.2	S-N/N-S
Line 4/5	1173/1175	0.05	58.6/58.7	248	0.4	99.2	W-E/E-W
3-D Grid 2							
Line interval	0.5						
Y-lines (11 lines)	101	0.05	5	248	0.4	99.2	N-S
3-D Grid 3							
Line interval	0.5						
X-lines (11 lines)	101	0.05	5	248	0.4	99.2	E-W
2008 2-D							
Maax Na							
Project 0							
Line 0/1	1564/1570	0.05	78.15/78.45	215	0.4	86	W-E/E-W
Line 2/3	3969/3920	0.05	198.4/195.95	215	0.4	86	N-S/S-N
Line 4/5	1938/1901	0.05	96.85/95	215	0.4	86	S-N/N-S
Line 6/7	2304/2226	5	115.15/111.25	215	0.4	86	W-E/E-W
Line 8, 10/9	1013/1011/1027	5	50.6/50.5/51.30	270	0.4	108	W-E/E-W/W-E
Line 11	15.55	5	312	270	0.4	108	N-S
Line 12	33.85	5	678	270	0.4	108	N-S
La Milpa							
3-D Grid							
Line interval	0.25						
X-lines (72 lines)	360	0.05	18	270	0.4	108	E-W
Y-lines(24 lines)	120	0.05	6	270	0.4	108	S-N
Pulse EKKO							
Frequency 100 MHz			Antenna Separation 0.5 m (CMP) and 1.0 m				
Maax Na							
Line 14 (CMP)	12	0.5	5.5	250	0.8	200	E-W
La Milpa							
Line 15	37	0.5	18	250	0.8	200	SE-NE
Line 16 (CMP)	17	0.5	8	250	0.8	200	SE-NE

Two CMP surveys were conducted in 2008; one parallel to the 2-D line south of the north structure at Maax Na, and the second along the edge of the pseudo 3-D grid at La Milpa. This was accomplished using the Pulse EKKO 100 MHz transmitter and receiver antenna units. Separation between the antennas was set at 0.5 m steps, with a total line length of 5.5 m.

Although our work was primarily conducted with Sensors and Software equipment, other manufacturers include GSSI (Geophysical Survey Systems, Inc.) and MALÅ. Each have a variety of products suited for specific applications and experience levels. As GPR technology has continued to evolve, multiple receiver arrays, advanced signal processing and improved display capability are now available. For more detailed specifications from each manufacturer, please refer to the reference list for a listing of their websites.

3.2 Survey design

In 2004 and 2008, several GPR surveys were conducted at Maax Na, templating the plaza area, an excavated pit and a ceremonial altar. Figure 3.5 shows the orientation of the 2-D lines and three pseudo 3-D grids surveyed at the plaza over a number of field seasons (2002 – 2008). The grids are not considered to be an exact three dimensional representation of the subsurface as found in seismic exploration. Due to the high cost of individual antennas, and their deployment complexity, GPR array acquisition is not standard practise for archaeological investigation. However, recent articles cited in the literature show successful examples of this emerging research and technology. According to Gustafsson and Alkarp (2007), seamless and high resolution 3-D images of the subsurface were generated based on exactly positioned parallel profiles using several separate transmitter and receiver antennas combined into one single antenna array unit at

surveyed for a total number of 40 2-D lines. The three 3-D grids were shot in the western plaza and across the altar feature just north of the ball court. In 2003, one of the 3-D grids was acquired in conjunction with a 3-component micro-seismic survey. Two archaeological pits were also excavated, within one of the 3-D grids in 2003, and at the intersection of two 2-D lines in 2004. As a common midpoint survey is not possible with the Noggin instrumentation, velocity information is determined by fitting a hyperbola to the observed diffraction events (Moldoveanu et al., 2002). Those diffractions, imaged on numerous 2-D lines at Maax Na, and from a piece of rebar wedged into the side of an excavated pit, allowed us to determine the velocities of the near-surface during our first visits to the site between 2002 and 2004. During the field season in 2008, we were fortunate enough to have a Pulse EKKO 100 MHz antenna unit which allowed for transmitter and receiver separation. As previously mentioned, two CMP surveys were conducted: one at Maax Na plaza along a 2-D transect south of the north structure, and the second at La Milpa, across the 3-D grid. Significant differences in velocities were obtained each field season. Since the measurements were conducted in virtually the same area, we now attribute these differences to variations in the air and water content of the limestone, precipitated by wet conditions in 2002, 2004 and 2008, and dry weather in 2003. Measured velocities in 2002, 2004 and 2008 ranged from 0.056 - 0.106 m/ns. Conversely, velocities from 0.119 – 0.140 m/ns were acquired in 2003. This represents almost a doubling of velocities at the extremes of the various ranges. Radar velocities, unlike seismic velocities, generally decrease with depth because of denser and consolidated rock, and increased water saturation.

3.3 Elevation and coordinate map using the Total Station Surveying Tool

To provide exact coordinates of the features delineated on the GPR images, total station surveys were conducted in the 2004 and 2008 field seasons. We used the Leica TC805L total station survey across the entire plaza, and over a ramp feature associated with the north structure. This survey tool allows for accurate spatial and topographic coordinates based on existing reference markers (turning points) set in place by the archaeologists. In previous years, a GPS system was used but accuracy concerns due to satellite and tree cover issues have demanded more dependable systems (Aitken and Stewart, 2004).

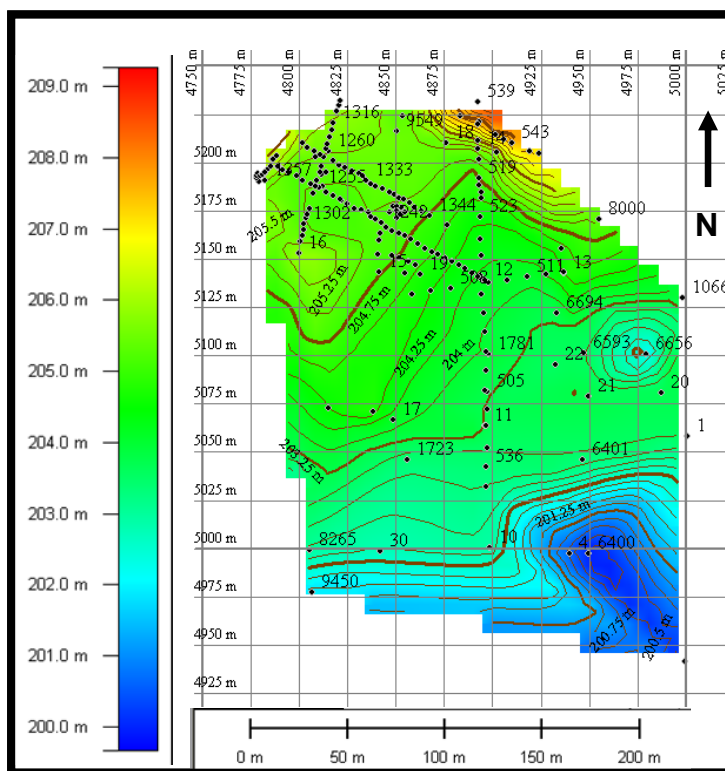


Figure 3.6 Topographic map of Maax Na incorporating total station survey data of GPR lines and archaeological turning points.

The resultant topographical map of the plaza, based on the positioning of the survey lines and turning point data, reveals a gentle sloping of the plaza to the south southeast (SSE) (Figure 3.6). The Maya engineered plazas such that their slope allowed for the drainage

of water away from pyramids and other structures during the torrential downpours associated with the rainy season. This was a means of protecting the temple and palatial structures from flooding and to collect the rainwater for future use. Interestingly enough, at Maax Na, the Maya created a large reservoir to the southwest as shown in Figure 3.7, and may have been in the process of building another to the southeast before they abandoned the site (Shaw, 2008, pers. comm.).

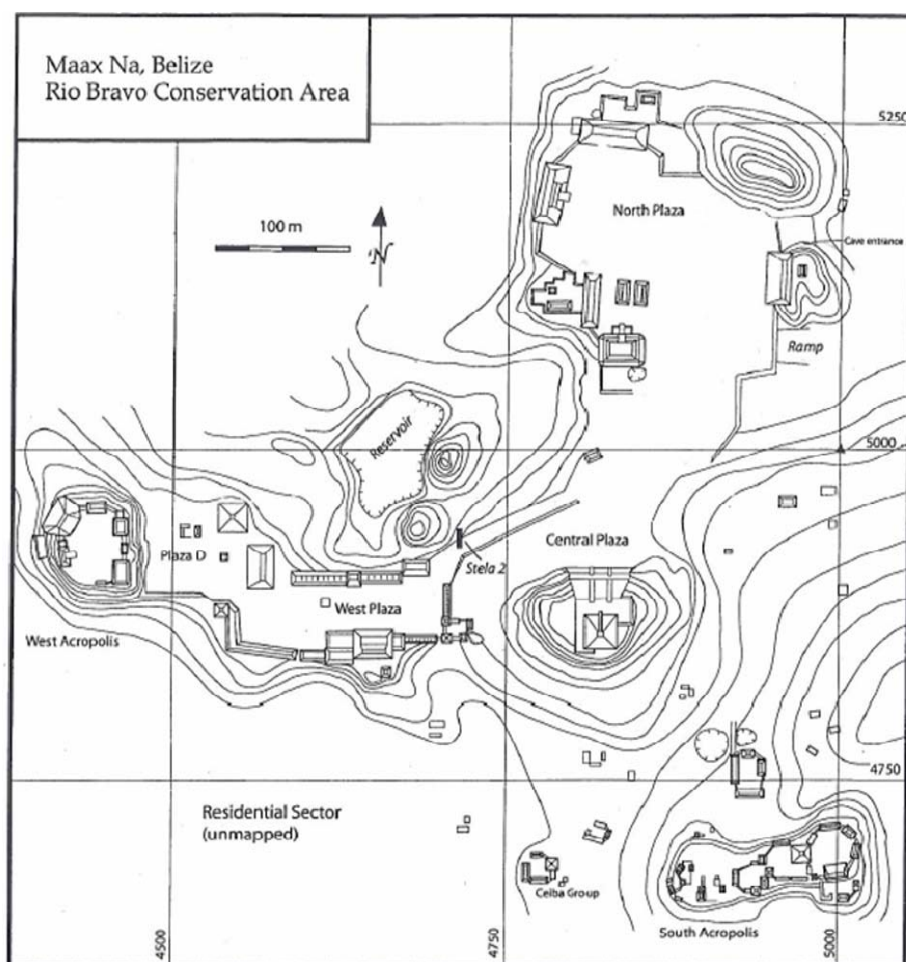


Figure 3.7 Ceremonial centre of Maax Na; note reservoir to the southwest of North Plaza (King, 2005, pers. comm.).

Chapter Four: RADAR VELOCITY AND MODELLING

4.1 Rock Properties affecting GPR

The success of GPR surveys is dependent on the composition of near-surface materials and conditions. The clay content of soils, the presence of saline fluids, and the saturation level of the material in general, play key roles in obtaining interpretable images of the earth. Radar velocity information collected over the four field seasons varied dramatically due to climatic conditions and wet versus dry environments. As dielectric permittivity is inversely proportional to radar velocity, it appears to be the property most sensitive to saturation of the near surface, assuming a non-magnetic and non-conductive medium.

4.2 Comparison of radar velocity measurements in the field

Velocity values in 2002, 2004 and 2008 ranged from 0.056 - 0.106 m/ns. These velocities appear to be consistent with a more saturated near-surface environment. Rainfall occurred in the area weeks before and during the field work. Conversely, velocities of 0.119 – 0.140 m/ns were acquired in the parched spring of 2003 when drought-like conditions prevailed, with a noticeable absence of insects and wildlife.

The velocity information observed in the field is summarised in Table 4.1.

Table 4.1 Velocity Information observed during the different field seasons.

Field Observations at Maax Na (Diffractions noted in subsurface)									
Year	Project	Line	Instrument Velocity Setting	Depth	Measured Velocities	Time *	Interval Velocity	Average Velocity	Field Conditions
			(m/ns)	(m)	(m/ns)	(ns)	(m/ns)	(m/ns)	
2002	2	3	0.08	0.40	0.100	10.00	0.100	0.082	wet
	2	3	0.08	0.60	0.082	15.00	0.013	↓	wet
	2	3	0.08	0.70	0.074	17.50			wet
	2	3	0.08	0.87	0.072	21.75	0.063		wet
2004	6	4	0.08	0.65	0.048	16.25	0.048		0.060
			0.08	1.04	0.072	26.00	0.100		wet
2008	0	3	0.06	0.57	0.056	19.07	0.056	0.058	wet
			0.06	0.63	0.057	21.07	0.066	↓	wet
			0.06	0.84	0.057	27.97	0.057		wet
			0.06	1.20	0.062	40.00	0.072		wet
2003		1	0.08	0.76	0.122	19.00			0.122
2003	Rebar set at:			0.74					
	Lines	1	0.08	0.75	0.122	18.75	N/A	0.135	dry
		3	0.08	0.74	0.134	18.50			dry
			0.08	0.76	0.138	19.00			dry
		4	0.08	0.78	0.140	19.50			dry
		8	0.08	0.75	0.140	18.75	↓	↓	dry

By measuring velocities and depth to the diffracted events, one can determine interval velocities as outlined in the above table. Interval velocity is the velocity of the wavelet through a single homogeneous layer and is calculated based on the Dix equation as follows:

$$V_i = \sqrt{\frac{V_n^2 T_n - V_{n-1}^2 T_{n-1}}{T_n - T_{n-1}}}, \quad (4.1)$$

where V_i is the interval velocity, V_n is the measured velocity and T is time.

Detailed interval velocities allow one to obtain a more correct velocity at a particular depth and in turn, create a more accurate depth model.

Average velocities are the mean velocity of the pulse averaged over the travel time (Hatton et al., 1988).

4.3 Water content and its effect on radar velocities

Based on our field observations, we were compelled to understand why the radar velocities between saturated and unsaturated materials differed so drastically. In the acoustic world, the Wyllie Time Average equation is often used, attempting to explain changes in field velocity by changes in the saturation of the pore space (Wyllie et al., 1958). We propose to use the same concept for radar velocity. Using the Wyllie equation, radar velocities are estimated for any porosity, rock matrix or fluid type. In this case, the plaza consists of repeated layers of cobble limestone topped with thick plaster. The porosity within the near-surface is a combination of the intragranular velocity within the limestone cobbles themselves, and the intergranular porosity of the void space between the cobbles. Within these voids, created through plaza construction, natural fracturing, or dissolution, pore space is filled with water or air, or a combination of the two. The velocity differences recorded in the field are the result of pore fill, since the rock matrix remains the same. Thus, we adapt the Wyllie Time Average equation to calculate the velocity of the medium by:

$$\frac{1}{V_A} = \frac{\phi}{V_F} + \frac{1-\phi}{V_M} \quad (4.2)$$

where V_A is the *actual* velocity measured, V_F is the velocity of *fluid* (air and/or water) within the pore space, V_M is the velocity of the rock *matrix* (limestone at 0.104 m/ns), and ϕ is the porosity.

To calculate the porosity of the medium, a simple rearrangement of the equation terms and a number of assumptions are required.

With the range of measured velocities recorded in the field during the drought of 2003, of V_A equal to 0.119-0.140 m/ns, V_M equating to the velocity of the limestone matrix at 0.104 m/ns, and dry conditions in which all the pore spaces are filled completely with air implying a V_F of 0.300 m/ns, it then follows that the porosity of the limestone medium (ϕ) is calculated to be in the range of 20 to 40%. This range is pretty high for limestone rock in general but possible for a combination of limestone detrital, cobbles, and plaster, and the fact additional void space exists between the cobbles in the man-made plazas. If we now assume wet conditions as encountered in 2002, 2004 and 2008, in which pore space or fill is saturated with water, and substitute the above range of porosities into the following equation,

$$V_A = \frac{V_F * V_M}{V_M \phi + V_F (1 - \phi)} \quad (4.3)$$

using V_M equal to the velocity of limestone *matrix* at 0.104 m/ns, and assuming the pore fluid to be water such that V_F is 0.033 m/ns, we can calculate a new set of velocities, V_A , and compare them to the field velocities determined at the site from the hyperbolic curve fitting to diffractors in the near-surface.

With water-saturated porosities ranging from 20% to 40%, we expect the actual velocities, V_A , to be 0.056 to 0.073 m/ns. Referring back to Table 4.1, our observed average velocities in the field were actually 0.058 to 0.082 m/ns.

4.4 Modelling of GPR data

Modelling of the GPR data was based on information garnered from the first excavation by the field archaeologists, of a two-by-one metre pit at the plaza at Maax Na.

The plaza levels, or lots, consisted of large limestone rubble at the base, with smaller cobbles filling in the remaining spaces, followed by a thick interval of plaster. Lots correlate with specific phases of Maya construction (Shaw, 2004, pers. comm.). Based on the detailed information about the layering and mode of construction from the excavated pit, a graphical representation was created in Excel and is shown in Figure 4.1. At least seven previous layers of construction were evident interspersed with rubble and cobble layering, with four major refurbishings of the plaza, and lots of little patching in between (King, 2005, pers. comm.).

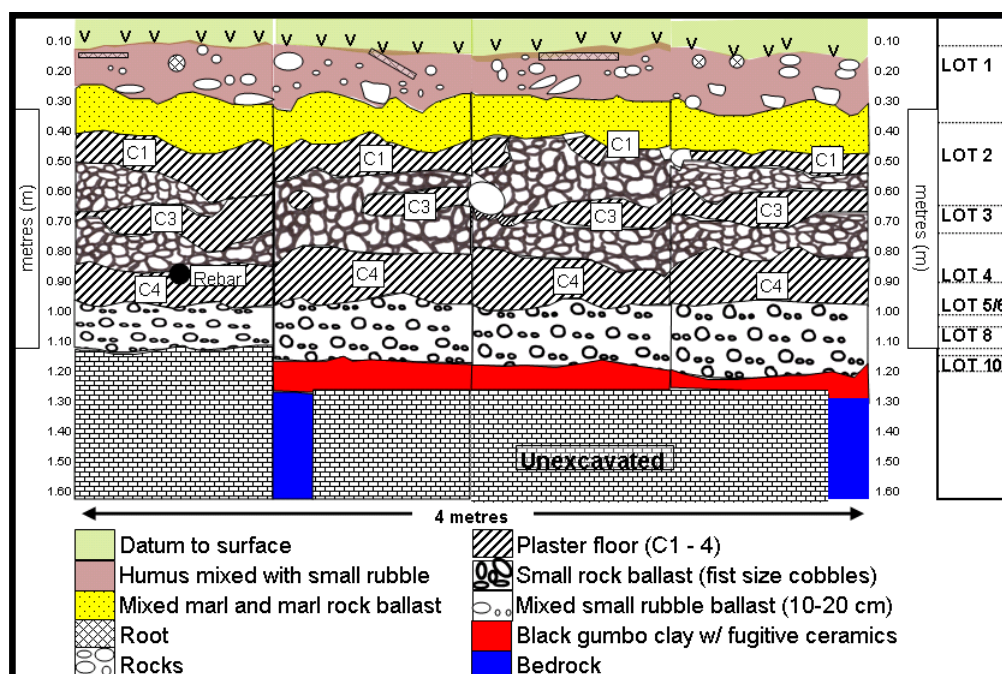


Figure 4.1 Schematic representation of the pit (reproduced from E. King).

As the plaza is constructed primarily of limestone from the base to the top, identifying what could cause contrasts and thus changes in impedance was challenging. The only real physical differences were the forms of limestone in terms of plaster, rocks and large cobbles, and the saturation of the materials. In the saturated conditions of 2002, 2004 and

2008, it was assumed that the interspersed cobble layers provided a permeable pathway for fluid flow. As the relative dielectric permittivity value of limestone is 8, compared to water at 80, it would follow that the dielectric constant for this interval should increase. In fact, average dielectric constants may increase up to 20 % with the infiltration of fluid along a preferential flow path (Hubbard et al., 1997).

Based on these assumptions, a GPR radargram was generated using CREWES software LOGEDIT and SYNTH (now SYNGRAM) developed at the University of Calgary.

LOGEDIT is a seismic based program which allows one to create and manipulate geophysical logs for input into a synthetic generation program called SYNGRAM.

Forward modelling of seismic reflection data is based on changes in seismic velocity and density. Often, this information is taken directly from borehole information, namely sonic and bulk density logs. Assuming a non-magnetic medium, ground-penetrating radar geologic models depict spatial variation in dielectric constant and conductivity as opposed to acoustic impedance (Anderson and Cardimona, 2002). In this case, these physical properties are not explicitly known so understanding the differences in the physical properties of radar necessitates the construction of “artificial” logs. Generating a GPR radargram entails a number of assumptions and requires the creation and manipulation of pseudo dielectric permittivity and conductivity logs from initial sonic and density logs. According to Equation 2.1, there is a direct relationship between radar velocity and dielectric permittivity. The sonic or slowness log was replaced, in this instance, by a dielectric permittivity log. The density log was manipulated to represent a constant “pseudo” conductivity curve using a constant value of 1 mS/m, representing the electrical conductivity of saturated limestone. According to the Sensors and Software

Inc., an attenuation log may also be used. Two different logs were created based on the velocities measured in the field in 2002 (saturated) and 2003 (dry).

The dielectric permittivity logs were created by assuming the plaster layers were impermeable and equivalent to the dielectric permittivity of limestone. The dielectric permittivity values were increased by 20 % (saturated) and 5 % (dry) respectively over those areas in the excavated pit that contained rubble or small rocks. The zones were also assumed to be at least 0.08 m thick, which is just above the vertical resolution for this type of system (i.e. calculated resolution of 0.072 m). Because the SYNGRAM program is designed for seismic modelling and not GPR, it was also necessary to multiply the velocity values by a constant to bring them into a more acceptable range. This of course will change the transit times of the new logs but can be accommodated by “stretching” or compressing the radargram. The logs were then convolved with a 250 Hz minimum phase wavelet. One of the resultant GPR synthetics is aligned with the archaeological information, the pseudo-conductivity log (blue) and the pseudo-dielectric permittivity log (red) for comparison (Figure 4.2).

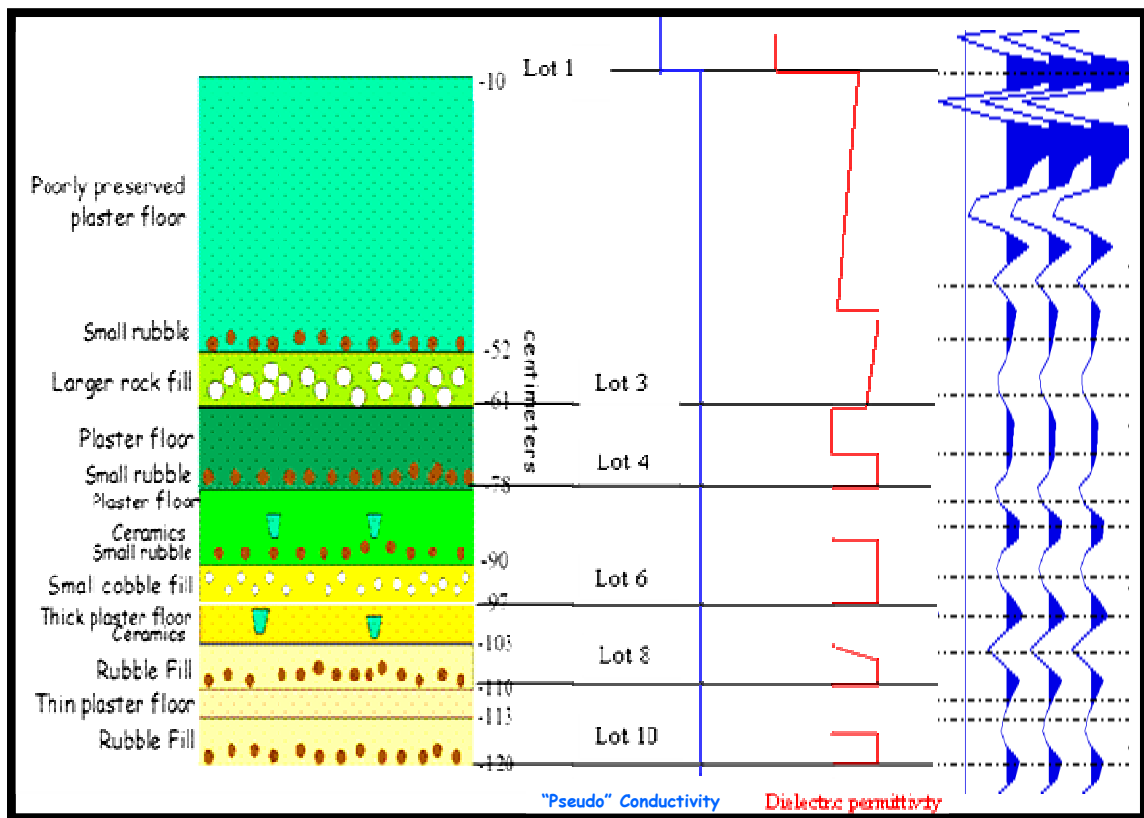


Figure 4.2 Radargram generation using a pseudo-dielectric permittivity and conductivity log.

Acknowledging the simplicity of model, and the huge underlying assumptions in its creation, two radargrams, specific to a saturated and dry environment were generated. Figures 4.3 and 4.4 show the rather promising similarity or tie of the radargrams, to the 2002 and 2003 GPR data.

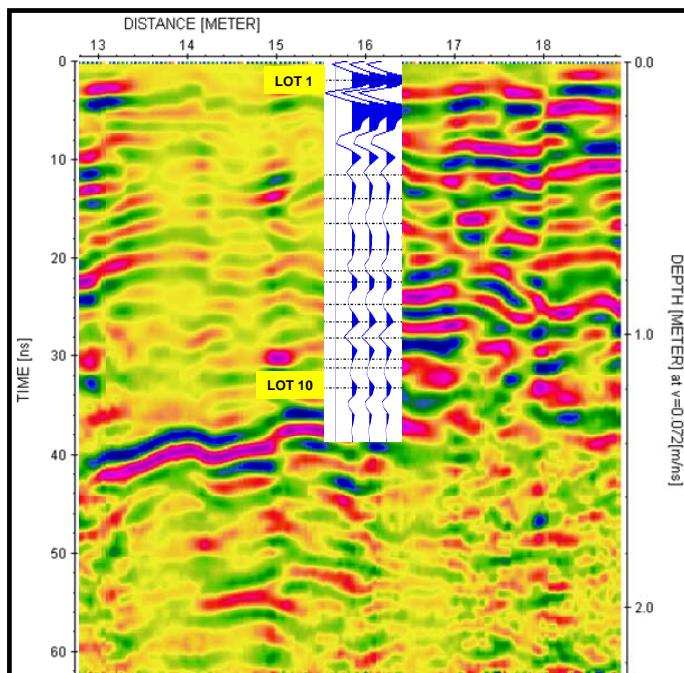


Figure 4.3 Comparison of 2002 data (wet) with GPR radargram.

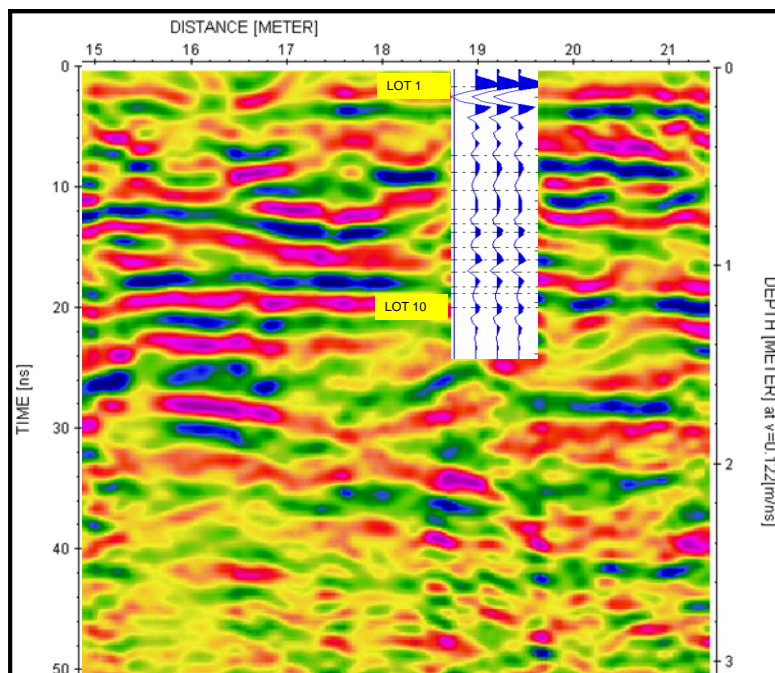


Figure 4.4 Comparison of 2003 data (dry) with GPR radargram.

This type of methodology allows one to determine approximately the depth of archaeological “lots” on the GPR record, assuming the lot is resolved (i.e. impedance

changes in the electromagnetic properties). The location of each individual lot is dependent on the radar velocity. This concept is best demonstrated by comparing the two datasets in time (Figure 4.5).

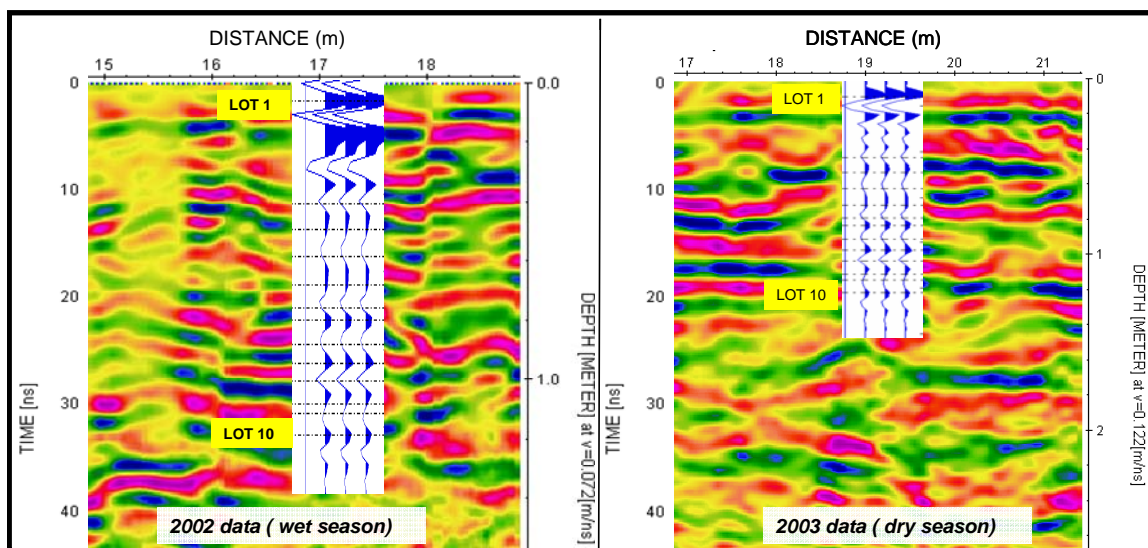


Figure 4.5 Time comparison between the 2002 and 2003 GPR data.

This figure reveals two important points. Radar velocity controls when an event occurs on a GPR record, and the resolution of that event. In 2003, the radar velocity is higher or faster, thus the travel time to that event is shorter. Conversely, while the 2002 data is slower, observe how much more information and resolution is displayed. For example, Lot 10 is imaged at approximately 33 ns on the left side and 19 ns on the right side of Figure 4.5. Assuming velocities of 0.072 m/ns and 0.122 m/ns for their corresponding radar velocities, and using equation (2.5), depths to Lot 10 are calculated to be at 1.18 m and 1.16 m respectively. The archaeologists mapped Lot 10 at 1.2 m.

Based on the velocities encountered in 2002 and 2003, and the frequency of the Noggin unit at 250 MHz, the wavelength of the data ranges from 0.29 to 0.49 m according to Equation (2.6). It follows then that the best theoretical resolution using $\lambda/4$, is 0.072 and

0.122 m respectively. The plus/minus 0.01 m difference determined from the depth conversion of the different vintages appears to be within the limits of our vertical resolution and confirms that the event is within the same pulse or cycle.

These variations in velocities, depth of penetration and resolution have a significant effect on the interpretation of events on a GPR record.

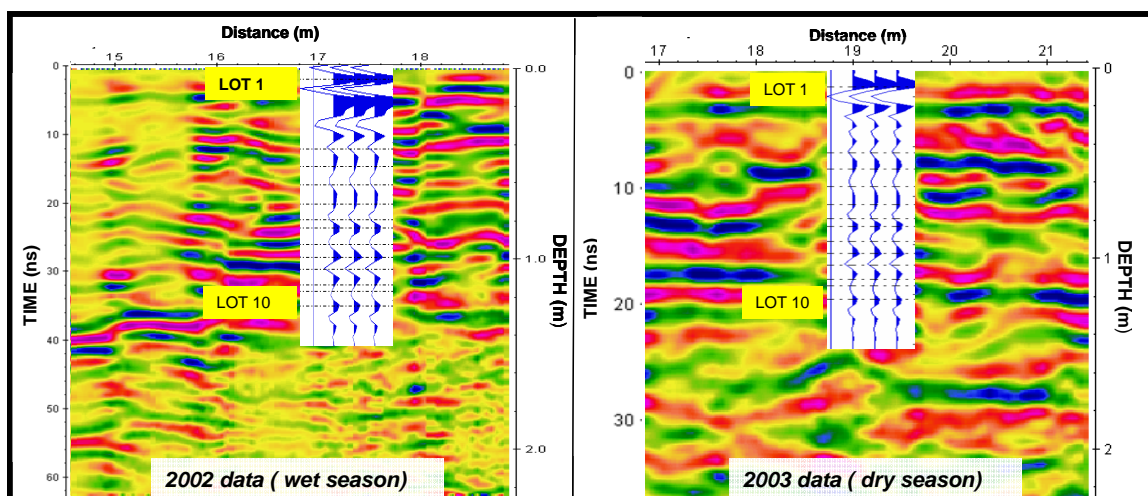


Figure 4.6 Depth comparison between 2002 and 2003 GPR data.

As shown, to tie the same archaeological event (Lot 10) in depth, one of the sections needs to be either stretched or compressed as demonstrated in Figure 4.6. The need to do this is often overlooked by non-geoscientists unfamiliar with the importance and dependency of near-surface radar velocities and how this can change from year to year.

4.5 Radar velocity measurement in lab

In 2005, a piece of rubble taken from the excavated pit was sent to a colleague, Dr. Elena Pettinelli at the Università Roma Tre. She is conducting a series of tests measuring dielectric permittivity and electrical conductivity under dry and saturated conditions. According to Annan (2003), dry limestone rock should typically have a relative dielectric constant ranging from 4-8, and an electrical conductivity of 0.50-2.0 mS/m.

I have unfortunately not received the results as yet, and did not plan to regenerate or research additional modelling packages until I had more realistic numbers. Quantifiable physical properties of the limestone samples, from the excavated pit, especially in saturated conditions, will serve to create a more realistic GPR radargram. Forward modelling is essential to understanding and interpreting GPR and should be used in all situations when possible to add confidence in the site interpretation (Goodman, 1994).

Chapter Five: PROCESSING

5.1 Processing Steps

In my research work, processing of the GPR data has been accomplished using various systems and different software programs and processing flows, including GEOX, EKKO-Pro, EKKO View, Promax, Vista, MATLAB and ReflexW. As time progressed, equipped with more knowledge, experience and understanding of the subject, it was felt that using or adapting seismic based systems was not the best approach. Converting time (milliseconds to nanoseconds), frequencies (Hertz to Mega Hertz) and velocities (m/s to m/ns) within each system was cumbersome and prone to error. Programs geared specifically to GPR and its associated units were a better alternative, which is why in the end, I preferred to do most of the processing using a software package called ReflexW, developed by Karl-Josef Sandmeier.

5.2 ReflexW Processing Flow and Examples

The GPR datasets were all processed using ReflexW, a program designed for processing and interpreting seismic, acoustic or electromagnetic reflection, refraction and transmission data (Sandmeier, 2004). The advantage of using this program is that many of the options available to the seismic processor, which I am familiar with, including 2-D and 3-D processing capabilities, are available and all the conversions to the appropriate GPR units are dealt with. The processing flow consisted of a dewow filter and gain, a smoothing operator, a band-pass filter (specifically a Butterworth filter), background removal, an F-K Stolt migration and a bulk shift to bring the start time to time zero. Several different filters were applied to the data both spatially and temporally, each providing a distinct and necessary function in optimizing the GPR record displays.

Challenges in processing the 3-D surveys in particular, were due to calibration problems, and the presence of skipped traces. Similar processing flows were established for the GPR lines for both 2-D and 3-D. Due to the acquisition procedure for the 3-D, namely a reversal in the direction of all the odd lines, an additional step to essentially flip the line is necessary such that all lines are aligned in the same direction. This is done automatically within ReflexW if imported correctly. The most effective processing flow is outlined in Figure 5.1.

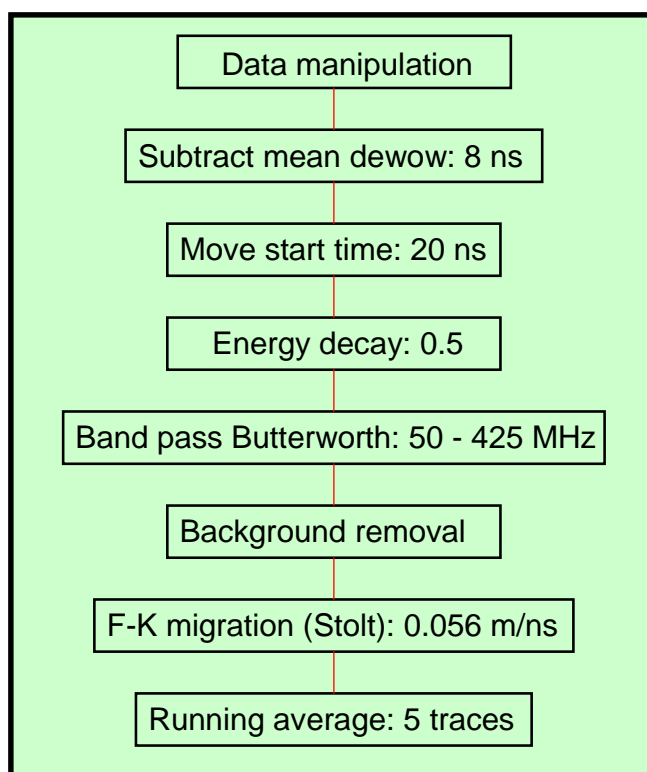


Figure 5.1 ReflexW processing flow applied to the GPR data.

The most important lesson I have garnered to date is the fact that elaborate processing flows are not necessarily the answer and do not particularly optimize GPR data. Keeping the flow simple seems to work well and great care should be taken when applying migration and the dewow filter.

A great deal of my research focussed on testing individual processing algorithms and creating processing flows for the GPR data. The following is an explanation of each processing step and its applicability to radar data.

5.2.1 Data manipulation

In order to create a 3-D grid of equal dimensions, several assumptions are necessary. Firstly, one must establish that the starting point of each line is correct, and that lines are identical in length or contain an equal number of traces. Consideration should also be given to the fact that if surveys are conducted in a forward-reverse acquisition mode, every second line needs to be reversed or the traces and common depth points renumbered, to reflect a consistent direction for processing.

5.2.2 Trace Interpolation

Skipped traces are common on GPR lines, and were evident on several of the lines in our survey as shown in Figure 5.2. Skipped traces are due to the cart moving too fast for data collection, by not allowing time for the specified number of stacks to be generated, or loss of contact with the wheel and odometer, resulting in a series of repeated traces. The position of each trace is correct, but a “true representative” trace fails to be collected. The traces should be edited in this case by either zeroing out or killing the trace, a process which I have adopted within ReflexW (Figure 5.3). An interpolation may also be applied to fill in the gap in the data. Several interpolation techniques were tested within Promax. A tau-p interpolation called INFILL DATA was the most successful technique applied to the stacked data. The process transforms a 21 trace aperture of x-t traces to a range of dip, or slant stacked traces. Each dip trace is then weighted, sample by sample, by the

semblance along that dip and then inverse transformed back to the x-t domain (Figure 5.4). ReflexW, however, does not contain a similar technique.

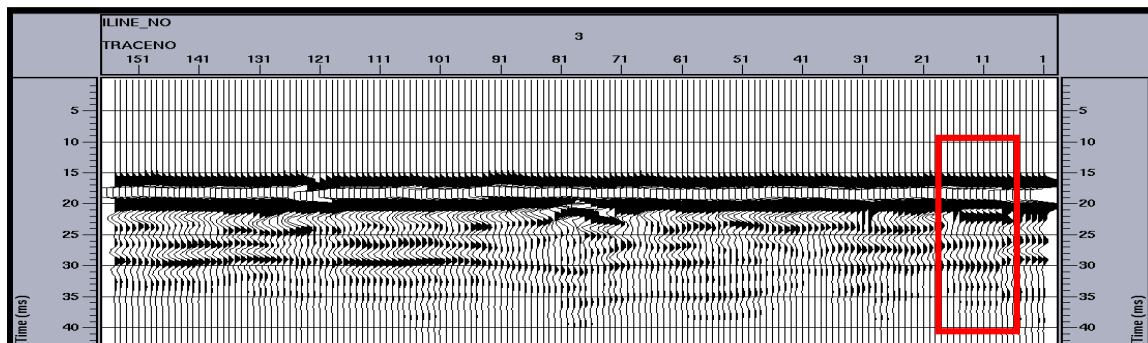


Figure 5.2 A GPR section showing skipped or repeated traces.

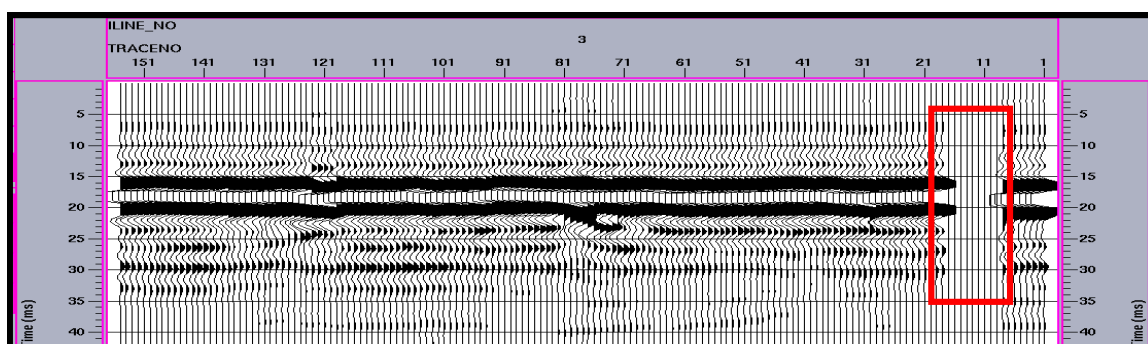


Figure 5.3 A GPR section with the skipped traces deleted or zeroed out.

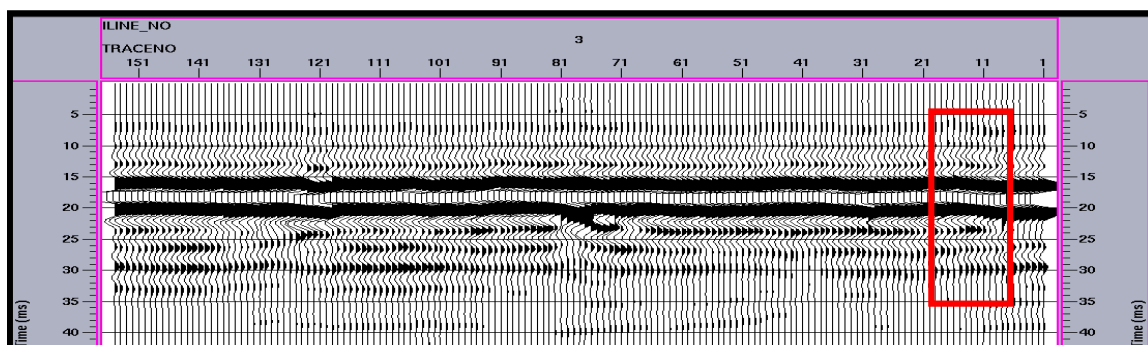


Figure 5.4 A GPR section showing the application of INFILL DATA to correct for the skipped traces.

5.2.3 Bulk Shift

The first two dominant events on a GPR record are the air-wave and the ground-wave. Important information contained in the subsurface data is considered to be anything below these two waves. Time zero is often difficult to pinpoint due to a time delay

between the emission of the transmitted pulse and the reception by the receiving antennae, the opposite polarity of the two pulses, and the ensuing likelihood of destructive interference. In this case, a bulk shift can be applied to the data with the assumption that time zero represents the start of or first deflection of the air-wave.

5.2.4 Normal Move-out

A zero offset section is one in which the source (transmitter) and receiver are co-incident and the travel path of the pulse is directly below the antennae and perpendicular to the reflecting boundary, assuming a flat surface and a constant velocity medium. The GPR data collected at Maax Na and La Milpa is not considered to be zero offset due to the separation of the transmitter and receiver within the Noggin antenna unit at 0.28 m, and the Pulse EKKO instrumentation at 1.0 m. The additional time delay for the transmitted pulse to reach the receiver is termed the normal move-out correction. The equation for calculating normal move-out is:

$$\Delta T = \left(T_0^2 + \frac{X^2}{V^2} \right)^{1/2} - T_0 \quad (5.1)$$

Assuming the depth to limestone bedrock at 1.5 m, and a radar velocity of 0.060 m/ns, the normal move-out correction is only 0.22 ns and 2.70 ns for the Noggin and the Pulse EKKO antennae units respectively. Due to this small difference for the Noggin instrumentation, calculated at less than a quarter of a nanosecond, applying the NMO correction to the processing flow proved unnecessary. According to Leckebusch (2003), in normal applications this value is constant and very small. Therefore, it is normally neglected without complications. Application of the NMO correction was applied to the Pulse EKKO Line 15.

5.2.5 Muting

Muting of the data, specifically the air wave and ground wave, is a good idea before applying gain. The strong amplitude of these events tends to be further enhanced if included in the gain window. Removing them through muting, before the gain application, results in more realistic true amplitude values and an even distribution of amplitude throughout the section.

5.2.6 Dewow Filter

All GPR systems contain a low-frequency component. The magnitude of the low frequency component and how it manifests itself in the data depends on the ground conditions around the antennas, and the distance between the antennas (Annan., 2003). A high-pass filter, known as a dewow filter, is used to eliminate this component by acting on each trace independently. Unfortunately, when the raw data are high-pass filtered, the wavelet is stretched in time with additional oscillations occurring before and after the original pulse (Annan., 2003). An example of this is shown below in Figure 5.5.

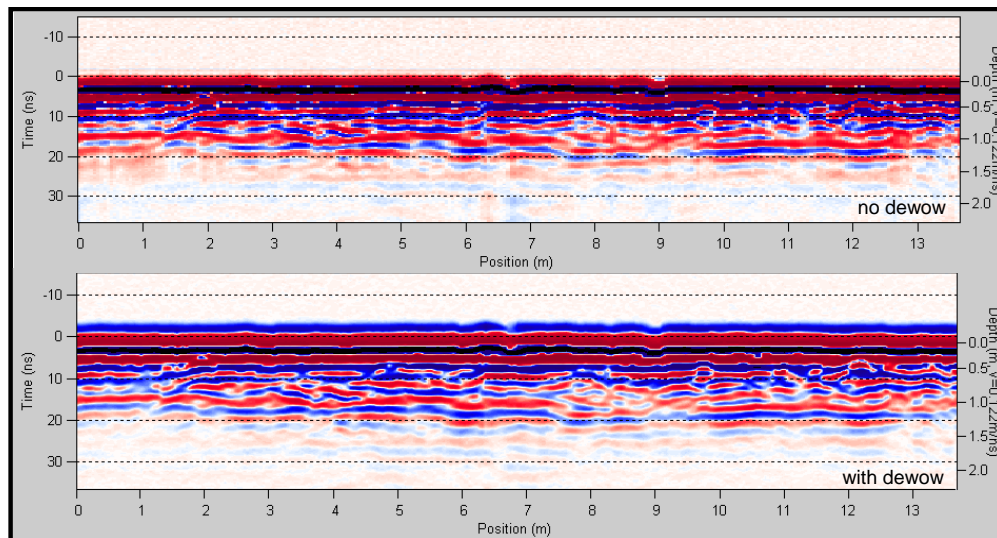


Figure 5.5 Example of a GPR record with and without a dewow filter.

Unfortunately, this particular process may also cause data artifacts and give rise to the pre-cursor in the data before time-zero when looking at plotted sections. Other filtering techniques such as an Ormsby filter, and removing or muting the non-data areas will address the presence of these unwanted artificially induced features. Care must be taken in selecting the correct time window (Berard, 2006).

5.2.7 Gain Function

The application of a gain function is especially critical to GPR data due to the rapid attenuation of electromagnetic energy with depth. This is due in part to heat conversion, and the rapid absorption of higher frequency energy in the near-surface. Several gain functions were tested, namely automatic gain control (AGC), a time-variant gain, and an energy decay function. The application of an AGC gain improved the amplitudes throughout the section but the true amplitude of the events is not preserved and any further amplitude manipulation is not valid. The AGC filter facilitates this through the generation of equally distributed amplitudes within a predefined time window (Sandmeier, 2004). Each sample is multiplied by a scalar derived from a window of data. The size of the window determines the severity of the equalization (Hatton et al., 1988). Small window sizes cause a strong equality distribution, while large windows result in a weak distribution of amplitudes. The time variant gain did a fairly good job of preserving the signal strength and continuity of the deeper events. However, it did appear to create a spurious event on the GPR record where the gain was ramped to accommodate the decrease in amplitude with depth. This event was not “real”. Having the ability to recognize the presence of “processing artifacts” from real world geology necessitates not just an understanding of the near-surface, but how these processes work. Based on a

comparison of the different techniques, the application of an energy decay curve was deemed the best for preserving amplitude information at depth (Figure 5.6).

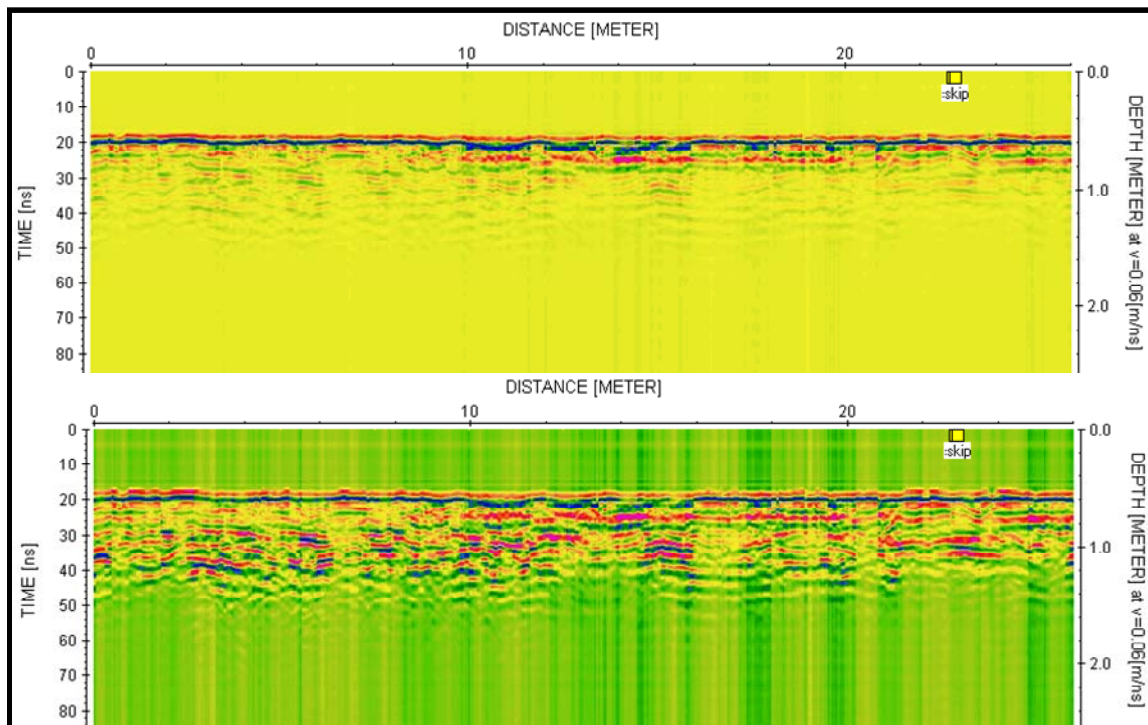


Figure 5.6 Comparison between a raw record and one with energy decay applied.

Another lesson to heed has been the need to look at the instrument gain applied to the data during acquisition. The instrument gain function is set in the initial stages as an input parameter, and controls how much the signal is amplified as the data is recorded on the digital video logger (DVL). This gain setting, which varies from 1 to 9, is for display purposes only and will not be applied to the data. A second level of gain is also available to the user (Sensors and Software manual, 2003). The linear gain parameter, set at 2, is usually adequate for most ground conditions but can vary from 0 to 5. One of the best anomalies we have come across during the last few years didn't show up when re-acquiring the lines because the instrument gain in the lower part of the section was not set correctly (too low). Even in field acquisition, this process is extremely important. The

user who may be looking for anomalies directly on the DVL would simply miss the feature if the data were not adequately gained enough. The critical thing here is the gain parameter is set automatically at a default value and unless the user is aware of this, such a mistake can easily be made.

5.2.8 Filtering

The running average filter is considered a smoothing spatial filter and performs a running average across a specified number of traces within a specified time interval. This filter method suppresses trace dependent noise and serves to emphasize horizontally coherent energy. A running mean value is calculated for each value of each trace within a specified time window, and is then subtracted from the central point. A band-pass filter is a filtering technique in which only certain ranges of frequencies are recovered in the data. This essentially rids the sections of low frequency interference and noise associated with higher frequencies. Based on the different tests, it appears the steeper the slope of the boxcar filter, the more ringiness or aliasing is apparent. A Butterworth filter is a subset of the band-pass filter, and does not have a boxcar shape. Instead it contains only two reference frequencies, in which frequencies within the range are passed and those outside the range are disregarded. The frequency response of the Butterworth filter is flat (with no ripples) in the pass band.

5.2.9 Migration

According to Sandmeier (2004), migration is one of the most important filters and imaging techniques. A simple time migration such as the Kirchoff migration of a two-dimensional profile based on a constant velocity, was performed on the GPR data.

Velocity measurements were determined from the hyperbolic fitting of curves to point

diffractors. The existence of diffractions, especially with GPR, allow for accurate velocity determination. If strong diffractions are present the migration tries to contract these diffractions to a minimum. This is useful for an interpretation using time slices for example (Sandmeier, 2004). In addition to the contraction of the diffraction energy, a goal of migration is to shift the arrivals to their "true" or original source position. This is especially important for steep dipping reflectors. Kirchoff migration is done in the x-t domain. For every migrated sample, energy is summed along a diffraction or hyperbolic path in the input section. The summed value becomes the amplitude value at the output location (Bancroft, 2004).

The Stolt migration of a two-dimensional profile was also applied. This fast fk-migration method works in the frequency-wave number (fk) domain. Within the fk-range, a variable transform is performed based on a constant velocity in which the frequency is transformed into the associated vertical wave number. This migration can only be applied if the time window is long enough (approximately 10-15 wavelengths). The Stolt migration is mostly preferable for the migration of extended or steep reflectors. When comparing the two different migration algorithms as shown in Figure 5.7, I found the results to be very similar; however, I felt the continuity and amplitude of the events were slightly better using the Stolt migration.

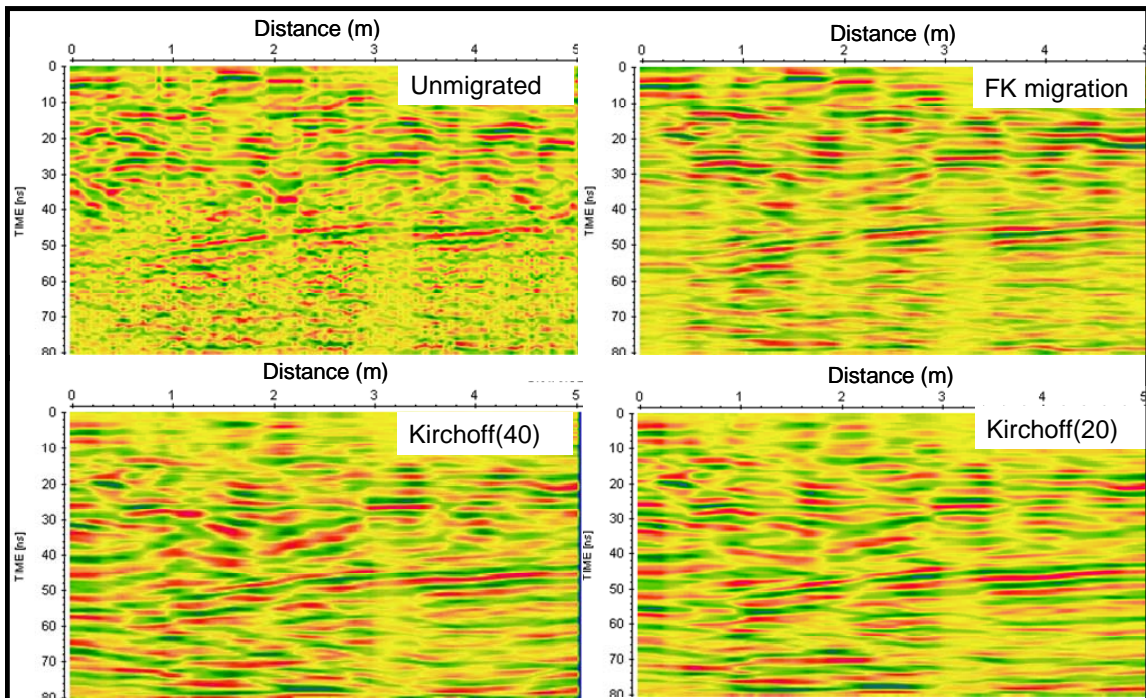


Figure 5.7 Different migration algorithms applied to the GPR data.

5.2.10 *Q-Filter*

Attenuation is the conversion of coherent energy into heat. It is manifested as the distortion of a wavelet as it propagates with time into the subsurface. This distortion, evident in the broadening of the wavelet and decreased amplitude, is due to higher frequencies being absorbed more than lower frequencies (Charles, 2007). Wavelet dispersion caused by frequency-dependent attenuation is often identified by the blurriness of the events with depth (Irving and Knight, 2003). To improve the deeper data, a deconvolution algorithm was investigated using an inverse-Q filter. It essentially calculates the subsurface Q from the reflection GPR data, assuming a constant Q type attenuation (Irving and Knight, 2003). As shown in Figure 5.8, a series of Q values from 20 to 100 were tested on the data. This approach was recommended by James Irving as

the values vary from one location to another depending on the composition of the near-surface. Note that a Q of 20-30 provides some indication of deeper strata.

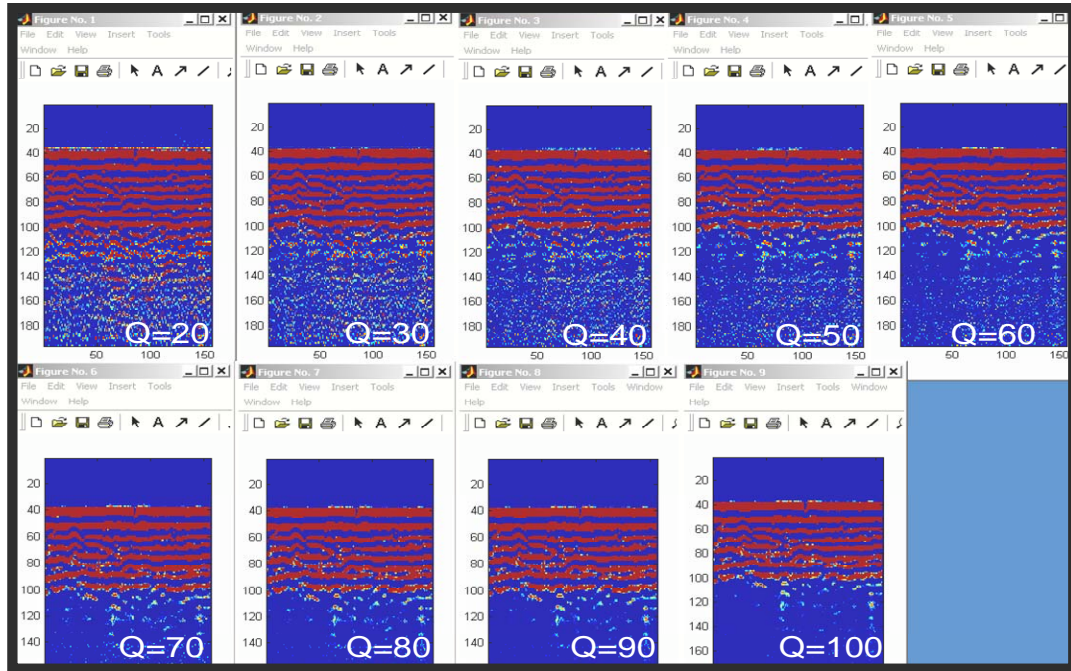


Figure 5.8 Comparison of Q-filter values.

The resultant section, as featured in Figure 5.9, is processed with the ReflexW flow and includes a spatial averaging 2-D filter. The image appears to be more continuous, less noisy and shows a marked improvement of amplitude at depth.

Based on a closer look at the GPR data at Maax Na, I now believe the decrease in energy with depth is due to the composition of the near-surface, namely the signal passing through and reflecting off the man-made layers of rubble and plaster representing past plaza surfaces, into the limestone homogeneous bedrock. In fact, the amplitude decrease serves to distinguish this important boundary.

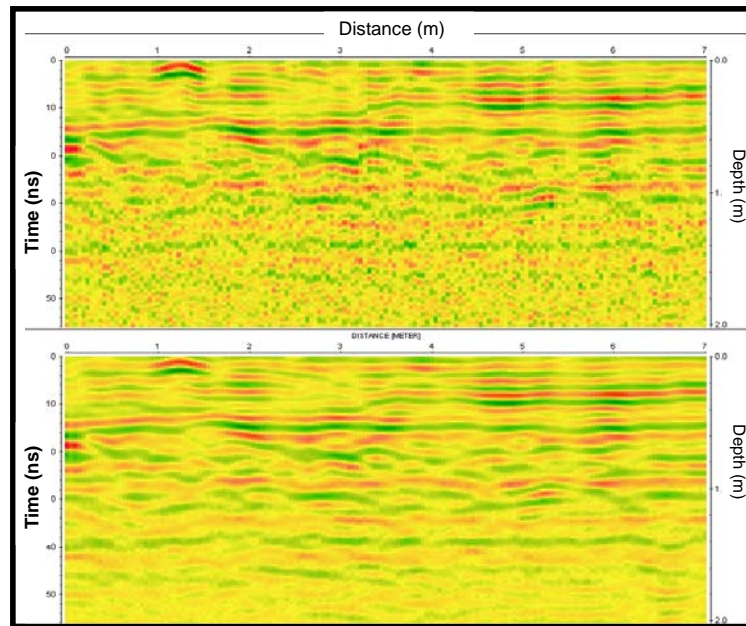


Figure 5.9 Comparison before and after a Q-filter and spatial filter.

5.3 Common Mid-point Survey (CMP)

Over the last several field seasons, velocity information was obtained by hyperbolic curve fitting to observed point diffractors in the subsurface. These measurements were a good approximation of the radar velocity of the near-surface but a more quantitative measurement should be taken by conducting a common-mid point survey. This survey involves a systematic separation between the transmitter and the receiver, by moving both antennas away from a central point or location, or by keeping the transmitter in a fixed position and moving the receiver antenna away (termed a shot-gather). In 2008, we acquired two CMP surveys with a Pulse EKKO 100 MHz system. The Maax Na survey will be discussed later in the report. At La Milpa, antenna separation was 0.5 m for a total length of 8.0 m (Figure 5.10). Processing was accomplished using the CMP(1-D)-velocity analysis within ReflexW. As recommended by Sandmeier (2008), prepping the CMP data for input into the semblance analysis required the application of declipping,

dewow, a subtraction average, gain, a static correction to flatten the air-wave, and a time cut.

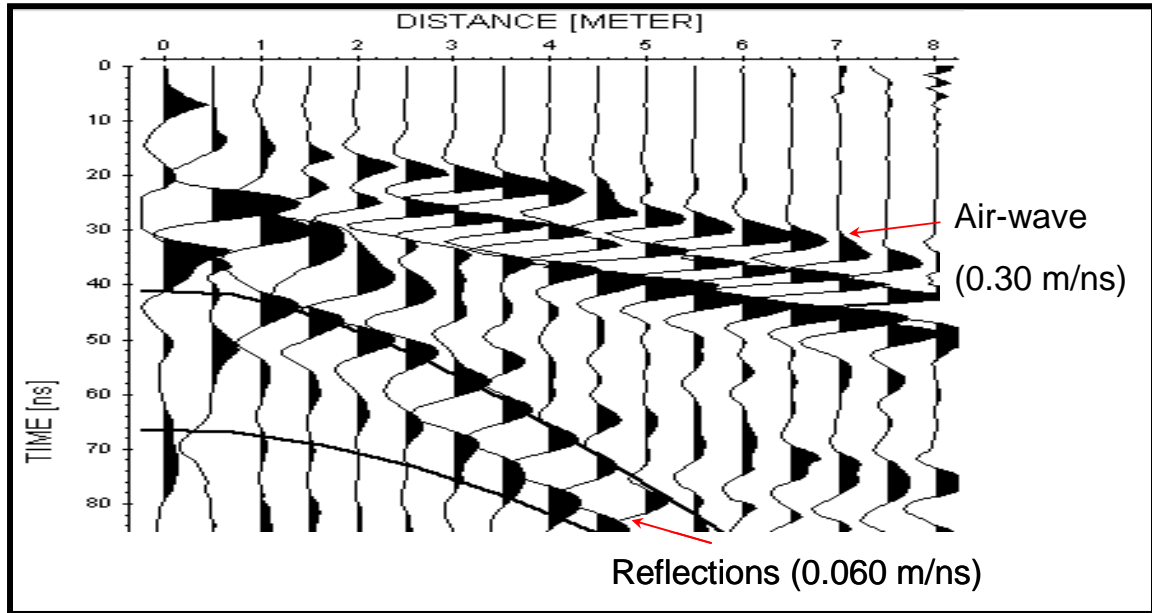


Figure 5.10 Raw CMP profile acquired at La Milpa.

5.4 Merging and Interpolation of 3-D Grids

The merging and interpolation of the 3-D grids has been one of the main thrusts of my initial work. As mentioned earlier, “real” three-dimensional GPR surveys are not routinely conducted due to the prohibitive costs of antennas. Instead, a series of closely spaced 2-D lines are acquired, (similar to the 3-D acquired at Maax Na in 2003) and interpolated in X, Y or both directions (Figure 5.11).

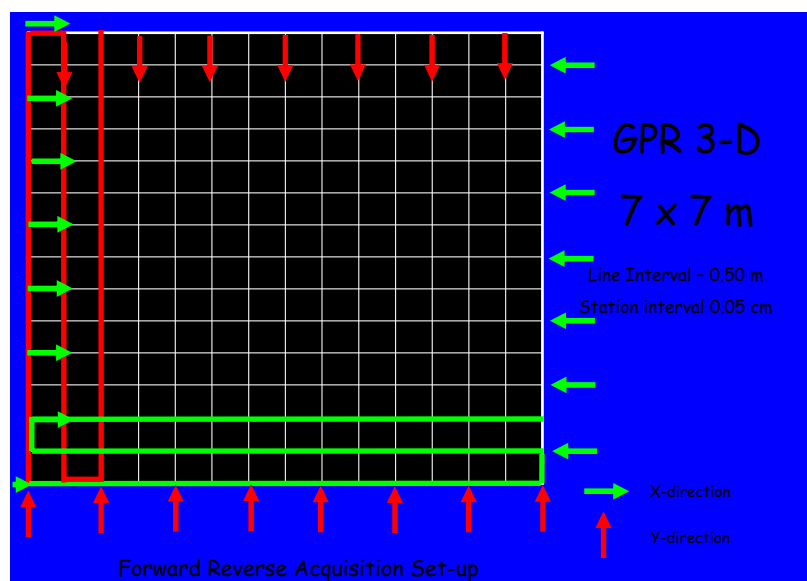


Figure 5.11 Acquisition layout of 3-D grid at Maax Na.

The two orthogonal datasets are often examined separately and compared, as opposed to analyzing the actual summation of the two (See Appendix C). Small variations in the datasets may discourage the merging of the two grids, but doing so ensures an averaging of all the possible GPR data points. Another benefit is that merging X and Y datasets meets the basic condition for migration in that energy sources are directional (Leckebusch, 2003). The interpolation method may range from simple averaging, to linear or square weighting. The software package, ReflexW, is geared for the latter within the “3D-datainterpretation module”. This program generates a 3-D file from 2-D lines using an interpolation scheme for freely distributed lines, or equidistant parallel lines without interpolation. The correct geometry is essential, as well as identical line lengths and trace numbers for each direction.

Chapter Six: INTERPRETATION

6.1 Interpreting GPR lines

The presence of continuous reflectors and changes in amplitude on a GPR record allow inferences to be made on the structure and stratigraphy of the subsurface. Anomalous features recorded on GPR images can be caused by numerous natural, man-made constructions such as the plaza, and acquisition/processing “artifacts”. The ability of the interpreter to differentiate such anomalous events is critical. It has been said that the interpretation of GPR data is even more dependent on the skill and experience of the operator than any other geophysical near-surface method (Gaffney and Gater, 2003). The interpretation process that I have employed with the GPR sections is one which the typical seismic interpreter would use in attempting to interpret seismic data. The first task is to gain an understanding of the rocks and geology in the particular area of interest, hence the first chapter about the near-surface geology and geography of the Maax Na/La Milpa region and sites. Next, the geophysicist would study nearby targets for an analogy to the particular “play” type, or look at any logs available in the area and model the expected seismic response through manipulation of the logs to the geologic scenario. This was accomplished in my research by using typical rock properties in creating a radargram, and acquiring a template line over a cave at La Milpa. The last stage would be to compare the seismic response or synthetic seismogram/radargram to the data (or excavated pit reconstruction) to look for similar features and to determine the correct placement of geologic/archaeological lot horizons. Thus, the interpretation of events in terms of isolating the depth to the various anomalies or features becomes much more accurate.

The first two major events on GPR sections are the airwave and the ground wave. The velocity of the airwave is equivalent to the speed of light in air at 0.30 m/ns. The ground wave is much slower with a velocity of 0.10 m/ns, and consequently arrives after the airwave. Typically the direct airwave will have a positive polarity, while the ground wave polarity is negative (Annan, 2003). It is often difficult to determine time zero due to the small separation, and destructive interference between the two pulses. To filter out the transmitted pulse to reveal shallow subsurface reflectors that may be masked by the transit pulse, a background subtraction spatial filter is recommended (Sensors and Software, 2003). In general, all subsequent events below the ground wave are considered to be subsurface information. The GPR lines acquired at the plaza appear to have imaged 2-3 metres below the surface which, according to the archaeologists, is the limit at which evidence of human habitation has been found at Maax Na. Theoretically, the limits of GPR data resolution requires that objects need to be larger than 0.07 m in order to be resolved using the Noggin.

Our work at Maax Na was focussed on providing archaeologists with a subsurface representation of the plaza based on state-of-the-art geophysical surveying tools. The objectives of this project included identification of the various levels of plaza layering on the GPR records, verification of the slope of the plaza to determine whether water drained away from the various structures to strategically placed reservoirs to the south-west, and the differentiation of natural formations versus man-made structures.

With the number of lines we have acquired over the past four field seasons, and the 2-D line and 3-D grid orientations across the plaza, I believe we are now in a position to address some of these queries.

Utilizing the ReflexW standard processing flow and software has resulted in interpretable images of the plaza. Reprocessing all of the GPR lines with the same processing software package, allows us to compare “apples to apples” despite different acquisition environments, and different vintages.

6.2 2-D lines crossing plaza

Three common lines have been surveyed and re-acquired across the main upper plaza over the various field seasons. The main reason was to extend the lines further to the east and to verify features which had been flagged after further processing back at the university. Most of the lines were shot consecutively, in the same position, but in forward and reverse directions as displayed in Figure 6.1.

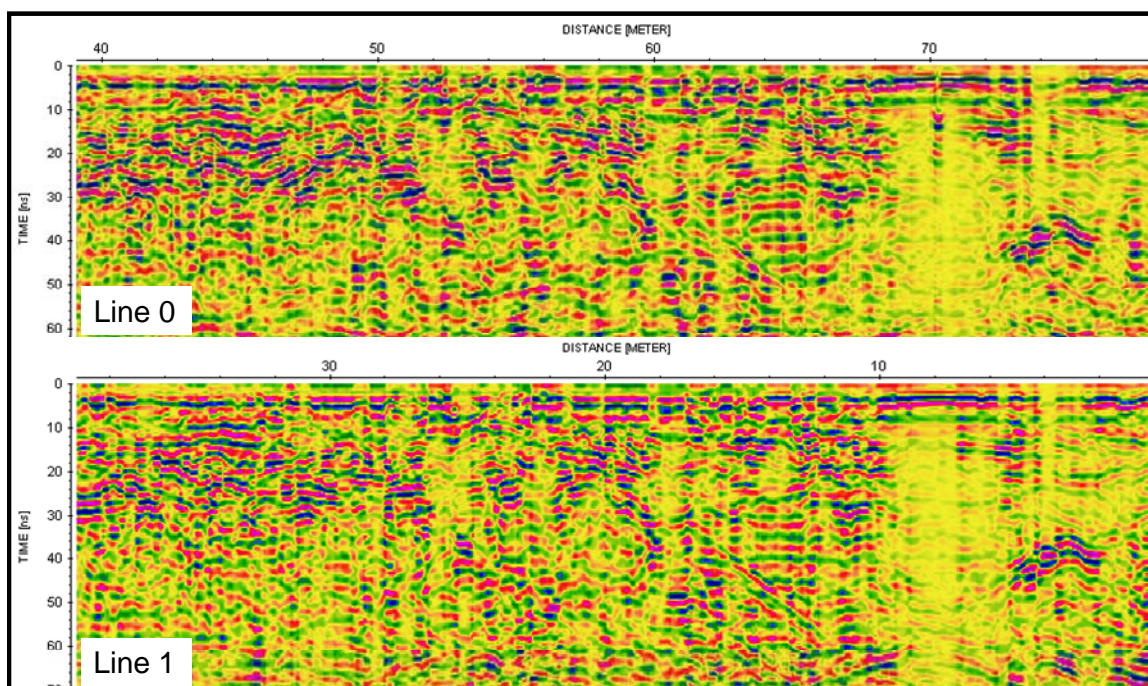


Figure 6.1 Comparison of GPR data acquired the same day in opposite directions.

The data shows similar features such as the anticline at ~ 74 metres (Line 0) and ~ 4 metres (Line 1), a steeply dipping linear event at ~ 64 metres on Line 0 versus ~ 14

metres on Line 1, and the significant dim zone at ~70 metres and ~ 8 metres, respectively, on each of the sections.

Figure 6.2 demonstrates a plausible interpretation of Line 4, acquired in May 2008, across the Plaza A at Maax Na. The GPR line images the multiple plaza levels and what I suspect is the top of the bedrock. At Maax Na, present day plaza levels can often overlie other levels of plaza, tombs, caches and even drainage systems (Shaw, pers. comm., 2003). Thus, when interpreting the sections, key elements to look for are:

- the presence of discontinuities in the data; anticlinal, synclinal or dipping events;
- apparent amplitude variations which may be indicative of structural and stratigraphic features;
- known archaeological features such as caves, walls, pits, or structures.

Buried objects are identified by the presence of point diffractors, which result in flattened hyperbolic patterns of energy when migrated. The surrounding material is often disturbed and the continuity of the geological layering is compromised.

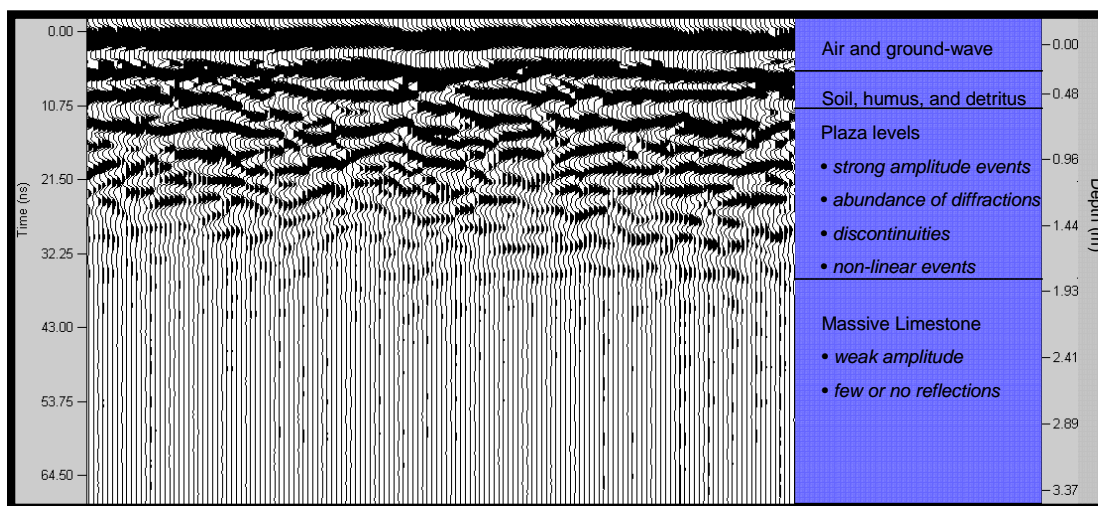


Figure 6.2 Interpretation of Line 4 across the Plaza A at Maax Na.

A number of features such as discontinuities, structural features, minor faults or fractures, and other anomalies can be discerned on this section and others at Maax Na. I interpret the large number of strong amplitude diffractions as emanating from the different layering of the plaza lots. An absence of reflections and weaker amplitudes corresponds to limestone bedrock. The amplitude of the pulse is not only decreasing with depth but loses significant energy with transmission through the karsted limestone. Several years ago I assumed this problem was a gain issue and attempted to resolve it through the application of a Q-filter. In this instance, however, I now believe that there is geological justification. The homogeneous nature of the limestone and lack of layering within this massive bedrock provides little opportunity for dielectric property changes and as a result shows little or no reflectivity. Strong events within the bedrock may be associated with possible caves or voids below the surface.

Areas of poor data from the top to the bottom are due to surface issues, namely the presence of tree debris, roots and rocks, causing instrument decoupling with the ground.

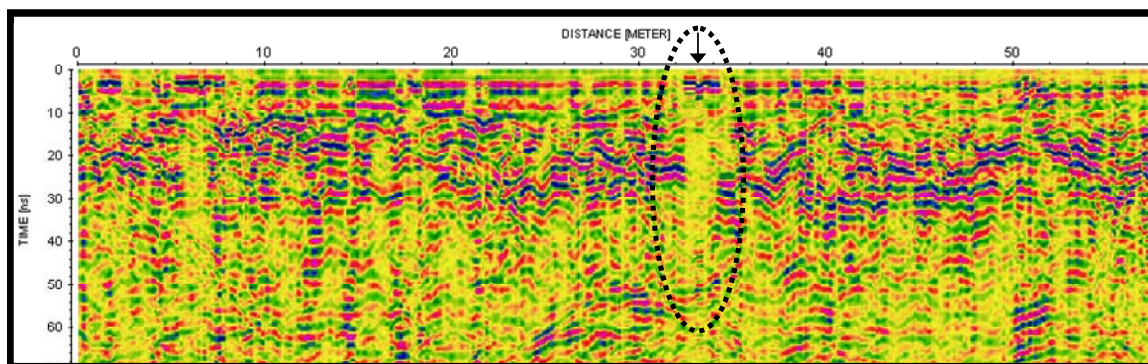


Figure 6.3 Line 6 showing the effect of surface debris on data quality of GPR lines.

A number of times, we were forced to lift the Noggin Smart-cart unit over rocks or logs along the surface, which, of course, led to a poor connection between the antennas and the surface. As we acquired the data, we documented such occurrences with the intention

of checking to see if it degraded the quality of the GPR records. For example, a mound of stones was encountered at 32.25 metres along Line 6, as shown in Figure 6.3. Note the disjointed and strong initial trough-peak-trough, and the dimming of the events below. This is evident on a number of lines at Maax Na due to the uneven and littered ground surface. A list of anomalies observed on the survey lines to date is found in Table 6.1

Table 6.1 Catalogue of anomalies observed at Maax Na.

List of Anomalies observed on the GPR lines					
Year Acquired	Project	Lines	Distance(m)	Time (ns)	Interpretation
2002	2	1	33-36	34-48	dimming throughout traces with strong dipping event
2002	5	1	13-16	34-48	dimming throughout traces with strong dipping event
2003		1	30-34	50-62	strong event cut off by zero traces
			55-57		
2003		3	33-38	50-58	weak diffraction feature?
2004	5	1	8.0-14.0	62-72	small sloping event
			106-110	40-50	collapse feature?
	5	2	11.0-18.0	40-60	dipping event
			54-60	65-78	dipping event
			86-88	30-50	collapse, fractures?
			90-116	60-78	weak diffraction feature?
2004	5	3	7.6-8.2	whole trace	weak signal at surface; strong event at 20 ns; altar
2004	5	4	3.0-4.0	whole trace	altar
2004	5	5	8-8.6	whole trace	altar
2004	5	7	3.9-4.7	whole trace	altar
2004	5	8	0.8-1.7	whole trace	altar
2004	5	9	17-30	50-70	strong diffraction event; best anomaly; similar to cave feature at La Milpa?
			9.5-12.5	72-80	strong event
2004	5	10	22-30	50-80	diffraction?
			37-39	70-80	strong amplitude event
2004	5	11	40-50	70-80	strong amplitude deep event
2004	5	12	10.0-18.0	70-80	possible diffraction?
2004	5	13	33-38	60-80	possible diffraction?
2004	5	14	0-4	70-80	more pronounced than previous line; cave feature?
2004	6	0	54-65	60-80	diffraction?
			37-105	50-80	weak sloping event and diffraction?
2004	6	1	57-68	60-80	weak diffraction?
2004		2	11.0-19.0	40-60	collapse feature?
			54-68	60-80	strong amplitude deep event
			100-102	60-70	weak dipping event
2008		0	66-74	whole trace	dimming throughout trace; dipping event at base
2008		1	6.0-12.0	whole trace	dimming throughout trace; dipping event at base
		2	4.0-28.0	40-80	series of strong dipping events; possible plaza collapse?
			46-54	60-70	diffraction?
			162-165	55-70	small dipping event
		3	32-34	60-70	strong but small dipping event
			140-150	50-70	strong event
			17-195	40-80	series of strong dipping events; possible plaza collapse?
		6	24-32	50-70	fair diffraction feature?
			85-90	32-45	strong discontinuous event
		7	20-24	60-70	strong event
			24-32	30-50	strong discontinuous event
			78-88	45-80	fair diffraction anomaly
		8	29-31	whole trace	dimming with strong event at 15-30 ns
			40-50	75-88	strong series of events-possible diffraction?
		9	0-10	70-88	diffraction feature
			20-23	whole trace	dimming with strong event at 15-30 ns
		10	29-31	whole trace	dimming with strong event at 15-30 ns
			40-50	75-88	diffraction feature

6.3 2-D lines across altar

During our visit to Belize in 2004, the archaeologists were interested in what they believed to be a ceremonial altar on the plaza surface. A number of 2-D lines and a 3-D GPR survey were acquired across the surface feature. Figure 6.4 is a picture of the altar,

and is recognized by the archaeologists as the placement of stones around a central depression.



Figure 6.4 Altar near ball court at Maax Na (photo courtesy of R. Stewart).

A 25 m² 3-D survey was acquired across the depression, with trace increments at 0.05 m and line separation set at 0.50 m. Lines were shot in both the X and Y directions for a total of 20 lines. Stones were left in place until the archaeologists had the opportunity to excavate the altar. As a result, data collection proved to be challenging as it required lifting the GPR instrument across the stones thereby affecting coupling with the ground surface. The quality of the 3-D, however, was remarkably good (Figure 6.5).

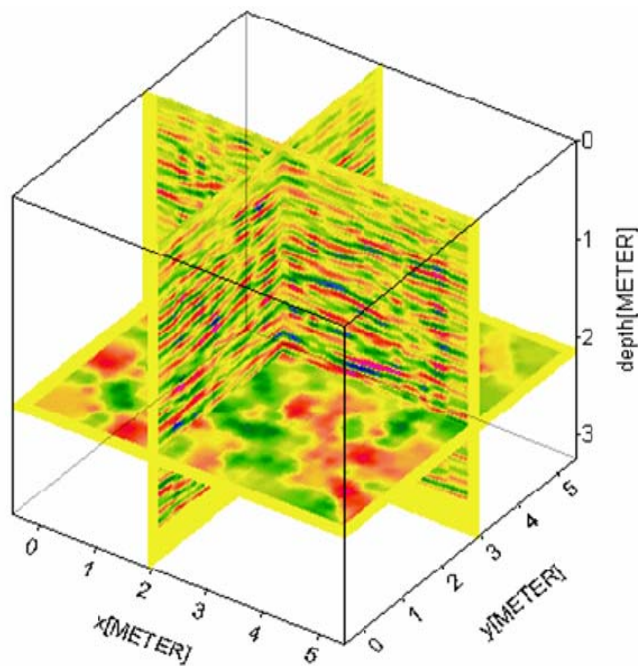


Figure 6.5 An X-cut, Y-cut and time slice from a 3-D across the altar at Maax Na.

Fig. 6.6 is a GPR 3-D image of the subsurface across the altar as outlined by the dashed oval. This particular time slice shows a strong amplitude event present at the apex of the diffraction seen on the 3-D lines.

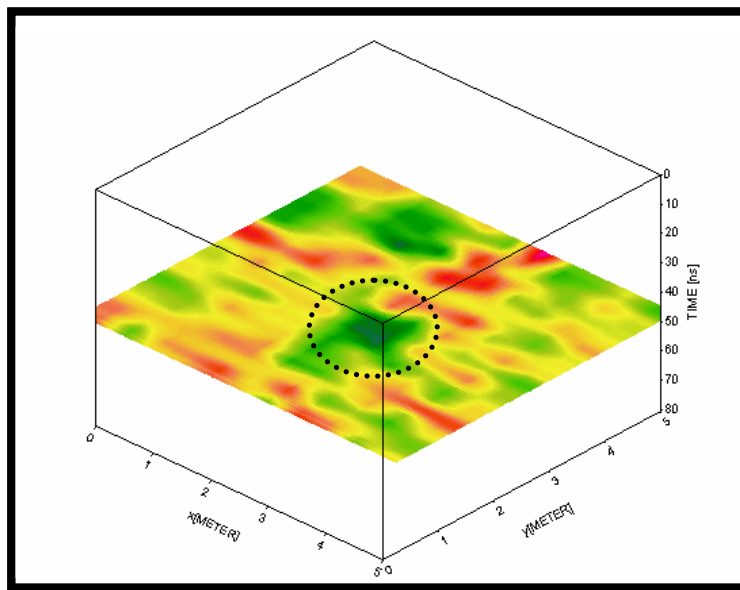


Figure 6.6 Time slice of 3-D across the altar.

An example of one of the lines from the 3-D, Line 4, acquired in the x-direction across the altar area, is nicely imaged in Figure 6.7. A strong amplitude event occurs in that vicinity at 8-16 ns, preceded by a discontinuity at the surface possibly due to the depression, as outlined by the dashed oval. A number of dipping events, possibly small fractures and shadow zones can also be observed.

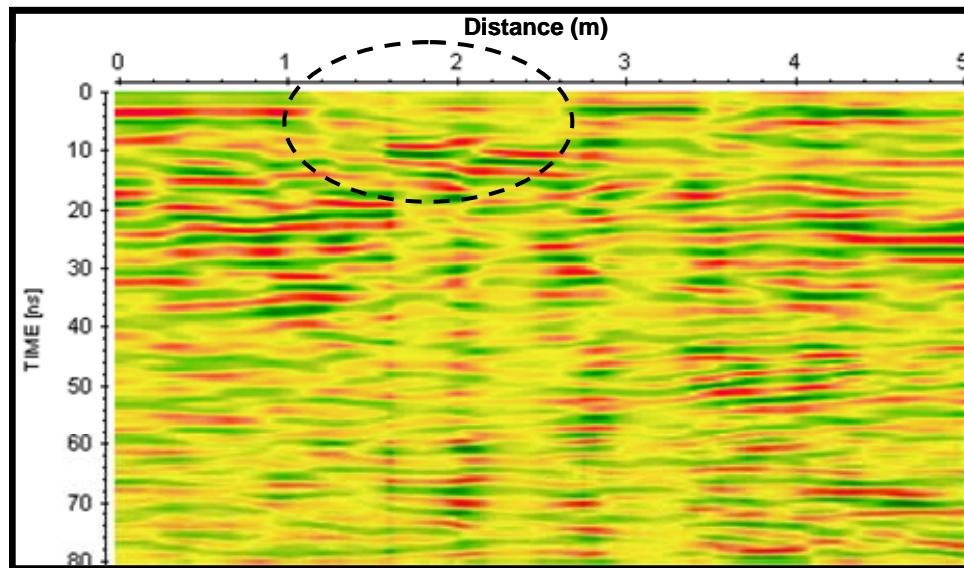


Figure 6.7 3-D GPR Line 4 across the altar.

Figure 6.8 is another 3-D line acquired across the altar but the interesting feature here is not the altar anomaly itself, but the presence of a strong wide-aperture dipping event deeper in the section that is very similar to the GPR template response encountered over the cave at La Milpa.

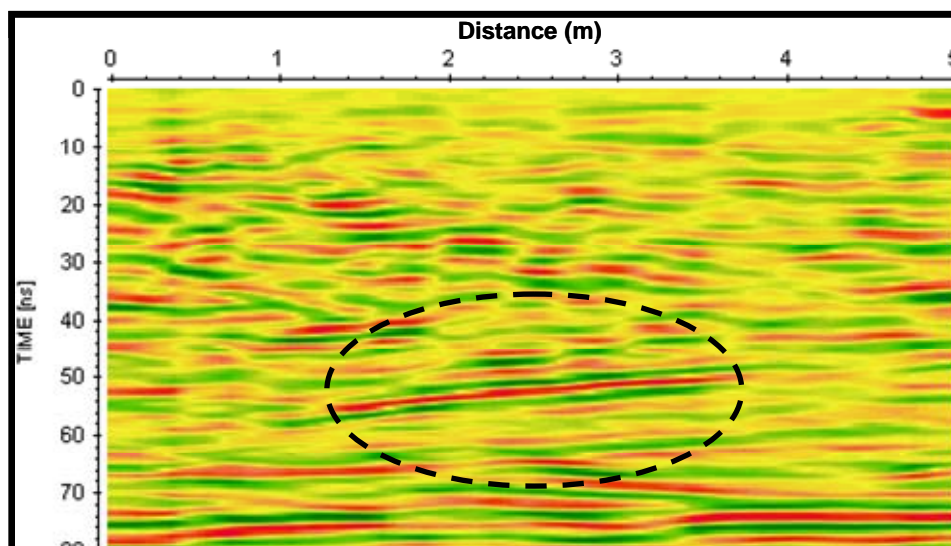


Figure 6.8 3-D GPR line across altar showing diffraction.

This event occurs between 48-56 ns, which equates to a depth of between 1.7 to 2.0 m, assuming an average radar velocity of 0.072 m/ns. A similar feature is present on a 2-D line acquired further to the south passing the ball court. The altar was excavated in 2004 but to a depth of 1.3 m only. This event appears to be almost half a metre deeper.

The anomaly could be caused by one of several things: a metal rod or surface feature, a buried structural feature, one of the diffraction tails from a cave, or a multiple. I attempted curve fitting the diffraction, and determined it was a velocity less than the speed of light (0.3 m/ns), making it unlikely to be a rod or metal object on the surface.

Airwave events caused by surface features such as these should theoretically travel close to the velocity of air (Annan, 2003). Multiples are more complex ray paths. They are generally reflections from one or more interfaces, and tend to arrive after the primary signals but at a predictable lag. Since there are no shallow events with a similar dip at earlier times, I would discount multiple energy. With two similar GPR responses in a relatively small area, I suspect that this anomaly may be some kind of diffracted energy

from the top of a void or cavernous feature, possibly connected. Another fascinating observation to note is that a change in the inclination of the plaza surface appears to occur at the vicinity of the altar too.

6.4 The Caves at Maax Na

Several caves have been discovered at Maax Na, and one notably was recently excavated as part of a grant from the National Geographic Society. This surface cave was located just east of Plaza A. Another two were discovered below the surface, south of Plaza A, and were part of the GPR surveying completed in 2002. Caves, with their evidence of Maya ceremonies and ritual offerings, were considered to be just as sacred as the temples overshadowing the plazas (Awe, 2007). The Maya appeared to have made extensive use of subterranean caverns and archaeologists have discovered many prehistoric remains, including ceramic artifacts, stone tools, architectural modifications, and cave art (Awe, 2007). An example of Maya ceramics (left) and an underground cave at Ma ax Na (right) are shown in Figure 6.9.



Figure 6.9 Maya pottery (www.parkerlab.bio.uci.edu), and Dr. Claire Allum in a cave at Maax Na (photo courtesy of R. Stewart).

In 2002, two known caves off the main plaza at Maax Na were surveyed. The lines were not acquired directly over the cave but a few metres off to the side. The near-surface consisted of humus and soil overlying homogeneous massive limestone, with no evidence of the typical plaza construction. Previous interpretation of these lines characterised the caves as areas with low amplitude and poor reflectivity, but after templating the cave at La Milpa, it is my opinion that the caves may be present but are not well imaged on this particular line. There appears to be a possible broad diffraction at 50-65 ns (dotted lines), suggesting a possible cave, with a fairly strong flat event at 30 ns (red arrow). The line contains areas of poor data too, which I attribute to inadequate surface coupling.

Figure 6.10 shows the GPR section acquired adjacent to the caves.

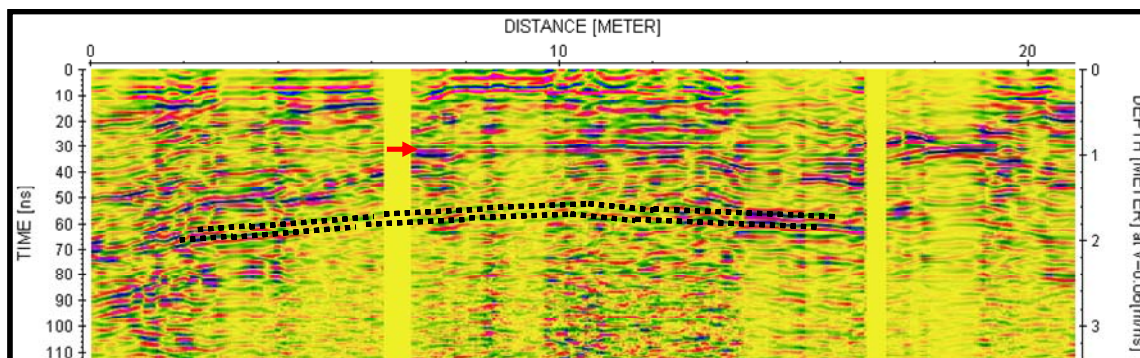


Figure 6.10 GPR Line adjacent to caves at Maax Na.

During our most recent visit to Maax Na in 2008, one of the archaeologists asked us to look at a ramp feature connected to the north structure, to ascertain whether it was natural or man-made. We attempted to acquire data across the ramp and a line perpendicular to the ramp, necessitating running the line from the top of the north hill to the plaza surface. At the top of the structure, we discovered a previously unknown cave. The cave was visible as a collapsed lenticular feature at the side of the hill, with a hole at the top which bore evidence of some modification. The cave was identical to the cave that was

currently being excavated at the site and has been flagged for excavation in 2009.

According to the interpretation of the GPR lines across the ramp, there appear to be strong amplitude, and continuous reflections similar to the GPR signature of the plaza. As a result, I believe that the ramp was constructed by the Maya.

6.5 2003 3-D grid and excavated pit

Two 3-D grids were acquired in 2003, one of which was associated with a 3-D micro-seismic survey. A pit was also excavated within the grid to provide some geologic ground truthing to the GPR records. The following figure represents the merging of the X and Y lines, and shows good data quality, continuity and amplitudes.

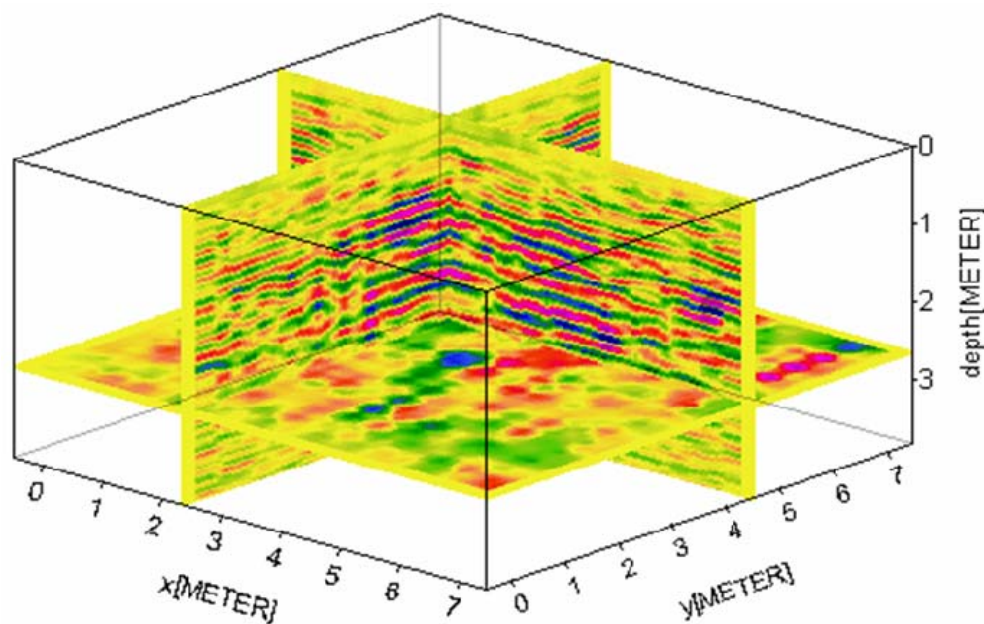


Figure 6.11 An X-cut, Y-cut and time slice of the 2003 3-D acquired at Maax Na.

The archaeologists, excavated a two metre north to south by one metre east to west pit in order to explain the plaza layering style implemented by the Maya. Figure 6.12 illustrates the tiered nature of the cobbled layers and plaster as pointed out by Dr. Eleanor King.



Figure 6.12 Dr. King explaining the plaza layering (photo courtesy of R. Stewart).

According to the archaeologists, there appear to be seven stages of plaza development.

With each new construction, the plaza was refurbished, or another layer added. Figure 6.13 illustrates the composition of the plaza, and the tie to the GPR data and radargram.

The correlation of the pit information with the GPR record validates that there is a noticeable change in amplitude at the base of the plaza layering and top of the bedrock.

The plaza layers are imaged as strong horizontal events. The GPR radargram shows good correlation with the GPR data.

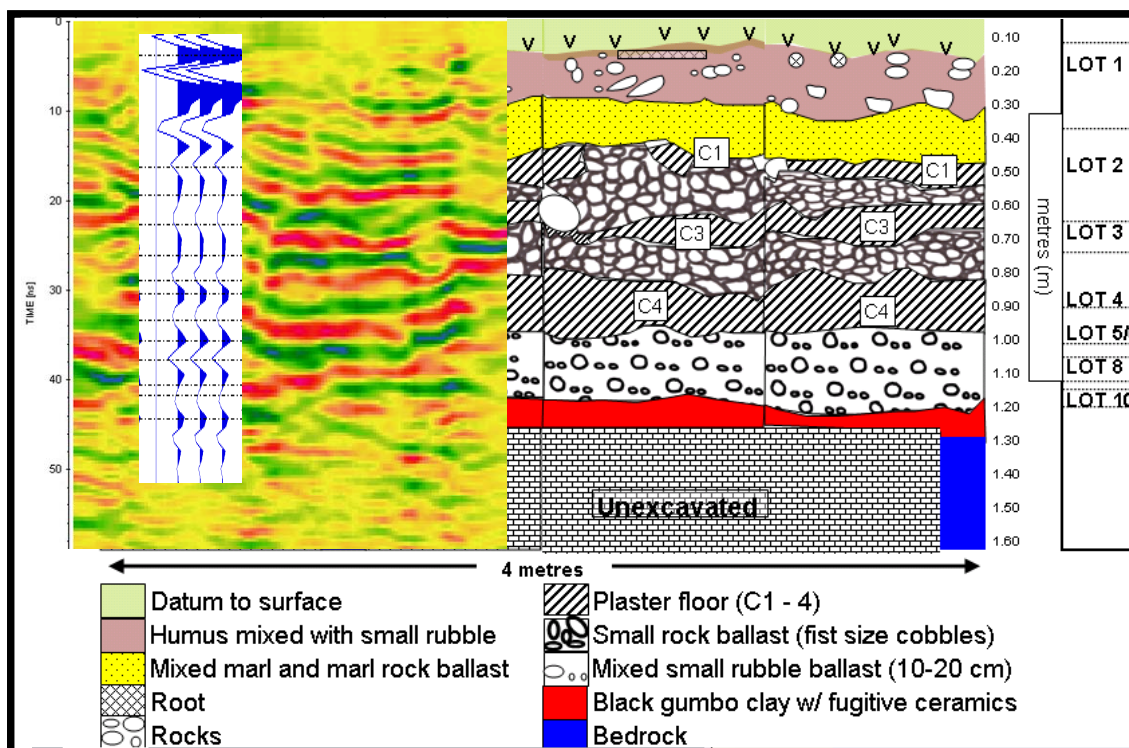


Figure 6.13 Schematic of excavated pit, GPR record and radargram.

6.6 Schematic of second pit and correlation with GPR data

One of the most significant anomalies that we encountered in our early visits to the site, namely a structural anomaly present on a 2-D line acquired in 2003, was highlighted for excavation as shown in Figure 6.14.

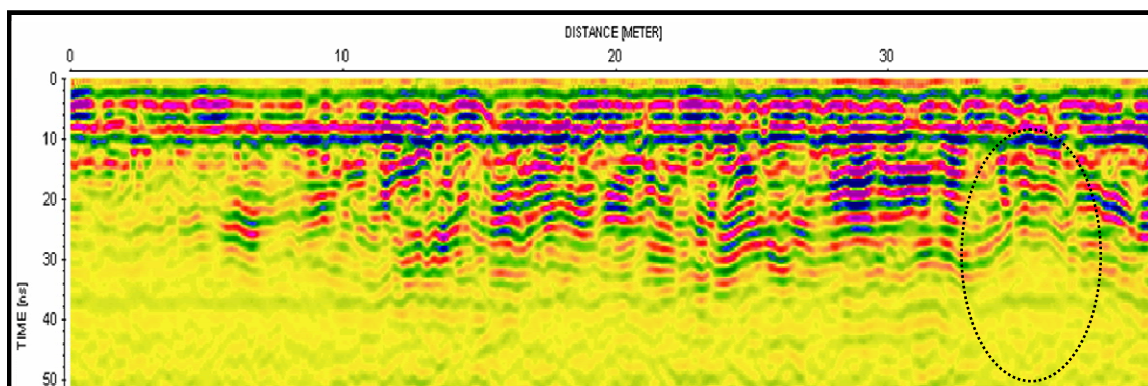


Figure 6.14 GPR Line showing anticlinal feature which was excavated.

The archaeologists did indeed excavate the site but found no evidence of buried artifacts.

A detailed geologic description of the pit is shown in Figure 6.15. According to the archaeologists, the anomaly turned out to be a thick wedge of plaza reconstruction, with large boulders, more air space and burnt plaster present in this area, unique to anything noted before (PfBAP, 2005). This additional wedge must have been at a higher radar velocity than the surrounding material causing a velocity pull-up in the data.

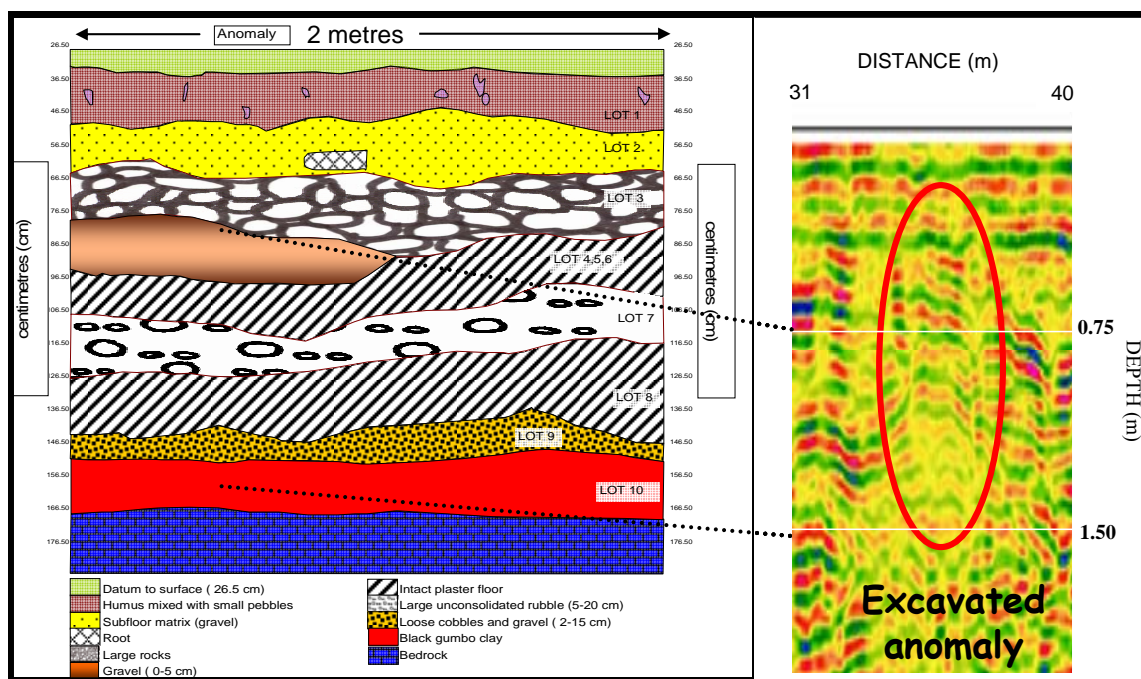


Figure 6.15 Schematic of the excavated pit (reproduced from the work of E. King, pers. comm., 2005).

6.7 Mapping of bedrock based on the GPR interpretation

Due to the fact we felt that we could identify the end of the plaza layering and the top of the bedrock, I attempted to interpret this ‘horizon’ on several of the 3-D lines. Figure 6.16 shows the picked surface identified by the separation of high amplitude horizontal events, which we attribute to plaza layering, to low amplitude and less coherent data.

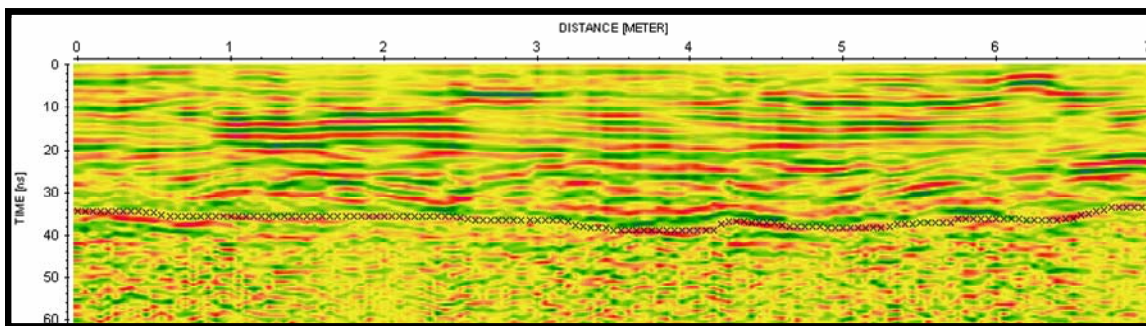


Figure 6.16 3-D line showing the pick values for the base of the plaza layering.

To create a surface map of the top of the bedrock, the base of the plaza layering (mnbopl2) horizon was picked on all the X lines from the 2003 3-D grid. The correct geometry of each of the lines was also required. Figure 6.17 represents the horizon map of the top of the limestone bedrock or base of the plaza layering. The interpretation shows dipping of the bedrock to the east with a small number of linear trending highs. The 3-D only covers a 7 by 7 m area, and this may only represent localized highs within the bedrock surface. Additional interpretation on all of the 2-D and 3-D lines is necessary to give a more realistic and complete picture.

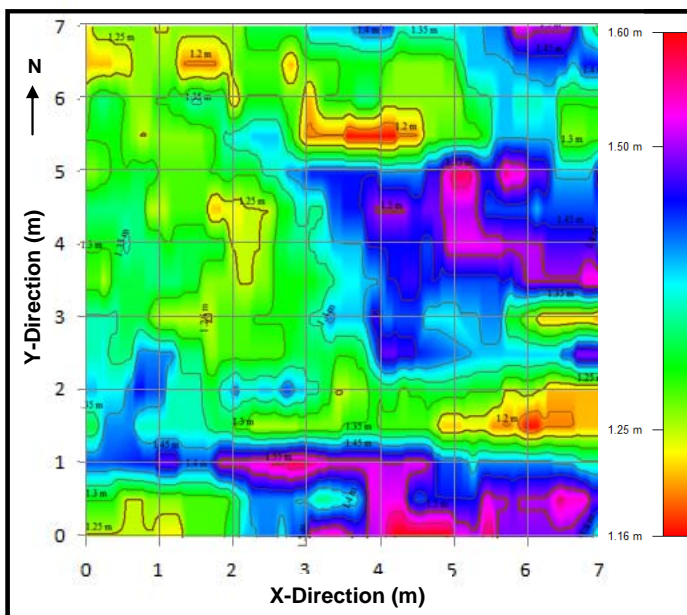


Figure 6.17 Mapped surface of the top of the bedrock.

6.8 Rebar experiment

During the 2003 field season, a length of rebar was pounded into the side of an excavated pit at a depth of 0.74 m. Our intention was two-fold; to determine an accurate velocity reading of the subsurface at that point, and to test the accuracy of depth determination. The rebar is made of corrugated steel and results in a strong diffraction pattern emanating from the apex of the bar as recorded in Figure 6.18. The GPR image was created in EKKO View, with an AGC gain applied. This program allows for calibration of the radar velocity by allowing one to compare different hyperbolas based on their associated velocities. As shown, the radar velocity of 0.119 m/ns best fits the diffraction pattern emanating from the rebar. Note the intersection of the asymptotes of the diffraction is not at time zero but time-shifted by approximately 9 ns.

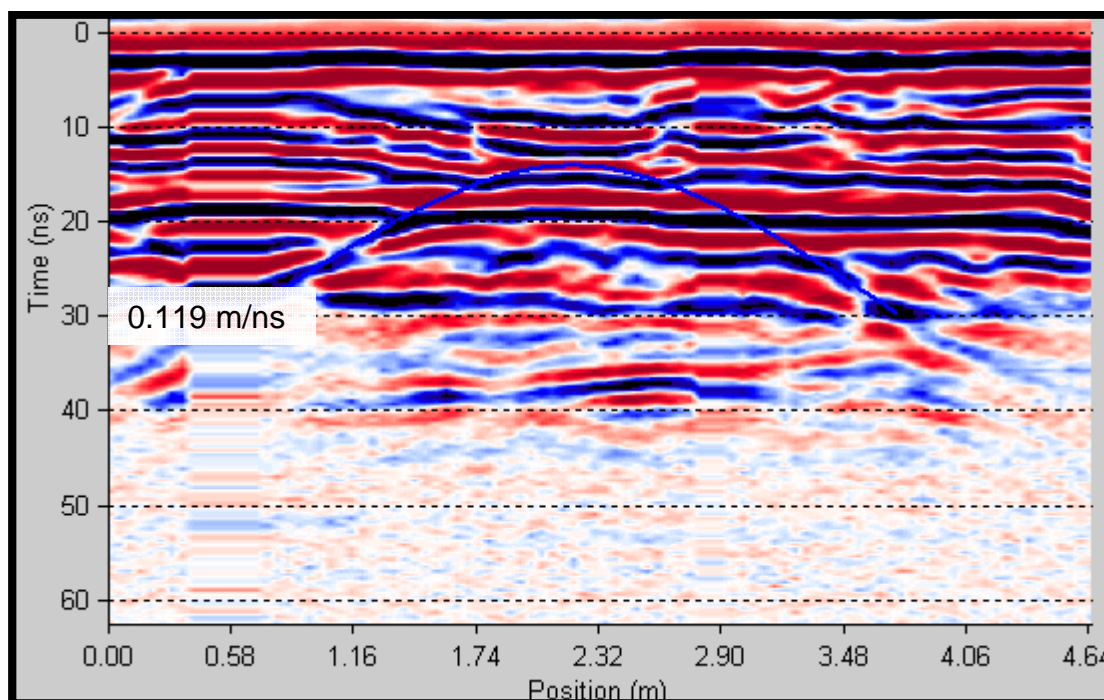


Figure 6.18 Diffraction from rebar line at Maax Na (Note repeated traces at left).

A series of eight GPR lines were acquired across the rebar ranging from 4.65 to 6.35 m in length. Curve fitting to the resulting diffraction hyperbolas determined the radar velocity as again ranging from 0.119 – 0.140 m/ns. Depth to the rebar was calculated at 0.74 to 0.88 m. These velocities proved to be higher than any measured previously, and represent a very dry subsurface environment.

The diffraction tails from the rebar were not symmetric in terms of energy distribution but were better imaged on one side than the other. Interestingly, we observed this was consistent with survey direction (Figure 6.19).

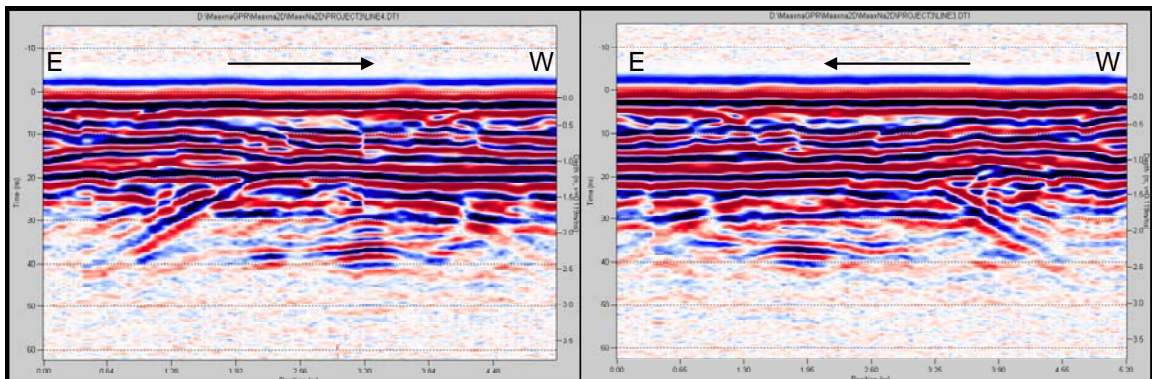


Figure 6.19 Difference in diffraction tails with survey direction.

The diffraction tail away from the survey direction was consistently stronger in amplitude, and was more continuous. This may be the result of the change in the radiation patterns of the antennas when moving from a positive polarity to that of a negative polarity, across an iron-bearing (magnetic) object. Since the influence of the Earth's magnetic field is strongest near the equator, and the fact the rebar was oriented north to south, parallel to the transmitter and receiver antennas, it follows that an induced magnetic field might interfere with the transmitter and receiver radiation patterns and cause destructive interference in the GPR data (Bancroft, 2008, pers. comm.). Another

possible explanation is that the antennas act like headlights. An object is best detected or imaged on approach and directly above, as opposed to having moved beyond and further away from it. This observation warrants more investigation, as this diffraction response is unusual. Future work might include using a brass rod instead of the rebar, or increasing or decreasing the speed of data collection.

6.9 Interpretation of CMP Analysis

The common-mid-point survey at Maax Na was very rushed due to limited time at the site. Unfortunately, we only acquired 5.5 m of data at 0.5 m intervals, equating to only twelve traces. As a result, the quality of the CMP is poor and only a limited number and extent of reflections are present. Figure 6.20 represents a CMP analysis displaying three panels. Panel a is a one dimensional velocity model of the near-surface based on the time and velocity of the interpreted reflections. The center panel, b, is the common-midpoint stack in which hyperbolas with their associated velocities are matched to the GPR data. Panel c is a 2-D color semblance plot which measures the coherence of the data to time and velocity pairs. The interpretation of the reflections verifies measured field velocities in the range of 0.90 to 1.20 m/ns. Note radar velocities are decreasing with depth.

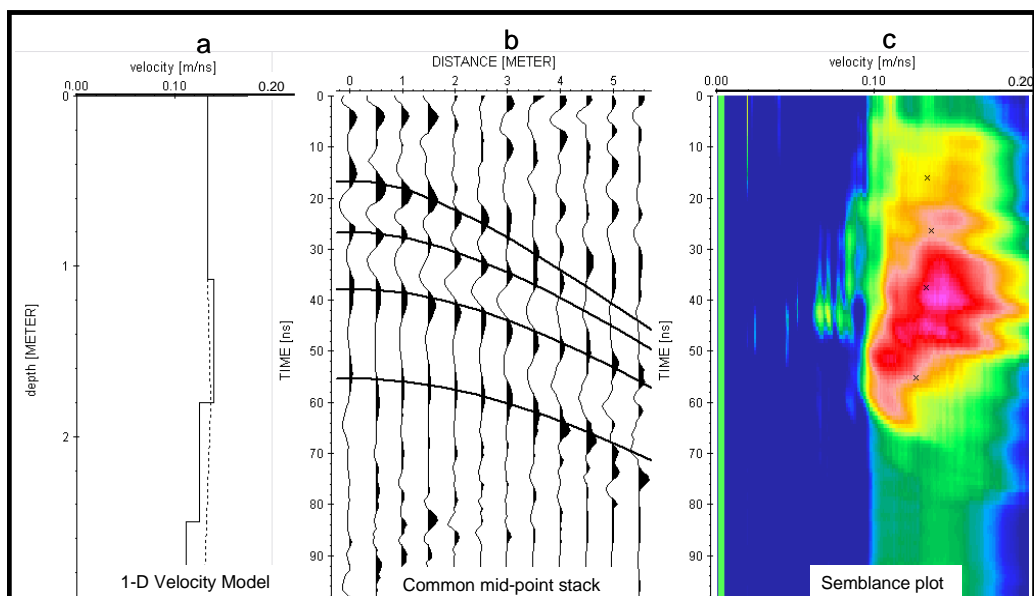


Figure 6.20 CMP analysis of data from Maax Na.

6.10 Interpretation of the Total Station Survey Data

Surveying the plaza with the Total Station instrument allows one to determine the correct positioning and elevation of the GPR lines based on existing archaeological turning points. Identification of the exact location of an anomalous feature aids the archaeologist in excavation planning. Identifying changes in the elevation readings across the plaza may provide the archaeologists with information on Maya construction. The resultant topographical map of the plaza at Maax Na was featured in Figure 3.6. This map represents two surveys conducted in 2004 and 2008 across the plaza and at the base of a pyramid, which necessitated some corrections to tie the two vintages to archaeological markers. Assessing the elevation and coordinates of the GPR lines individually, however, highlights some interesting features (Figures 6.21 - 6.25).

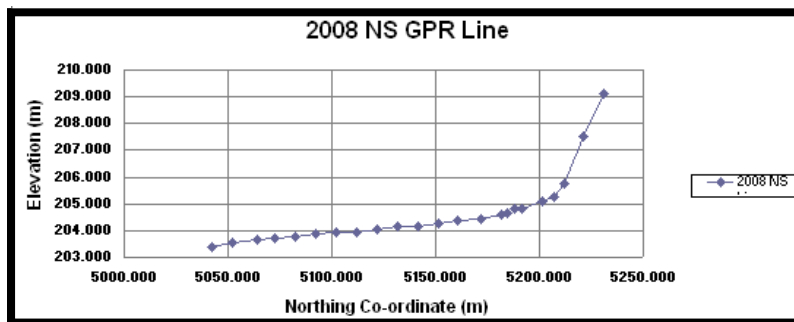


Figure 6.21 Charting of the elevation coordinates for 2008 N-S GPR Line.

Lines 2 and 3, acquired in 2008, were shot in a north to south orientation across the plaza surface and up towards the north structure. The elevation shows a strong dip to the south and a rapid climb in elevation to the north as we approached the hill. Note how smooth the incline appears.

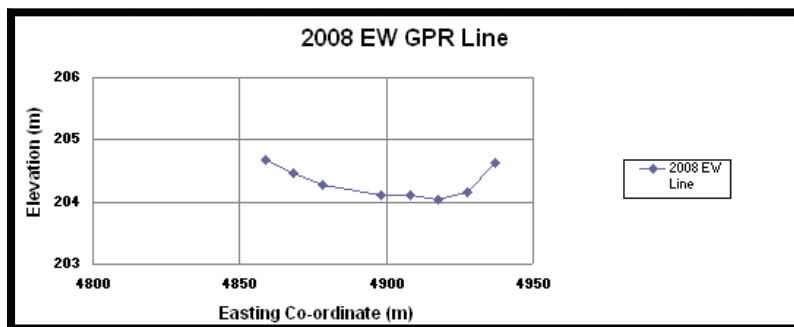


Figure 6.22 Charting of the elevation coordinates for 2008 E-W GPR Line.

Lines 0 and 1, acquired in 2008, were shot east to west and vice versa. A strong dip to the east is apparent, with a climb in elevation toward an eastern structure within which a Maya cave was being excavated during the recent field season.

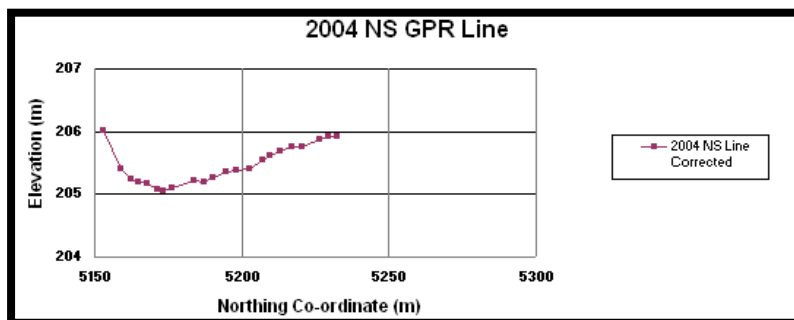


Figure 6.23 Charting of the elevation coordinates for 2004 N-S GPR Line 2.

The elevation profile for Line 2, acquired in 2004, verifies the strong slope of the plaza to the south and a rapid elevation increase when one approaches a structure.

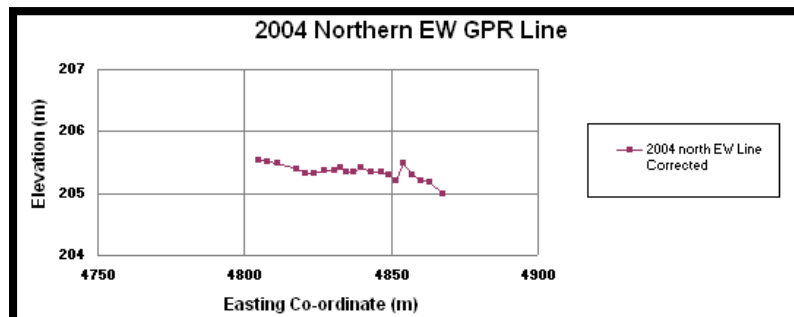


Figure 6.24 Charting of the elevation coordinates for 2004 Northern E-W GPR Line.

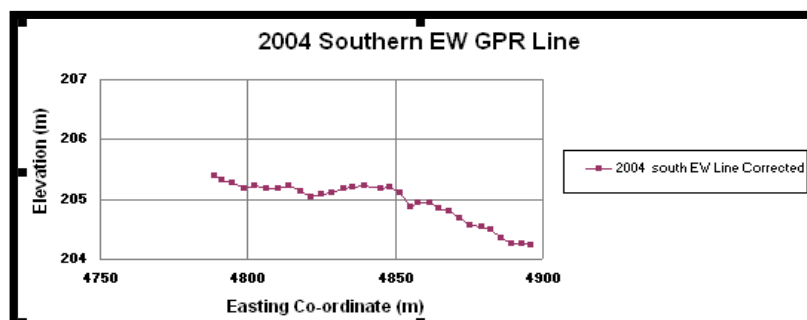


Figure 6.25 Charting of the elevation coordinates of the 2004 southern E-W Line.

Figures 6.24 and 6.25 represent the graphing of the topographic coordinates of Lines 1 and 3 acquired in 2004. These lines were shot at the western side of the plaza and show a gradual sloping to the east, with an abrupt change in the slope for both lines in the area of the ball courts and altar.

A hand contoured map of the plaza using only the elevation data from the Total Station survey and pertinent archaeological turning points is displayed in Figure 6.26. A series of arrows outline the slope direction of the plaza to the south and west of the site (See Figure 3.6). Flow direction is the result of the inclination of the plaza surface and the fact the plaza is bounded by elevated pyramids and structures. From the north-west end of the

plaza, it shows a south-west to south-east flow direction. Mapping also indicates a subtle incline to the south of the western plaza, and a dramatic low to the south east.

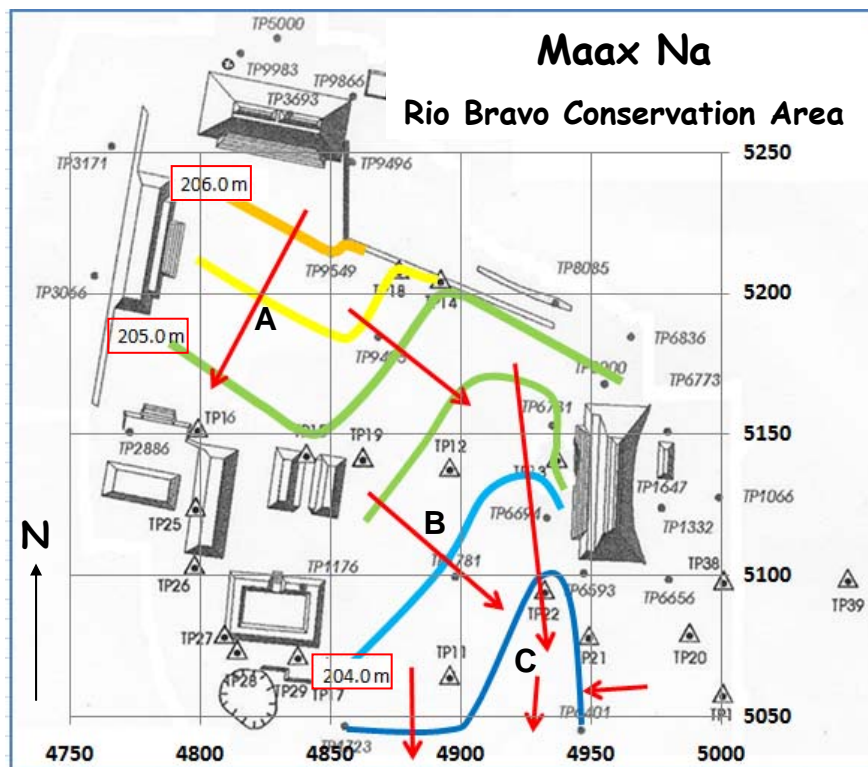


Figure 6.26 Elevation contour map and likely flow direction of rainwater.

One of the most significant accomplishments of the Maya is the incredible engineering involved in the construction of the plaza surface. Not only is there a definite inclination, but the surface is largely planar. The plaza was sloped in such a way as to direct any rain water away from the structures, into strategically positioned reservoirs to the south-west, and possibly to the east prior to abandonment of the site (Shaw, 2008, pers. comm.).

These reservoirs contained sufficient water to last throughout the dry season (Coe, 2001). Based on an elevation increase of 1 m over a distance of 75 m, the inclination of the north plaza (A) is calculated to be 0.76 degrees. The slopes of the south-eastern parts of the

plaza increase to 1.3 degrees (B) and 2.1 degrees (C) respectively. These slope calculations are based on the present surface topography and may not have reflected the slope during Maya construction. Local subsistence may have occurred during the last millennium as illustrated in the mapped surface of the bedrock (Figure 6.17), and as indicated by small fractures and discontinuities in the GPR plaza data. Tectonic activity in the area is unlikely due to the fact the structures are intact.

Chapter Seven: THE MAYA RUIN SITE OF LA MILPA

7.1 GPR 3-D template over known cave

In March of 2008, we had the opportunity to visit the Maya archaeological site of La Milpa. La Milpa is also part of the Programme for Belize, within the Rio Bravo Conservation area, and is six miles from Maax Na (Figure 7.1).

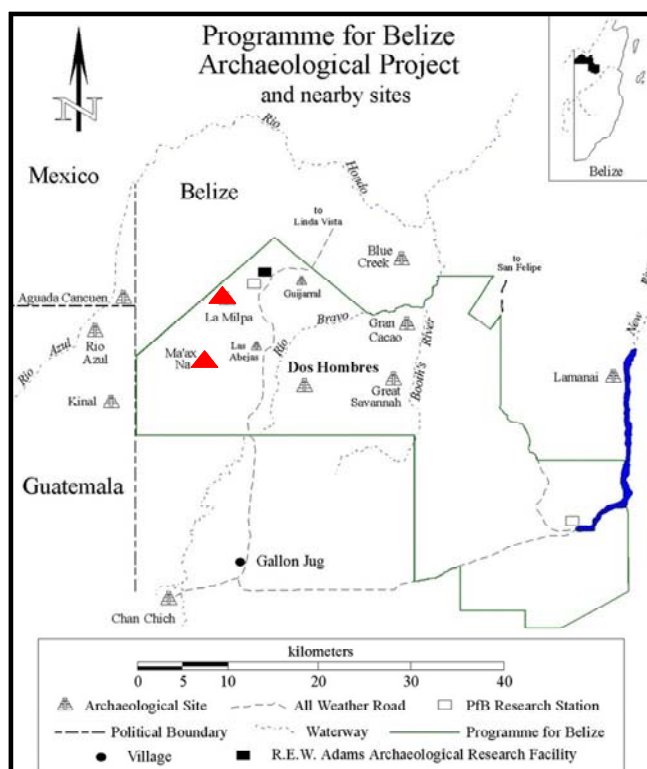


Figure 7.1 Location of La Milpa in northern Belize (MARL).

La Milpa is an ideal site to conduct GPR surveys because the plaza area is cleared of tree trunks, roots and debris. Another advantage is the existence of two known caves or chultunes beneath the plaza surface. Thus, a three dimensional GPR template was acquired across the cave to obtain the characteristic image of a subterranean cavity. A total station survey was also carried out. Figure 7.2 outlines the layout of Plaza A, a

topographical map, and the location of our 3-D grid at the archaeological site of La Milpa. The inclination of the plaza to the southeast is indicated by red arrows.

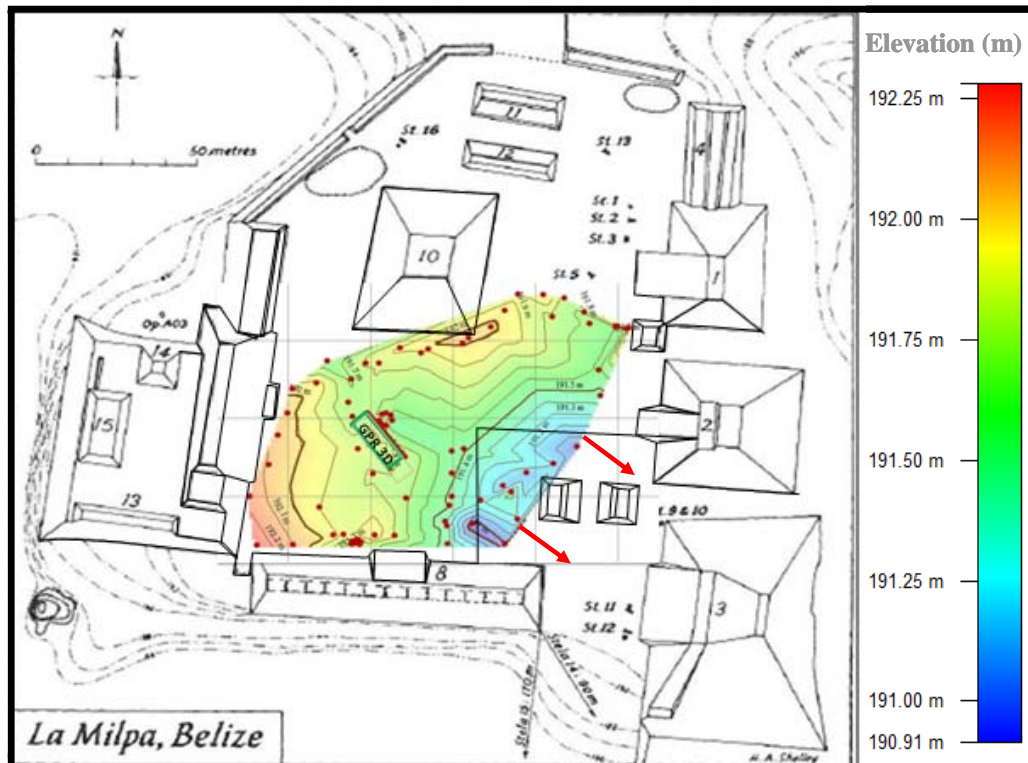


Figure 7.2 Topographic map of Plaza A at La Milpa, outlining the 3-D GPR survey across chultune (reproduced from Tourtellot et al. 1993).

Figure 7.3 is a photo of the cave and the placement of the GPR 3-D survey.



Figure 7.3 La Milpa plaza with 3-D grid and cave (photos courtesy of B. Cameron).

The cave is fairly extensive, with its entrance about 5 metres in diameter and the depth at approximately 1.7 metres below the surface. The grid encompassed an area of 18 metres x 6 metres across the plaza. Each of the lines was 0.25 m apart and was collected in orthogonal x and y directions.

The 3-D grid composed of a series of closely spaced lines using the Noggin 250 MHz Smart-Cart antenna unit. Velocities at the site were determined from curve fitting to point diffractors and with a CMP survey shot within the grid employing the Pulse Ekko 100 MHz antenna. The data acquisition consisted of 24 x-lines shot from the south-east corner of the grid at a length of 18 metres. Seventy two orthogonal lines were acquired in the y-direction at a length of 6 metres each. Parameters included a line interval of 0.25 m, a trace interval set at 0.05 m and a temporal sampling of 0.4 ns.

The first set of lines acquired in the x-direction contained a large number of skipped traces which I believe was due to the fact that data collection was too fast for the instrument to calculate the pre-programmed number of stacks. Once the problem was

observed, we cut back the number of stacks at each point from 32 to 8. With this small change, we no longer obtained any skipped traces. Another issue we encountered was blacked out data ranges when shooting the data. We attributed this to decreasing battery power (at the end of the day) and luckily we were able to re-acquire the problem lines. Observing the data collection on the DVL enables one to see immediate problems, and any interesting features or anomalies one might wish to focus on. Limestones are largely transparent to GPR signals, and the karstic cavities (filled with air or water), common in limestone, give strong radar return signals (Annan, 2003). Figure 7.4 illustrates a limestone cavity response on a GPR record according to Annan.

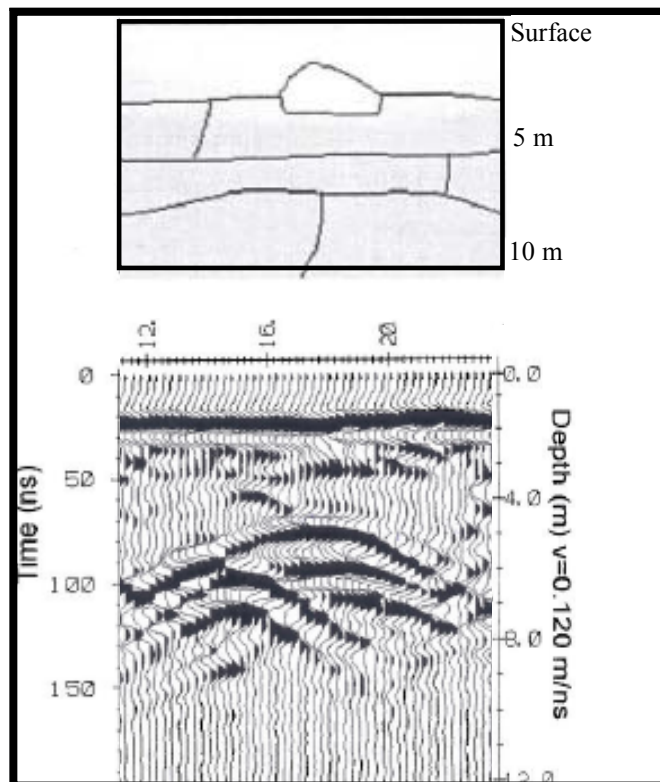


Figure 7.4 GPR Response from a limestone cavity (reproduced from Annan, 2003).

Figure 7.5 is one of the 3-D lines which nicely imaged the cave. As depicted, the line over the chultun appeared to exhibit a strong wide-aperture event within the massive limestone bedrock which otherwise shows poor reflectivity and weak amplitude. This is consistent with what to look for according to the Sensor and Software Inc. example. As the onset of the cave is a limestone/air interface, we would expect a strong reflection coefficient as is the case. The wide aperture GPR response is likely due to the geometry of the cave itself and the fact the top of the cave is a rugose and uneven surface. An interpretation of the different layers within the plaza is shown to the right of the figure. The record is a dewow filtered and gained display using Sensors and Software EKKO View program. Figure 7.6 is a photograph of the cave entrance at La Milpa.

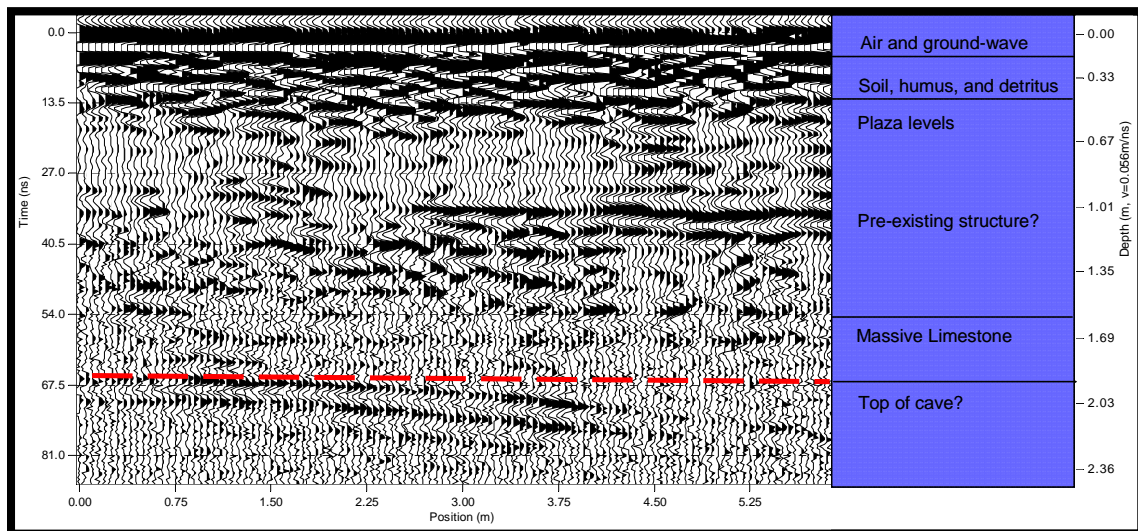


Figure 7.5 Anomalous event observed on y-line 60 at La Milpa.



Figure 7.6 Photograph of the top of the cave at La Milpa (courtesy of B. Cameron).

Interpolating the lines to create a three dimensional cube of the near-surface serves to image the cave even better and allows one to see the areal extent of the feature.

According to Figure 7.7, the 3-D shows the diffraction imaged on the x-line, y-line and the time slice. The feature consists of a strong peak-trough-peak event over the entire y-lines and the last few metres of the x-lines. The apex of the diffraction is consistent with the measured depth of the cave at 1.7 m. The horizontal expression of the cave on a timeslice is a semi-circular feature which appears to exhibit a fairly linear trend to the northwest.

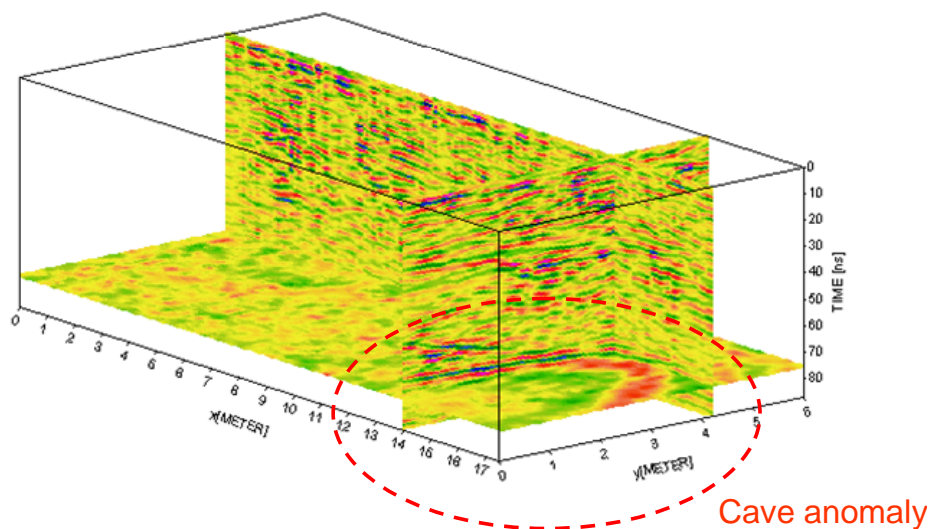


Figure 7.7 3-D image of cave feature below the plaza surface.

A closer examination of the time slice at 71.6 ns, at a depth of 2.15 m based on a velocity of 0.06 m/ns, suggests a cavity about 4.5 m wide and 3 m in length (Figure 7.8). The caves are designated by dashed ovals.

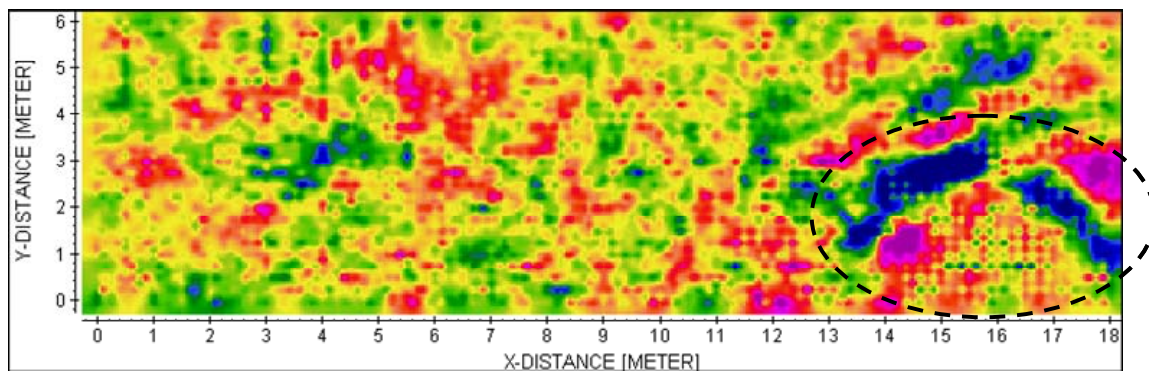


Figure 7.8 Timeslice outlining circular feature of cave in lower right.

If one continues to slice the dataset in time, the same cave appears to open up to the south-west (Figure 7.9).

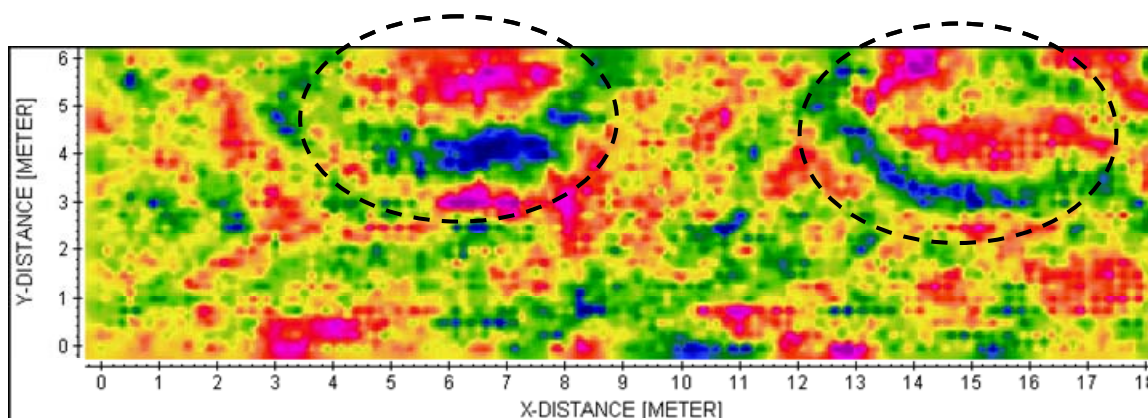


Figure 7.9 Time slice of 3-D at 82.4ns, outlining two caves below La Milpa plaza.

Further analysis of the 3-D time slices uncovered another semicircular feature, possibly another cave, at the south east corner of the grid.

One of the exciting results of this template study is the fact that this same feature has been observed under the altar at Maax Na, and on another 2-D line close by. A portion of what might possibly be a strong amplitude, wide aperture event is apparent 1.7-2.0 m below the surface there, suggesting another possible cavity.

Picking the horizon or event which I have interpreted as the cave, results in the validation of two separate anomalies as shown in Figure 7.10. This event was difficult to interpret on some of the GPR lines due to the weakening (decreasing amplitude) of the diffraction tail. The caves appear localized and not connected, but this may be due to data quality and the fact I was unsure of the pick in the intervening areas. Additional picking of the cross lines will improve the interpretation. The possible cave feature on the left may be an extension of a chultun located about 40 m SE of the GPR grid.

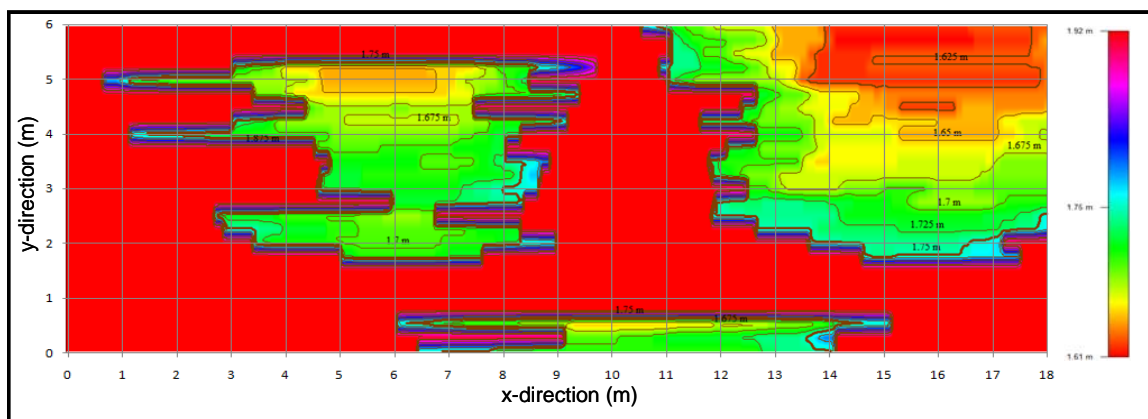


Figure 7.10 Map of picked cave horizon at La Milpa.

7.2 Pulse EKKO line and CMP across cave feature

A 2-D line was also acquired across the cave using a different instrument and lower frequency antenna, namely the Pulse EKKO 100 MHz unit. The lower frequency penetrates deeper into the near-surface but the resolution of the GPR data is somewhat compromised. This unit has separate transmitter and receiver antennas which allowed for the acquisition of a common mid-point survey (CMP) at the plaza.

The GPR line is displayed in Figure 7.11.

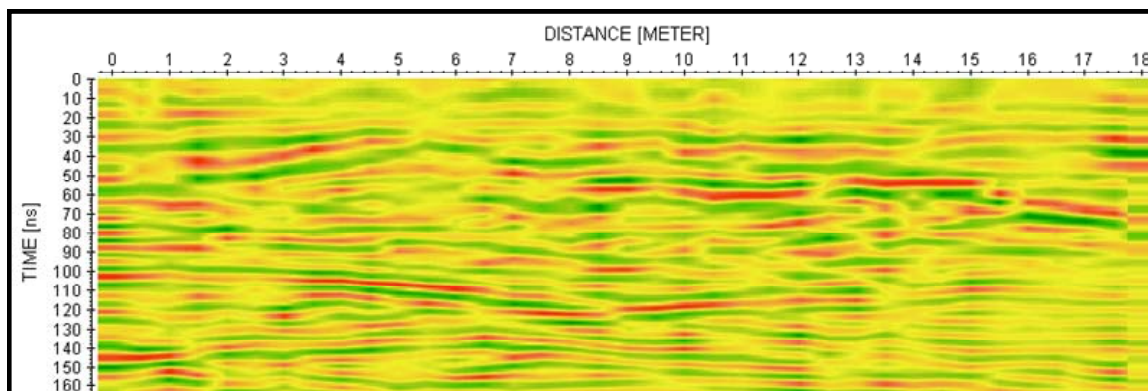


Figure 7.11 Pulse EKKO line acquired across the cave at La Milpa.

The cave is nicely imaged by the presence of an anticlinal type feature on the right starting at about 110 ns. This signature is likely a diffraction from the top of the cave.

The GPR section also shows another dipping event on the left, which I believe is a second diffraction from an additional cavern beneath the plaza. As previously discussed, this is either a new cave or an extension to the cave entrance further to the south and east of the grid. The two events exhibit destructive interference and break up where the two intersect.

The common mid point survey line was displayed in Chapter 5 (Figure 5.10). Picking the deeper hyperbolic events was difficult on the CMP line due to the decreasing amplitude with distance and depth, and aliasing due to the separation distance between the transmitter and antenna. This was the first time we had conducted such a survey so we were not aware that antenna separation was problematic. Next time I would recommend a smaller interval between steps.

Referring to Figure 5.10, I believe only a couple of strong hyperbolas, which represent the plaza cobble layer alone, are present. As previously discussed, the bedrock is identified by a low amplitude interval. Thus, picking the position of the base of the plaza layering and the top of the bedrock was challenging, but the velocity profile appears to be in line with expected values.

Figure 7.12 illustrates the CMP analysis of Line 16 at La Milpa. The associated velocity profile indicates velocities between 0.06 -1.1 m/ns, a velocity range indicative of a saturated, limestone environment. Although, there was some correspondence with the measured velocities ascertained from hyperbolic fitting of diffractions in the subsurface of 0.056 m/ns, the first one to two metres appear to have higher velocities than expected. This may be due to the quality of the CMP itself.

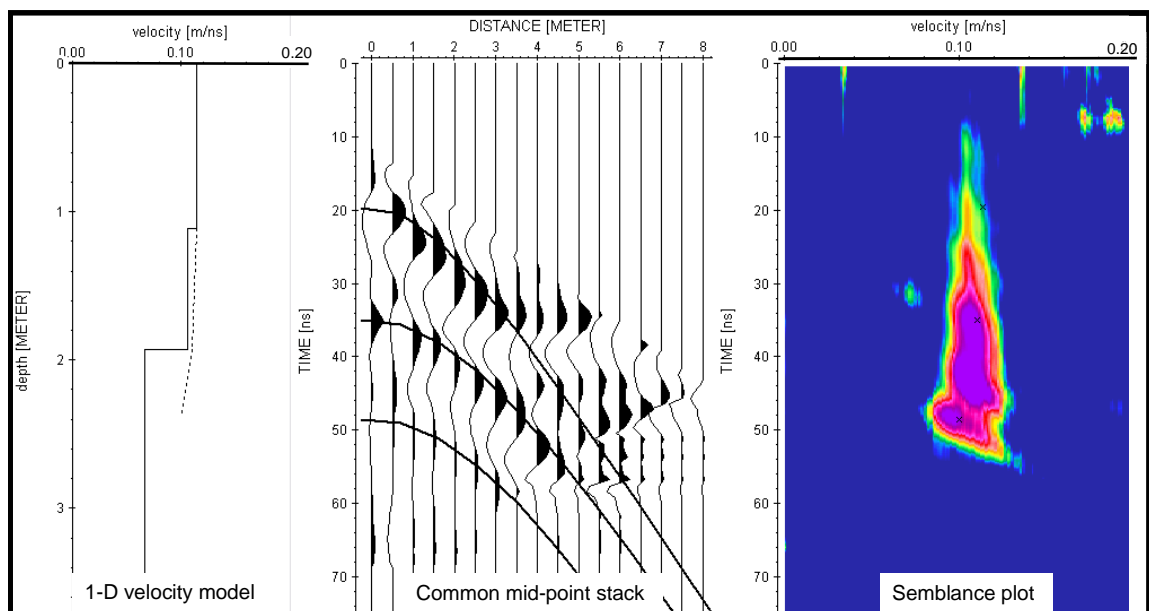


Figure 7.12 CMP analysis of Line 16 at La Milpa.

Chapter Eight: CONCLUSIONS

8.1 Benefit to archaeology

The objective of this thesis was to develop GPR methodologies to assist in exploring the plaza near-surface, acknowledging the similar work done at other Maya sites by Conyers (1995), and Valdes and Kaplan (2000). In particular, to provide archaeologists with a catalogue of geophysical anomalies encountered during our research work at Maax Na and La Milpa. These may be indicative of such archaeological features as caves, buried artifacts or structures. The advantage of geophysical surveying is that it provides a quick and efficient look at large areas, in an effort to focus archaeological field work. Many archaeologists sanction this activity because it allows for a non-invasive, non-destructive assessment of the subsurface. A number of lines, both 2-D and 3-D grids, have been acquired, surveyed, processed and interpreted for such features.

A number of interesting features have been highlighted, and providing a basis for possible excavation. One must be cognizant, however, that anomalous features recorded on GPR images can be caused by numerous factors, both natural, or of man-made construction. That being said, geophysical surveying still provides a much needed scientific service and the failure to unearth artifacts should not deter one from continuing to make recommendations to the archaeologists.

8.2 Recommended acquisition procedure and processing flow

Having undertaken several surveys at the archaeological site of Maax Na and La Milpa, I would make the following observations and recommendations:

- The opportunity to visit La Milpa and template a known cave aided in the interpretation of anomalous features at Maax Na.

- More care must be taken with distance calibration of each line within a 3-D grid survey.
- Finer distance separation is required between 3-D line acquisitions.
- Continued integration between total station and/or GPS survey and ground-penetrating radar survey is critical.
- Gain and other input parameters must be carefully looked at and possibly changed during field acquisition.
- Familiarity with the GPR instrument is important before field acquisition.
- More planning is warranted for the common mid-point survey in terms of the separation between the transmitter and receiver, and line length.
- Additional investigation is recommended to determine velocities in situ by using a brass rod instead of rebar.

The GPR method provided coherent and interpretable images of the subsurface of the plaza, in which structural, stratigraphic and other features were resolved. Although the interactive image on the digital video logger (DVL) showed some information about what lay beneath the surface, the application of a simple processing flow did improve the resolution and continuity of the events. This was accomplished with a flow which grouped together simple basic processes but proved effective.

Velocity differences determined over the various field seasons were observed and explained using the Wyllie Time Average equation. Lower velocities were noted to be typical of a wet regime and higher velocities indicative of dry near-surface conditions.

Processing recommendations include:

- A simple flow works best.
- The application of Q-filtering does improve the continuity and amplitude of deeper events. However, there may not be a need for it as was the case here.
- More investigation is required in the use of deconvolution, and the determination of the “correct” transmitted pulse.
- Further work needs to be done in applying some seismic-based algorithms to GPR data as they don’t appear to be as effective.
- The summing and interpolation of both the x and y line data results in a more accurate 3-D image incorporating all the information in both directions.
- Incorporating both x and y orthogonal data satisfies the directionality requirement for migration.

Chapter Nine: FUTURE WORK

9.1 Recommendations

Further processing research entailing GPR, should focus on three main thrusts, namely interpolation, migration and deconvolution. I believe if more work is done in creating new algorithms or fine-tuning the existing ones, we will see major improvements in near-surface imaging using ground-penetrating radar. Some of the work has been initiated but not completed due to the already large scope of the research project. Due to the inability to frequently visit the Maya sites in Belize, some of our ideas were tested out by using other sites and datasets acquired closer to home.

The University of Calgary shot a small survey on a property east of Fish Creek Park over a septic field in 2005 to help answer some of our questions regarding interpolation. In this particular survey, line separation was reduced to 0.20 m (compared to 0.50 m at Maax Na), with trace interval set at 0.05 m. The trace interval cannot be changed to a smaller value. Line separation was controlled to some extent by the width of the instrument itself. The Noggin Smart-Cart was approximately 0.25 m in width from wheel to wheel which makes acquiring smaller intervals cumbersome. Questions pertaining to line separation distance, spatial resolution, suitable trace intervals, and the importance of acquisition direction were addressed. Interpolation using the full dataset and subsets of the dataset were compared in an attempt to determine best practices in terms of parameter selection. The results of this work also focussed on how to improve data acquisition. The paper is included in Appendix C.

Another focus of further research should involve a more rigorous approach to estimating the “true” wavelet or propagating pulse using the data acquired over a rebar experiment both at Devon Island and at the Maax Na site. The idea is to create a window around the diffraction from the rebar, flatten the window and then sum the traces. The resultant wavelet would be representative of a “true” GPR signal which could then be used to design a decon operator and to generate more realistic radargrams. If we could successfully identify the shape of this wavelet, and extract or deconvolve it through the use of a suitable inverse filter, the resultant image should be a “true” picture of the subsurface. Fisher et al., (1992) maintains that deconvolution is not necessary because the radar source already produces a compact wavelet. To further complicate matters, pulse radar systems have undefined phase and do not fulfil the requirement of a minimum phase signal for deconvolution (Leckebusch, 2003). Despite this, the deconvolution algorithm attempts to define the reflectivity of the GPR data, but with limited knowledge of the composition of the plaza, and phase information, determining the accuracy of standard decon testing is guesswork.

References

Aitken, J. A., and Stewart, R. R., 2002, A geological/geoscience overview of the hydrocarbon potential of Belize, Central America: CREWES Research Report, **14**, 1-18.

Aitken, J.A., and Stewart, R. R., 2004, Shallow GPR and seismic surveying in a carbonate environment: Belize, Central America: CREWES Research Report, **16**, 1-17.

Allum, C., 2004, Welcome to the Monkey House: Bowdoin, **76**, No. 1, Bowdoin College, Maine, 19-25.

Anderson, N., and Cardimona, S., 2002, Forward seismic modeling: The key to understanding reflection seismic and ground penetrating radar (GPR) techniques: Geophysics 2002: The 2nd Annual Conference on the Application of Geophysical and NDT Methodologies to Transportation Facilities and Infrastructure, Federal Highway Administration, 22 p.

Annan, P., 2003, GPR principles, procedures and applications: Sensors & Software Inc.

Awe, J., 2007, Maya Cities and Sacred Caves – A Guide to the Maya Sites of Belize: Cubola Productions, 104 p.

Bancroft, J.C., 2004, A practical understanding of pre- and poststack migration, Course notes Vol. 1, p. 4.2.

Belize Tourist Board: www.travelbelize.org

Berard, B., 2006, Multioffset ground penetrating radar data - acquisition, processing and interpretation in diverse archaeological contexts, MSc. Thesis, University of Calgary.

Berman, A., 2008, Another discovery in Belize: World Oil, Vol. 229, p. 23.

Bristow, C.S. and Jol, H. M., (eds), 2003, Ground penetrating radar in sediments, Geological Society, London, Special Publications, 211 p.

Campbell, S., Gibson, J., Holder, M., Leslie, R., Rempel, B., Panton, F., Ruiz, C., and Wright, C., (eds), 1997, A geography of Belize: Cubola Productions, 139 p.

Charles, E. E., 2007, Using electrical resistivity imaging to apply an inverse Q-filter to ground-penetrating radar data, MSc. Thesis, University of Calgary.

Coe, M. C., 2001, The Maya: Thames and Hudson Ltd. New York, 256 p.

Conyers, L.B., and Goodman D., 1997, Ground penetrating radar- an introduction for archaeologists: AltaMira Press, 232 p.

.

Conyers, L. B., 1995, The use of Ground-Penetrating Radar to map the buried structures and landscape of the Ceren Site, El Salvador: *Geoarchaeology: An International Journal*, **10**, No. 4, 275-299.

Daniels, D.J., 2004, Ground Penetrating Radar 2nd edition: The Institution of Electrical Engineers, London, England, 726 p.

Daniels, J. J., 2000, Ground penetrating radar for imaging archaeological objects, Institute of Conservation Science for Cultural Heritage, Korea, 247-265.

Demarest, A., 2004, Ancient Maya – the rise and fall of a rainforest civilization: Cambridge University Press, New York, 373 p.

Davis, J.L., and Annan, A.P., 1989, Ground penetrating radar for high resolution mapping of soil and rock stratigraphy: *Geophysical Prospecting*, **37**, 531-551.

Dixon, G. G., 1956, Geology of Southern Honduras with notes of adjacent areas: Government Printer, Belize, 91 p.

Fasquelle, R. A., and Fash Jr., W. L., 1991, Maya Artistry Unearthed: National Geographic, **180**, no. 3, 94-105.

Fisher, E., McMechan, G.A., and Annan, A.P., 1992, Acquisition and processing of wide-aperture ground penetrating radar data: Geophysics, **57**, 495-504.

Gaffney, C., and Gater, J., 2003, Revealing the Buried Past: Geophysics for Archaeologists: Trafalgar Square Books, 200 p.

Goodman, D., 1994, Ground-penetrating radar simulation in engineering and archaeology: Geophysics, **59**, p. 224-232.

Geology and Petroleum Office Ministry of Science Technology and Transportation, 1995, Petroleum Potential of Belize, Central America, Belmopan, Belize.

Geophysical Survey Systems, Inc., GSSI: <http://www.geophysical.com/>

Goldberg, P., 2001, Earth Sciences and Archaeology: 513 p.

Gustafsson, J., and Alkarp, M., 2007, Array GPR investigation of the cathedral at Uppsala: Near Surface Geophysics, **3**, p 203-207.

Hatton, L., Worthington, M.H., and Makin, J., 1988, Seismic data processing: theory and practise: Blackwell Scientific Publications, 177 p.

Hubbard, S.S., Petersen, J.E., et al, 1997, Estimation of permeable pathways and water content using tomographic radar data: The Leading Edge, **16**, 1623-1628.

Henley, D.C., Birch, R.A., and Stewart, R.R., 2002, Near - surface imaging: refraction tomography and reflection imaging: CREWES Research Report, **14**, 1-15.

Jol, H.M., DeChaine, R.J., and Eisenman, R., 2002, Archaeological GPR investigations at Rennes-Le-Château, France: Proceedings of SPIE (the International Society for Optical Engineering), **4758**: 125 - 129.

Jol, H.M., Broshi, M., Eshel, H., Freund, R.A., Shroder, Jr., J.F., Reeder, P. and Dubay, R., 2002, GPR investigations at Qumran, Israel: Site of the Dead Sea scroll discovery: Proceedings of SPIE (The International Society for Optical Engineering), **4758**: 91 - 95.

Johnson, G., 2006, personal communication, Sensors and Software, Inc.

King, E., 2003-2008, Personal Communication, Howard University, Washington, D.C.

Irving, J., and Knight, R., 2003, Removal of wavelet dispersion from ground-penetrating radar data: Geophysics, **68**, 960-970.

Lechebusch, J., 2003, Ground-penetrating radar: A modern three-dimensional prospection method: Archaeological Prospection, **10**, 213-240.

MALÅ Geoscience: <http://www.malags.com/>

Miller, M. E., 1999, Maya art and architecture: Thames and Hudson, New York, 240 p.

Moldoveanu, M., Stewart, R.R., and Aitken, J.A., 2002, Shallow imaging using ground-penetrating radar (GPR) data in a carbonate environment: Belize, Central America: CREWES Research Report, **14**, 1-13.

Moorman, B., and Michel, F.A., 2000, Glacial hydrological system characterization using ground-penetrating radar, *Hydrol. Process.* **14**, 2645-2667.

Morrice, S., 1993, Discovery of a pull-apart basin may signal oil potential in Belize: *Oil and Gas Journal*, **91**, 100-103.

Nieto, Carlos, 2005, Multicomponent seismic exploration and ground-penetrating radar surveying in the Canadian Arctic, MSc. Thesis, University of Calgary.

Northern Belize.com, 2008, <http://www.northernbelize.com/vegetation.html>

Olehoef, G.R., 2000, Maximizing the information return from ground penetrating radar: *Journal of Applied Geophysics*, **43**, 175-187.

Olhoeft, G.R., and Capron, D.E., 1993, Laboratory Measurements of the Radio Frequency Electrical and magnetic Properties of soils from Yuma, Arizona: US Geological Survey Open-File Report, **93-701**.

Rao, R. P., 1982, Exploration in Belize gains momentum: *Oil and Gas Journal*, **80**, 308-318.

Reynolds, J.M., 1997, *An introduction to applied and environmental geophysics*: John Wiley & Sons, New York.

Sensors & Software Inc., 2004, GPR Course notes.

Sandmeier, K., 2004-2008, ReflexW v 4.5 program for processing and interpretation of reflection and transmission data: Sandmeier-Geo.

Sharer, R. J., 1994, *The Ancient Maya*: Stanford University Press, 892 p.

Shaw, L., 2003-2008, Personal communication, Dept. of Sociology and Anthropology, Bowdoin College, Maine.

Shaw, L., King, E., and Chiarulli, B., 2005, and Valdez Jr., F., Programme for Belize Archaeological Project: Report of activities from the 2004 Field Season, Mesoamerican Research Laboratory Occasional Papers No. 4, University of Texas at Austin.

Stuart, G. E., 1989, City of kings and commoners – Copan: National Geographic: **176**, No. 4, p.494.

Tchakirides, T. F., Brown, L. D., Henderson, J. S., Blaisdell-Sloan, K., 2006, Integration, correlation, and interpretation of geophysical and archaeological data at Los Naranjos, Honduras in Proceedings of 2006 SAGEEP Conference, Columbus, Ohio, 10 p.

The Ma'ax Na Archaeology Project, 2001, <http://www.neararchaeology.org/project>.

Valdes, J. A. and Kaplan, J., 2000, Ground-Penetrating Radar at the Maya site of Kaminaljuyu, Guatemala: Journal of Field Archaeology, **27**, No. 3, 329-342.

Valdez Jr., F., and Shaw, L., 2006, Preliminary report of fieldwork at Maax Na, Belize, 2005, Programme for Belize Archaeological Project: Report of activities from the 2005 season, Mesoamerican Research Laboratory Occasional Papers No. 6, University of Texas at Austin.

Wilson, W.L. and Wilson, D.C., 1990, Investigation of Mayan structures at Caracol, Belize, using ground penetrating radar: Third International Conference of Ground Penetrating Radar, U.S Geological Survey, Open-File Report **90-414**, p. 74.

Wyllie, M. R. J., Gregory, A. R., and Gardner, G. H. F., 1958, An experimental investigation of factors affecting elastic wave velocities in porous media: *Geophysics*, **23**, 459-493.

APPENDIX A: A GEOLOGICAL AND GEOPHYSICAL OVERVIEW OF NORTHERN BELIZE AND ITS EXPLORATION POTENTIAL

(from Aitken and Stewart, 2002)

A review of the exploration history of Belize has led to the recognition of its possible untapped potential. Since the onset of oil exploration in Belize began in 1938, a total of only forty-seven wells have been drilled on the mainland and offshore. Well results indicate the presence of oil reservoir but as yet in sub-commercial quantities. Commercial quantities of oil however have been discovered within the stratigraphically equivalent Peten basin in the neighbouring countries of Mexico and Guatemala. Northern Belize is considered to be one of the most prospective areas of Belize. As of the mid 1990s, thirty wells have been drilled in northern Belize. A number of undrilled anomalous structures and possible play types have been identified. With the onset of new technologies, a more in-depth look at the prospectivity of Belize, particularly northern Belize, may be warranted.

Recent articles in World Oil and the Belizean newspapers, and evidence of deep muddy tracks left by heavy seismic trucks and/or rigs at Maax Na, indicate increased exploration activity. In 2007, Belize Natural Energy Ltd (BNE) tested light, sweet oil from several Cretaceous carbonate reservoirs, the same Albaina-Turonian Yalbec formation that produces at the Spanish Lookout field discovered in July, 2005 (Berman, 2008).

A.1. Introduction

This overview of the geology and geophysics was initially undertaken to become familiar with the surficial geology in and around several Mayan ruin sites in northern Belize namely Maax Na and Chan Chich (Figure A.1).

Understanding where the Mayans built their impressive pyramidal structures and plazas, and the materials they used, required the examination of the regional geological setting and lithological information. Several geophysical surveys conducted by the University of Calgary at these sites over the past several years have provided good images of the near surface confirming the existence of caves, a looter's trench and other important archaeological features. This research however, has also uncovered a virtually unexplored area of considerable oil potential. Thirty wells have been drilled in the Corozal basin over the last seventy years of petroleum exploration history with encouraging results, namely several live oil shows but as yet non commercial oil production. The intent of this appendix is to summarize the information and findings of several sources, and those presented by the Geology and Petroleum Office - Ministry of Science and Technology and Transportation of the Government of Belize.

A.2. Regional and Stratigraphic Setting

Belize is located in southeastern Central America and is bounded by Mexico, Guatemala, and the Caribbean Sea. It has an areal extent of 22,700 square kilometers and is the only Central American country with no Pacific coastline. According to Morrice (1993), “From an explorationist’s viewpoint, Belize is exciting because of its placement on the rim of the prolific Southern Gulf of Mexico basin, containing most of the major Mexican oil production. Belize offers access to the same stratigraphic sequences of source, reservoir and seal facies.”

A.3. Tectonics

The evolution of Belize’s tectonic history began with the super-continent Pangaea and its subsequent break up into the continents of North and South America over eighty million years ago. The associated rifting along fracture zones within what would become the Gulf of Mexico, and periods of juxtaposition between the North American and South American plates resulted in the Yucatan area being bounded by a series of faults. The Yucatan basement is extended and linear stretching produced a series of horst and grabens (Figure A.2). According to World Oil, “it is likely that organic-rich source beds accumulated in graben areas as they did elsewhere along the rifted Atlantic and Gulf of Mexico margins”. Continental drift of the North American plate precipitated the formation of new oceanic crust in an area adjacent to Belize, forming the Caribbean plate. Continued tectonic activity led to the eastward movement of the Caribbean plate which deformed the Central American region and is responsible for the dominant and structurally controlled features of Belize today: the Maya Mountains, the offshore atolls and the coral barrier reefs (Figure A.3).

A.4. The Stratigraphy and Paleogeography of the Corozal Basin

The Belize mainland can be subdivided into three geological provinces: Northern Belize, Southern Belize and South-Central Belize. The Corozal Basin of Northern Belize is an extension of the Yucatan platform, a geologically complex province, and is stratigraphically part of the North Peten Basin of Guatemala. Southern Belize contains the Belize basin and the Maya Mountains are part of the South-Central Belize geological province. This report will focus on Northern Belize and the Corozal Basin. The Corozal basin is comprised of a thick sequence of non-clastic sediments deposited during a 50 million-year history of tectonic uplift, erosion, faulting and transgressions. It is characterized by a predominantly marine carbonate sequence. From a geomorphic perspective, the Corozal basin, is comprised of three distinct units: a coastal plain with swamps and flood plains of Quaternary age, a central plain with gentle topography and lakes created by subterranean karsting, and overlain with a cover of Lower and Upper Tertiary carbonates and clays, and a western expanse of hills ranging from 100 to 250 meters in elevation, with rivers and flood plains. Upper Cretaceous and Lower Tertiary carbonate rocks make up the surficial expression of this latter region. The most striking feature of the rivers north of the Maya Mountains is their remarkably straight courses (Dixon, 1956). Faults and fractures appear to dominate the drainage patterns throughout this region.

Northern Belize contains a series of WNW-ESE trending anticlinal structures that plunge to the northwest, and may be of interest to petroleum exploration (Geology and Petroleum Office, 1995). These structures are confined to the western area of Belize and are part of the Peten basin of Guatemala in which commercial quantities of petroleum have been discovered in the Reforma, Campeche and North Peten areas. It has been postulated that the trending pattern of these structures is associated with the uplift of the Maya Mountains in the early Tertiary. Figure A.4 represents a geological cross-section through part of the Corozal basin and is a fair representation of the stratigraphy of the Maya ruin sites of Maax Na and Chan Chich. The geologic sequence and paleogeography of the Blue Creek 1 well, which represents the northern limit of the cross-section shown in Figure A.5, is arranged from the oldest to youngest deposits:

A.4.1. Santa Rosa Group

The creation of a geosynclinal trough due to tectonic activity led to the deposition of the Paleozoic sediments and metasediments of the Santa Rosa group which essentially form the basement rocks in the Yucatan Platform, Corozal Basin, Guatemala and southeastern Mexico. The Blue Creek 1 well was drilled to a depth of 3200 meters and encountered Paleozoic shale with minor graywackes, but other wells in the Corozal Basin have penetrated carbonates, with metamorphosed slates, phyllites and schist within the Santa Rosa group.

A.4.2. Hillbank Formation

Following a period of uplift, erosion and faulting, a major transgression occurred in Early Cretaceous flooding the Corozal Basin in its entirety. The Maya Mountains provided high topographic relief, and northern and southern boundary faults set limits to sediment

deposition. Within the Corozal Basin, the Belmopan-Shipstern subsurface ridge split the basin into two geologic environments resulting in the creation of a hypersaline lagoonal basin in the west and a shallow marine sea to the east. The Hillbank formation consisting of clayey dark tan microcrystalline calcareous dolomite with interbedded sand and shale was deposited during this period.

A.4.3. Yalbac Formation

The Yalbac formation represents a period of sequential deposition of carbonates and anhydrites in the evaporitic basin of northwestern Belize. A thickness of over 2250 metres was encountered while drilling the Blue Creek 1 well. This formation appears to be the most prospective for light oil as evidenced by the successful wells by the Belizean Natural Energy Ltd. at Spanish Lookout and east of Belmopan.

A.4.4. Barton Creek Group

A stable marine environment in the Late Cretaceous period led to the deposition of over 200 metres of limestone and dolomitic limestone and marls. The Barton Creek Formation refers to the entire sequence above the Yalbac Formation.

In the Early Eocene, a significant tectonic event resulted in thrust faulting, folding and uplift in the basin and shelf environments. During the Miocene, a major transgression submerged most of the Corozal basin and reefal structures were created alongside areas of high relief. Lagoonal sedimentation consisted of limestone with boundstone/grainstone to wackestone textures. Subsequent regression of the seawater and the uplift of the mainland during Pleistocene times have led to Belize's present day geographical framework.

A.5. Geophysics

Although Belize has a history of oil exploration since the 1930s, from a geophysical point of view, a large part of the area is generally unexplored. Oil companies including Gulf, Anschutz, Chevron, Placid Oil, Petro Belize and American Eagle drilled in the Corozal Basin from 1956 to 1994, and results established the presence of oil, but at that point in time failed to find economic quantities. With the onset of new technologies such as 3-D seismic, computer workstations, improved instrumentation and seismic processing software, it may be possible to take a fresh look at the hydrocarbon prospectivity of northern Belize. This has indeed occurred as indicated by the article in World Oil. "BNE has identified four prospect areas using an impressive technology workflow to interpret and integrate seismic data, surface and subsurface geology, geochemistry, reprocessed gravity, magnetic data, and space-shuttle imagery."

A.5.1. Gravity and Magnetism

The Corozal Basin contains a number of Bouguer anomalies according to the Geology and Petroleum Office. Gravity lows in the north, trend NW-SE and may signify the continuation of the Peten Basin embayment or a low-density granitic pluton. Two

anomalously high gravity readings are evident in the central part of the Corozal Basin and trend in a north-south orientation. The southwestern part of the basin consists of low gravity values suggesting a gradational thickening of the regional sedimentary sequence to the northwest.

Two major sub-basins within the Corozal Basin are present due in part to the existence of the Hillbank Fault. The Sand Hill sub-basin is part of the Yucatan platform while the Hillbank sub-basin represents the eastern expression of the Peten basin. Structures on the SW side of the fault would be potential targets for petroleum exploration (Geology and Petroleum Office, 1995).

Although the magnetic anomaly map of the Yucatan Peninsula does not include coverage over Belize, it does confirm the existence of a magnetic low in the northwestern part of Belize, which corresponds to the extension of the Peten Basin of Guatemala. This possible embayment was also postulated from gravity lows. The presence of the NW-SE trending Hillbank Fault was also confirmed on the magnetic anomaly map.

In 1974, an aeromagnetic survey to the magnetic basement was conducted in Belize, covering a total of approximately 14,000 square kilometres. In the Corozal Basin of northern Belize, anomalies trend in a NW-SE orientation with values increasing toward the eastern region, and toward the Maya Mountains. These anomalies appear to reflect lithological variations in the basement composition and are not structurally related (Geology and Petroleum Office, 1995). Estimates of the depth of the magnetic basement range from almost zero in the vicinity of the Mayan Mountains to over 5500 metres in the northwest region of the Corozal Basin.

A.5.2. Seismic

Various oil companies have acquired nearly 10,000 kilometres of 2-D seismic lines in Belize over the last several decades, concentrated mainly off-shore (Figure A.6).

According to Rao (1983), “The majority of wells drilled within the Corozal basin have been delineated on the basis of gravity data or poor seismic data. So it is possible that wells were not located on the highest part of the structures.” It is believed that poor seismic recordings are caused by near surface karst structures that are prevalent in the area. These cave-like voids result in seismic interference, which leads to poor-signal-to-noise and the lack of continuity of events. Recent ground penetrating radar surveys have easily detected such features and may provide a means of establishing a better layout of seismic lines at a negligible cost.

A.5.3. Play types

Two possible play types in the Corozal Basin are structural closures bounded by faults and pinchouts (Figure A.7). The play concepts as presented indicate normal faulting downthrown to the south-east, creating potential trapping mechanisms for Mesozoic

sediments. Exploration companies have mapped approximately twenty faulted anticlinal structures in this basin (Geology and Petroleum Office, 1995).

The two most likely formations with reservoir/seal potential are considered to be the Yalbac and Hillbank formations. Both formations have notable oil shows. Drilling to deeper Paleozoic rock however is another potential target. In Central America, the Paleozoic and Pre-Cambrian formations have been rather neglected owing to the greater importance of the younger oil producing formations (Dixon, 1956).

A.6. Conclusions

A review of the geology and geophysics of northern Belize has uncovered some interesting undrilled geological structures. The government of Belize is committed to encouraging the participation of foreign investment in hydrocarbon exploration. Belize's stability, democratic government and investment incentives with respect to the petroleum sector make it an attractive place to invest in. At this point it is premature to comment on the quality of the plays outlined in this report as more work is warranted in integrating the geological and geophysical data. Near-surface geophysical methods such as ground-penetrating radar could provide means of determining karst topography and allow for the acquisition of better quality seismic data. New technologies such as three-dimensional seismic acquisition could better image the subsurface and aid in quantifying the risk of potential exploration targets. This has been the case based on recent developments in Belize.

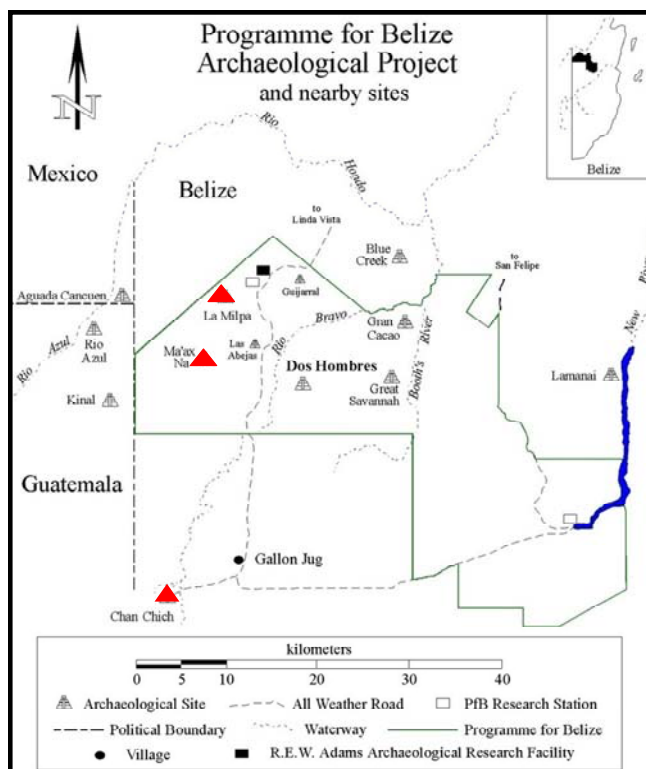


Figure A.1 Location of Maya study sites in Northern Belize (MARL).

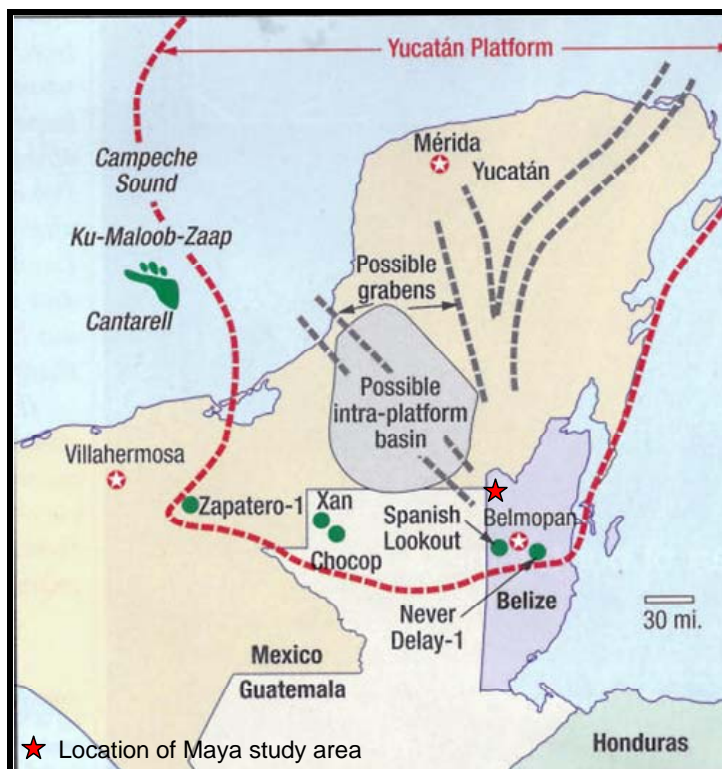


Figure A.2 Extension of Yucatan Platform and associated faults (World Oil, 2008).

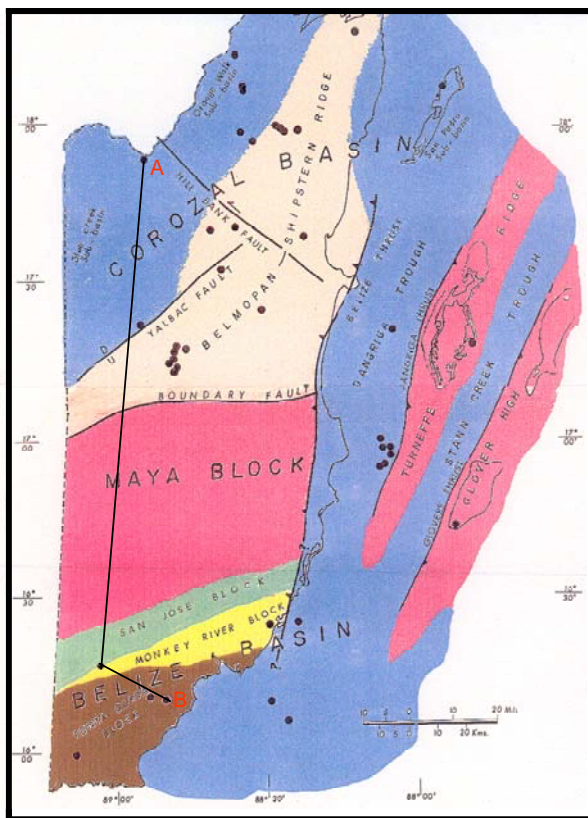


Figure A.3 Tectonic Map of Belize with location of cross-section A-B (Geology and Petroleum Office, 1995).

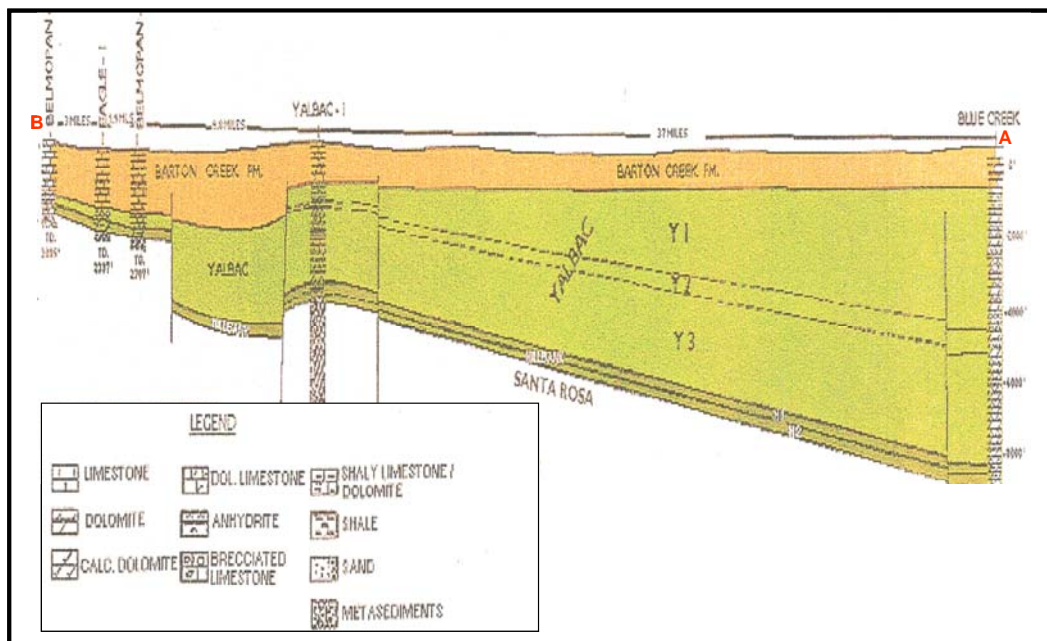


Figure A.4 Geological cross-section of western Belize (Geology and Petroleum Office, 1995).

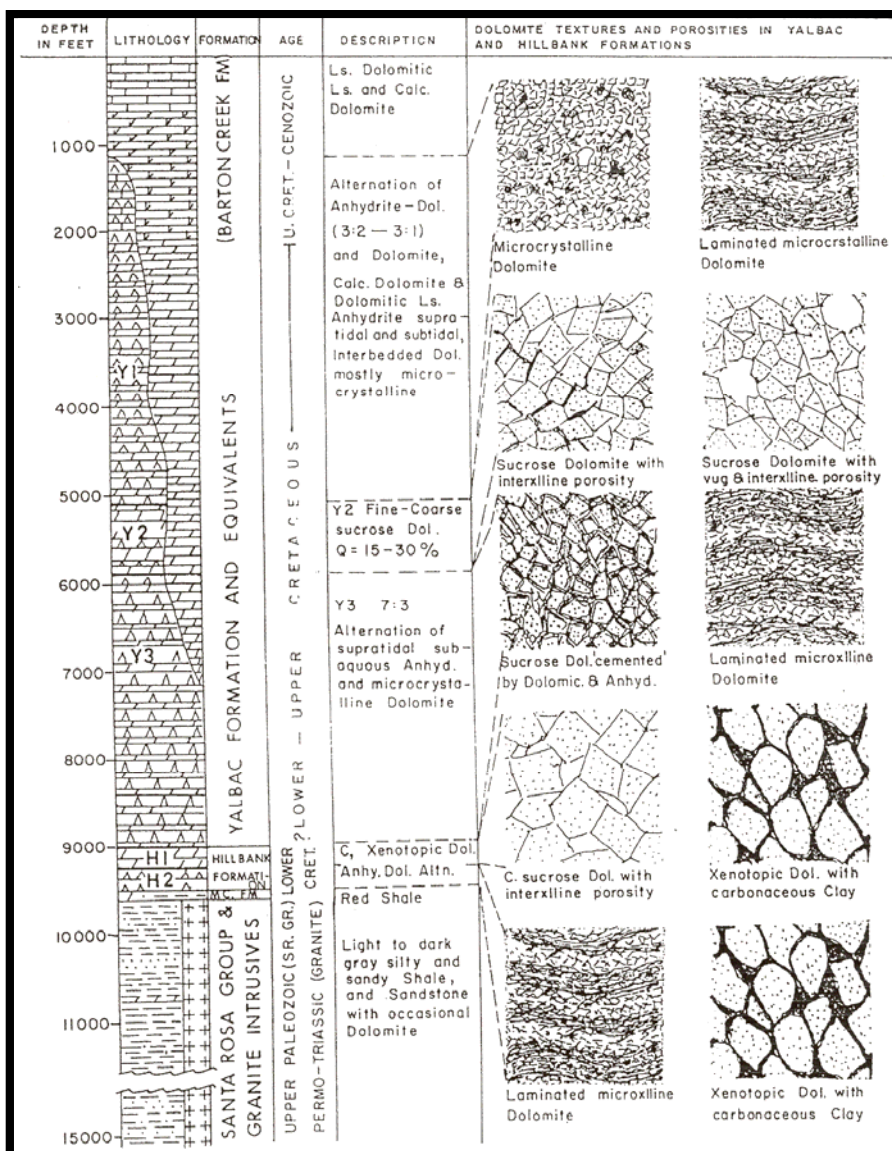


Figure A.5 The stratigraphic column of the Corozal Basin (Geology and Petroleum Office, 1995).

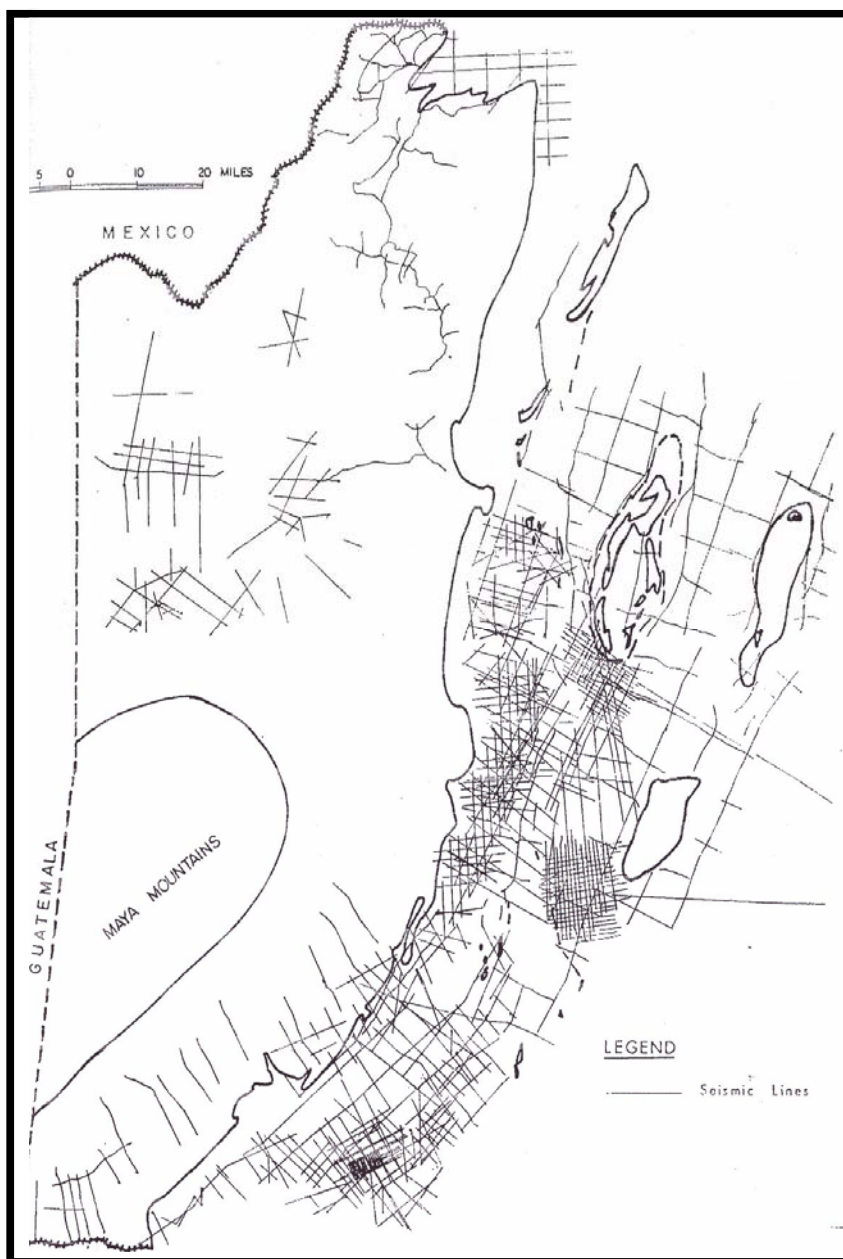


Figure A.6 Seismic Base Map of Belize (Geology and Petroleum Office, 1995).

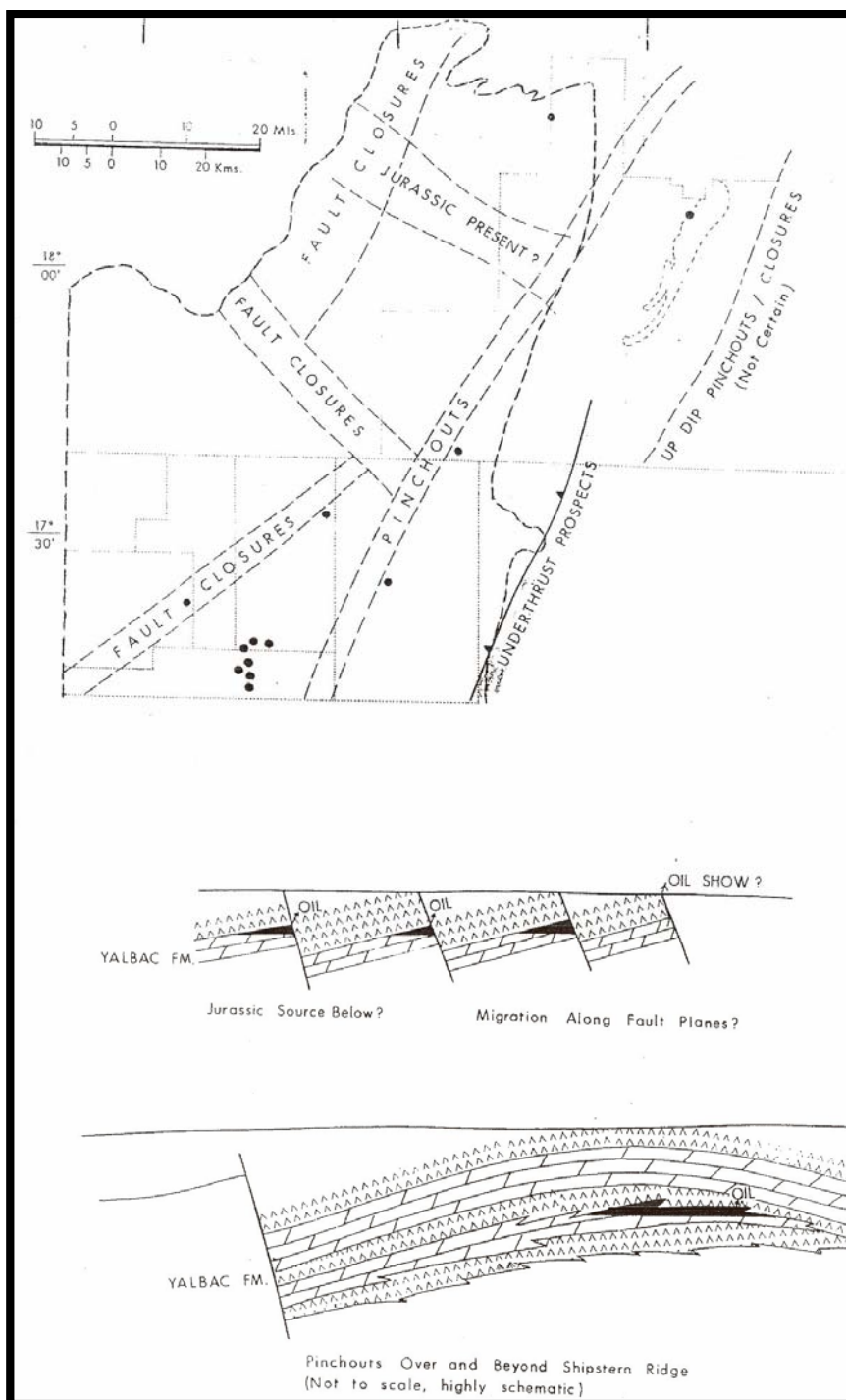


Figure A.7 Possible play concepts in northern Belize (Geology and Petroleum Office, 1995).

APPENDIX B: CATALOGUE OF GPR LINES

This appendix contains the majority of the GPR 2-D lines acquired at Maax Na during 2002-2008. The lines have been divided into the different field seasons (years). All lines have been processed with a similar processing flow using ReflexW, although some have not been migrated due to the poor quality of the data and the presence of strong isolated events. A number of the lines are lengthy which necessitated breaking the GPR sections up into two or three parts. A map outlining the layout of the GPR acquisition survey at the site accompanies each part in 2002/2003 and 2004, and 2008.

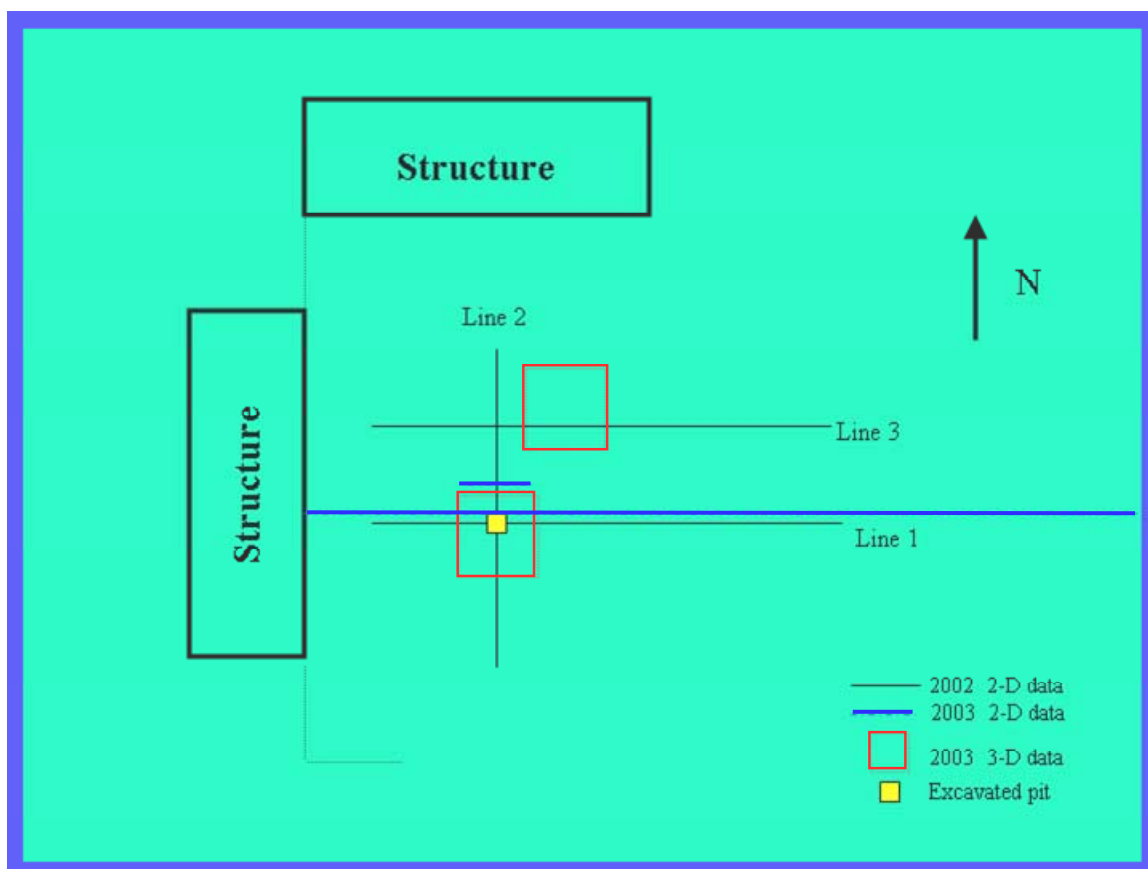
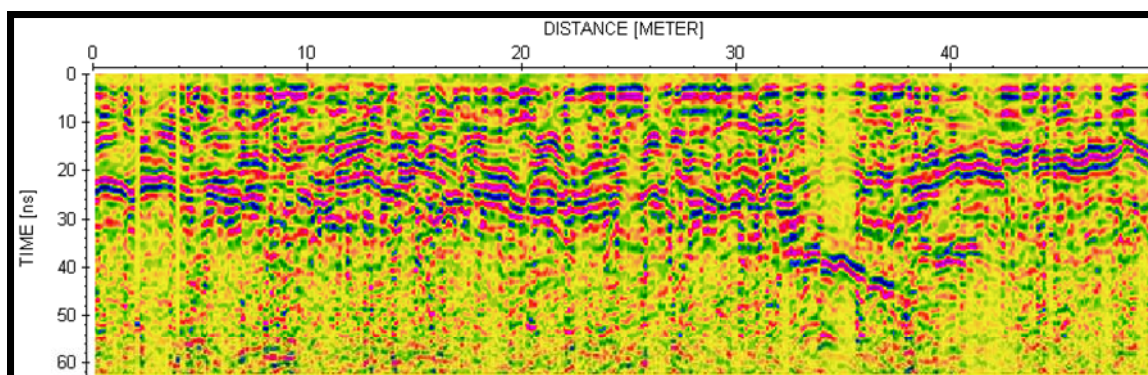
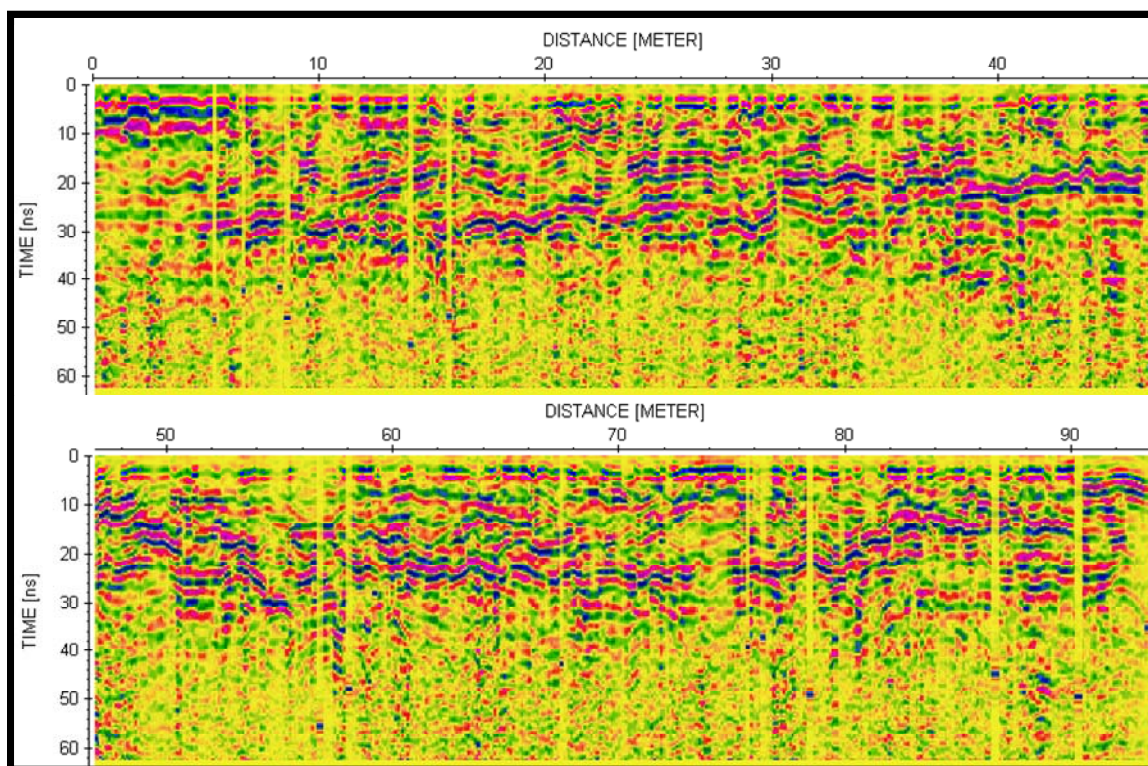


Figure B.1 Schematic of GPR line locations across Plaza A in 2002 and 2003 (not to scale).

B.1. 2002 GPR Data:**Figure B.2 E-W Project 2: Line 1 across north plaza.****Figure B.3 S-N Project 2: Line 2 across north plaza.**

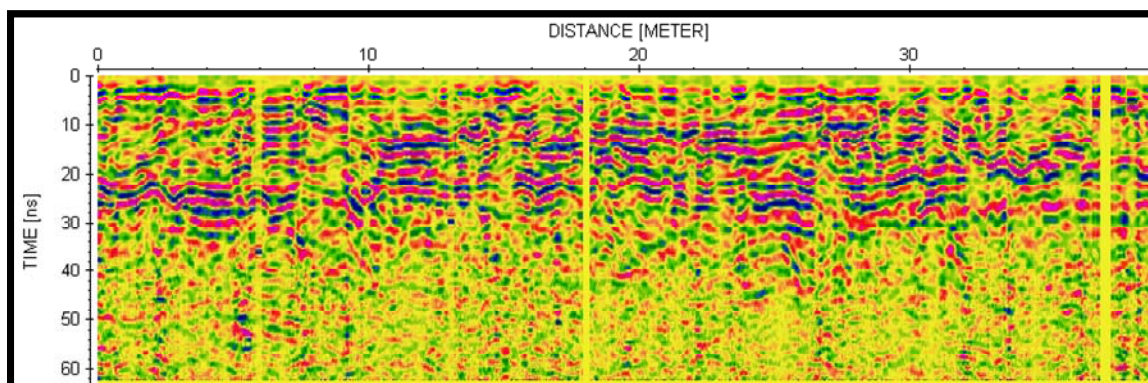


Figure B.4 E-W line: Project 2: Line 3 across north plaza.

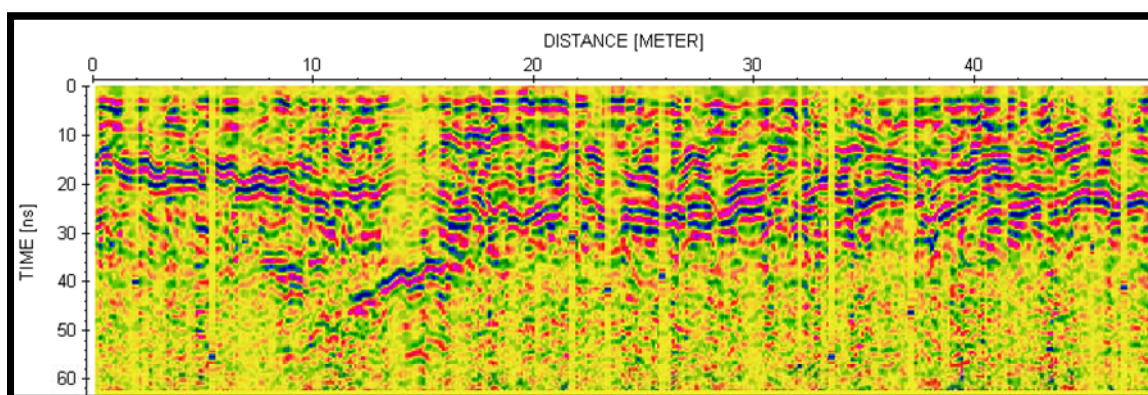


Figure B.5 W-E Project 3: Line 1 across north plaza (reverse direction to Project 2 Line 1).

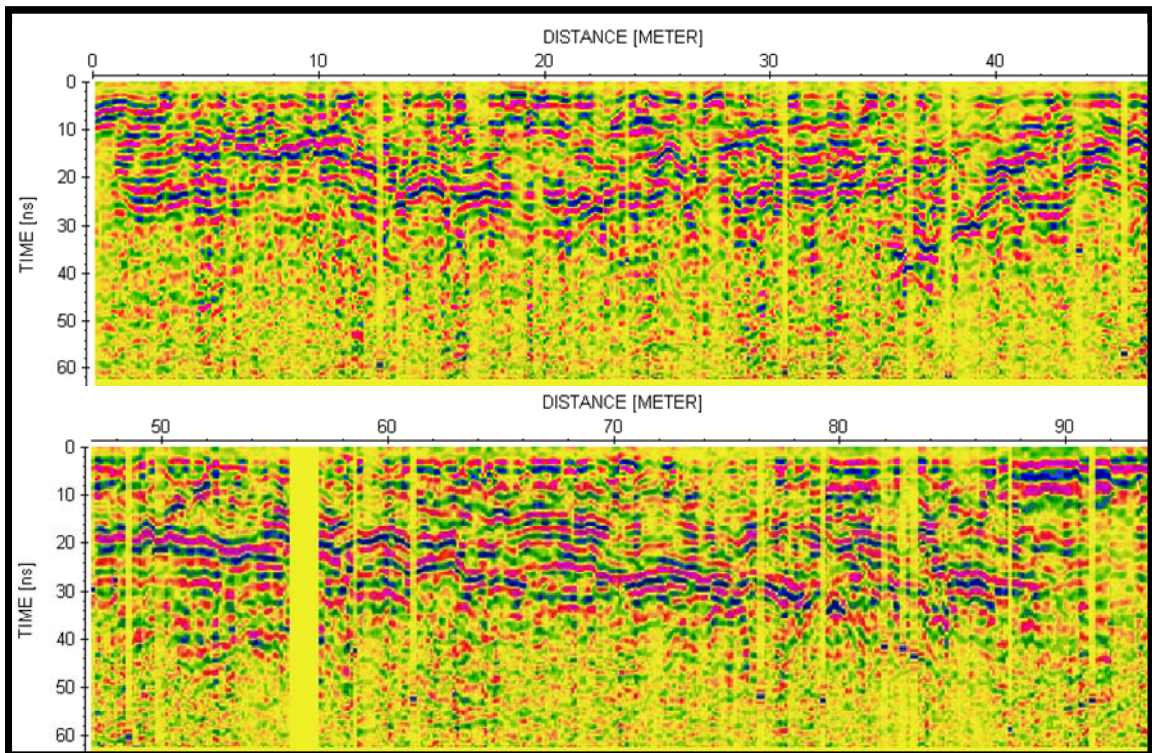


Figure B.6 N-S Project 3: Line 2 across plaza (reverse direction to Project 2 Line 2).

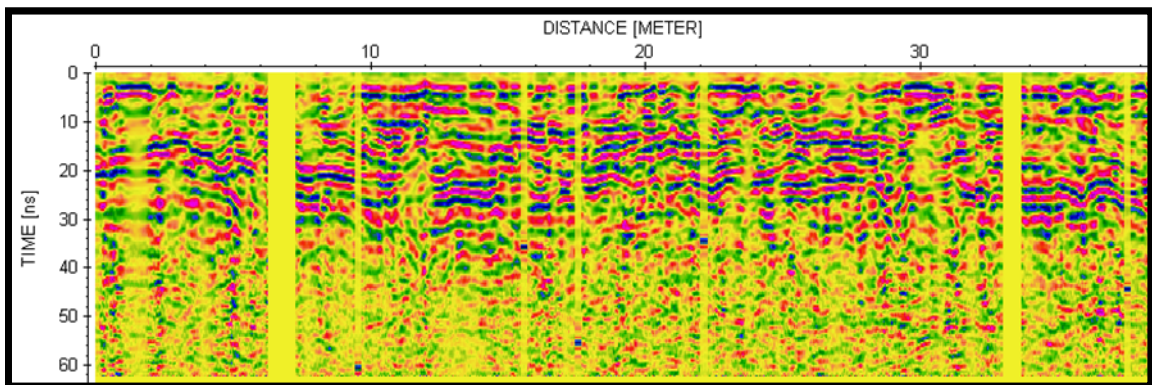
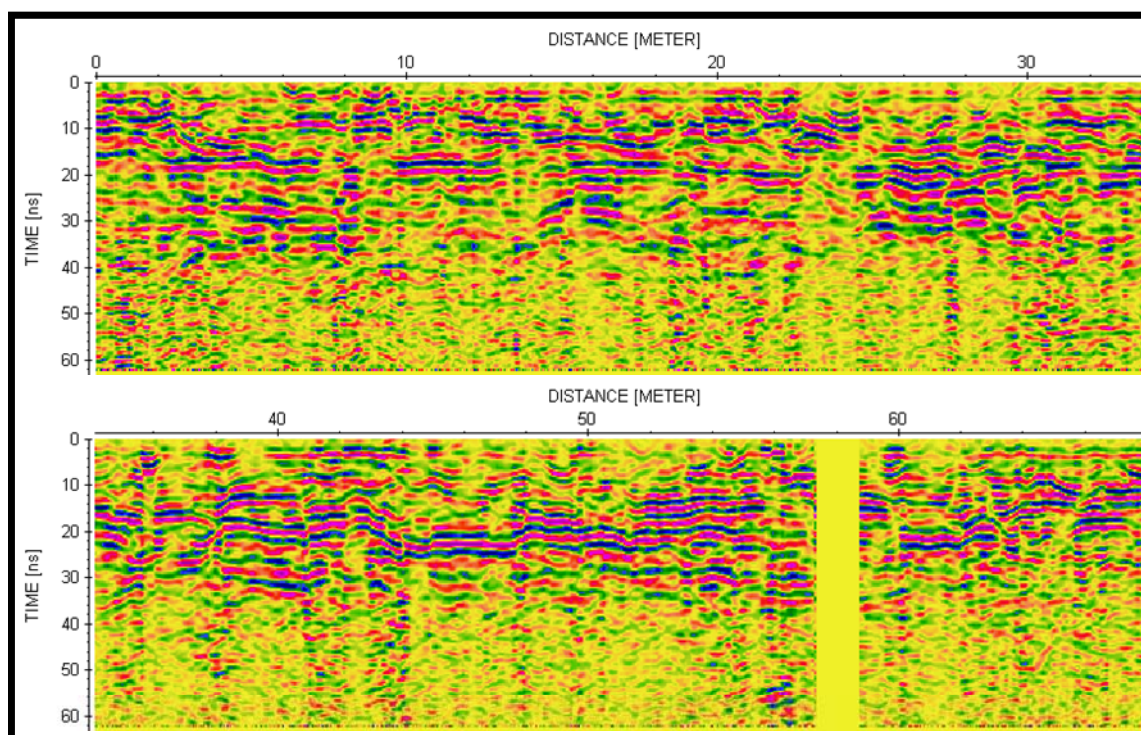


Figure B.7 W-E Project 3 Line 3 across north plaza (reverse direction to Project 2 Line 3).

B.2. 2003 GPR Data:**Figure B.8 W-E Project 1: Line 1 across plaza.**

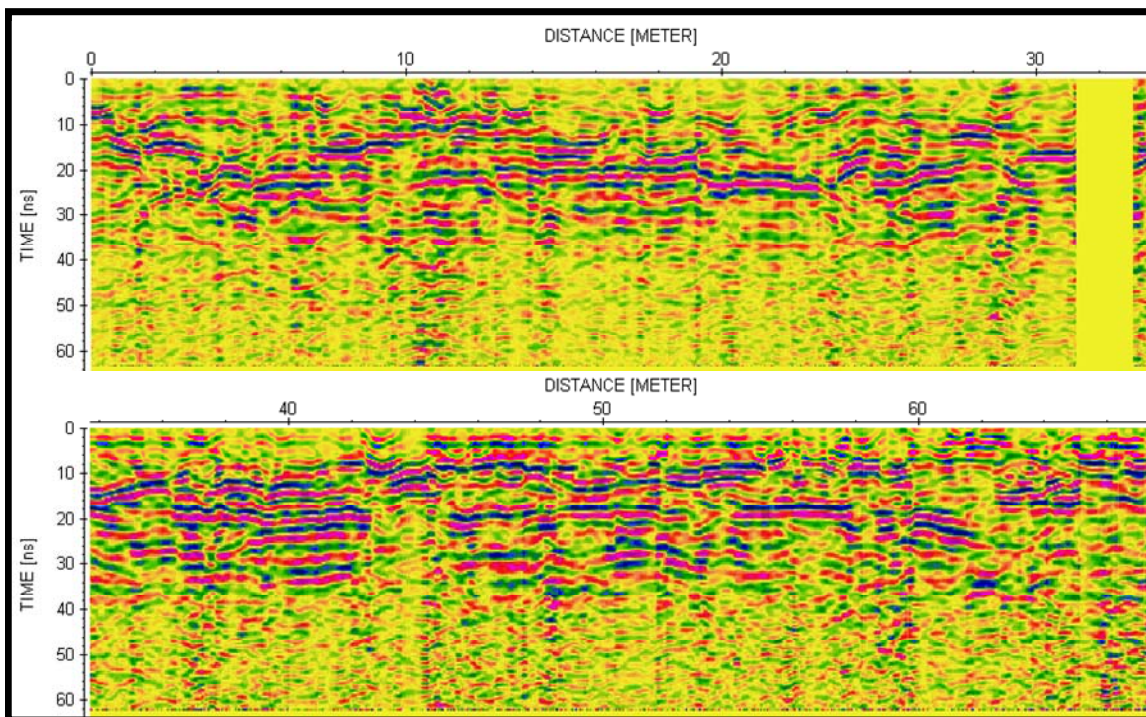


Figure B.9 E-W Project 1: Line 3 across plaza (reverse of Line 1).

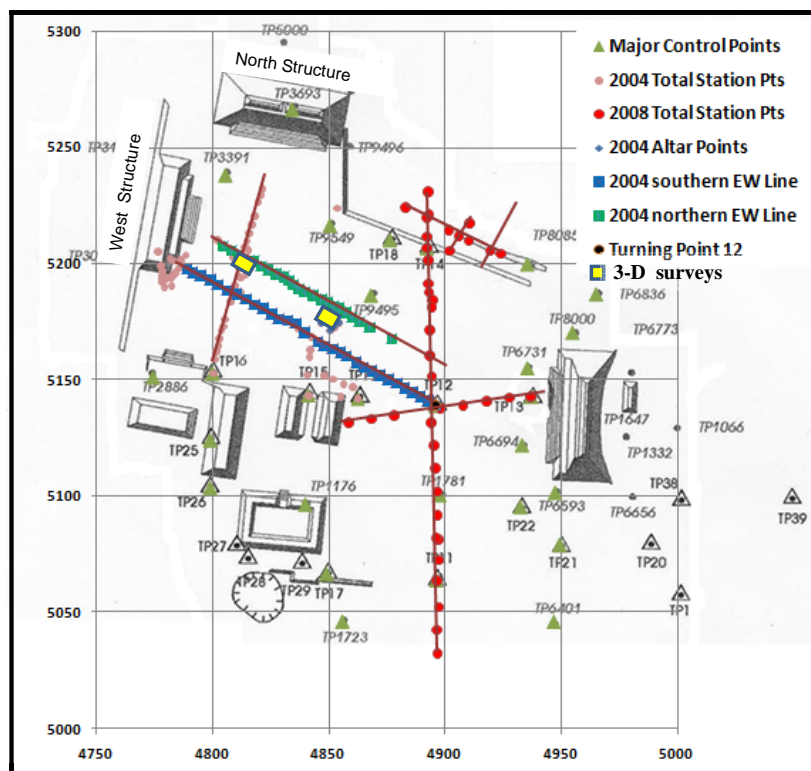
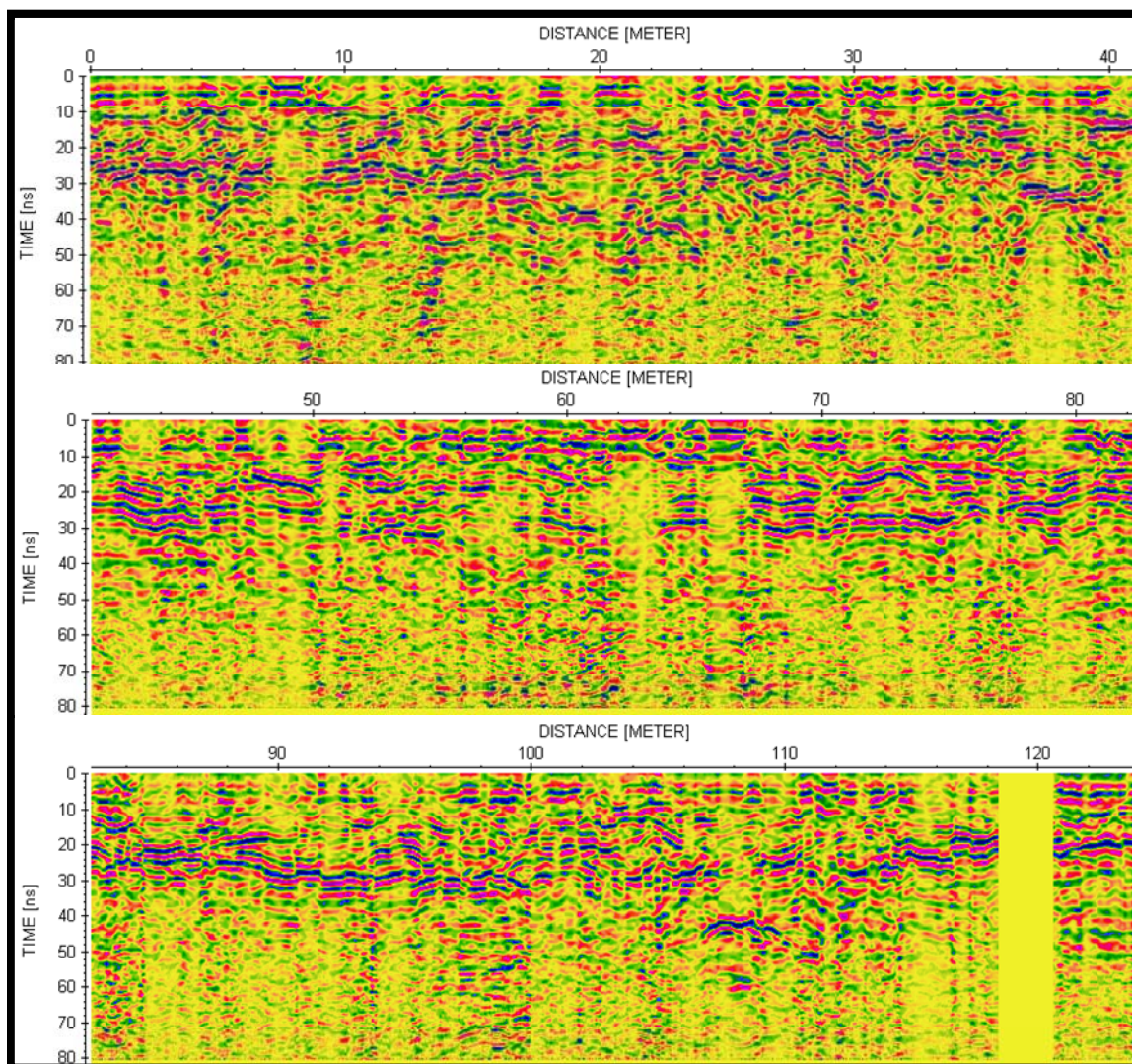


Figure B.10 Total station survey and GPR lines acquired in 2004-2008.

B.3. 2004 GPR data:**Figure B.11 Project 5: Line 1 across plaza.**

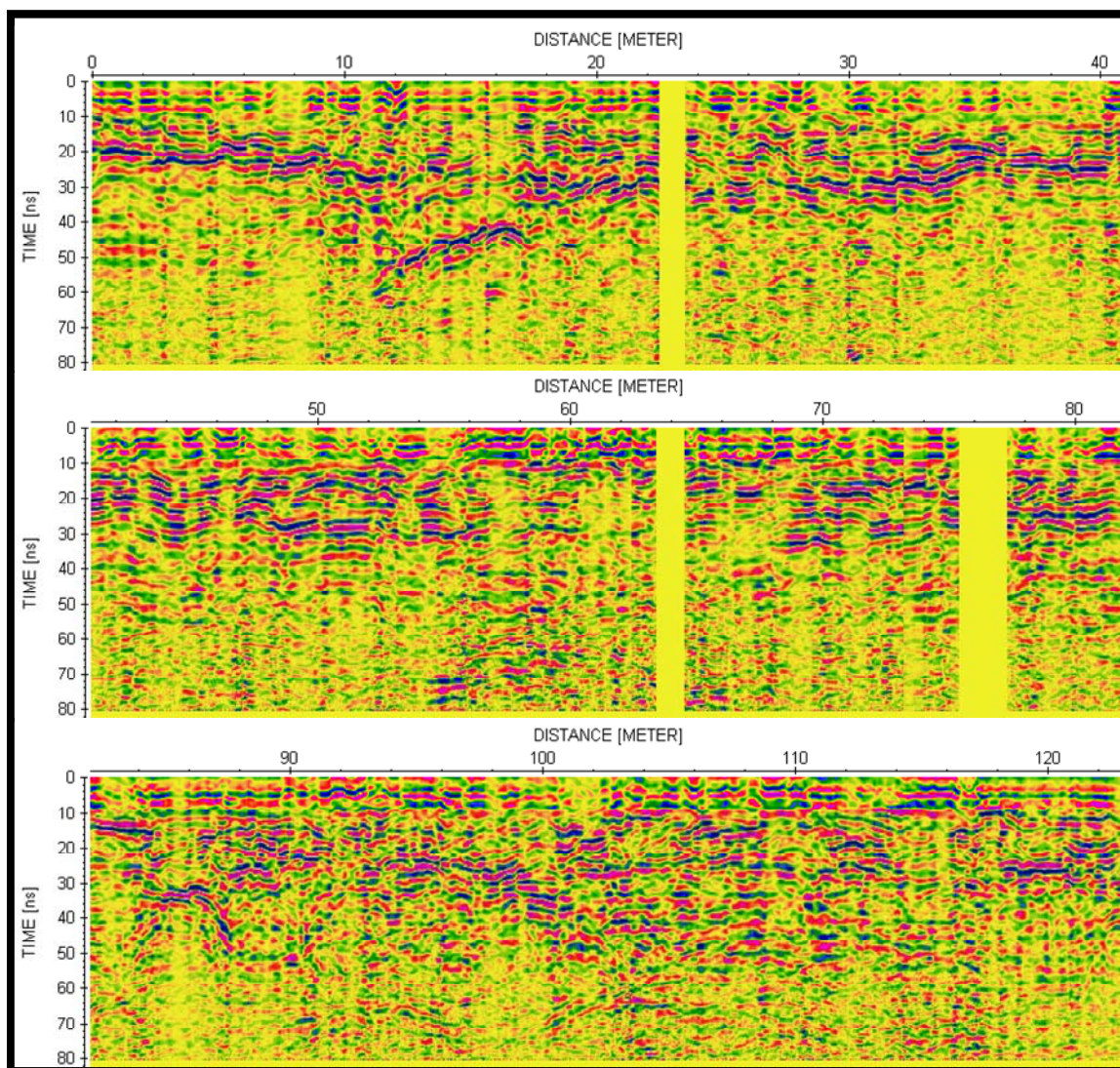


Figure B.12 Project 5: Line 2 across plaza.

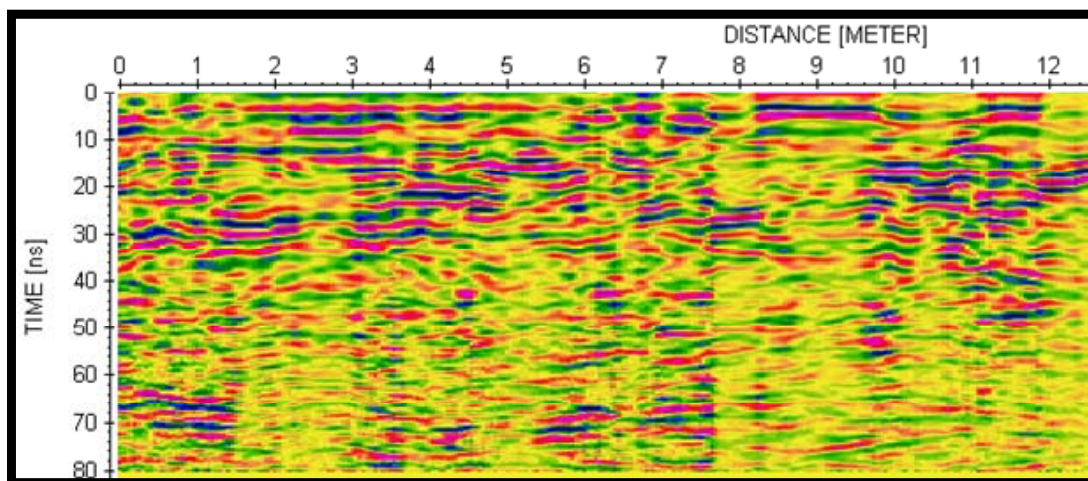


Figure B.13 Project 5: Line 3 across north plaza.

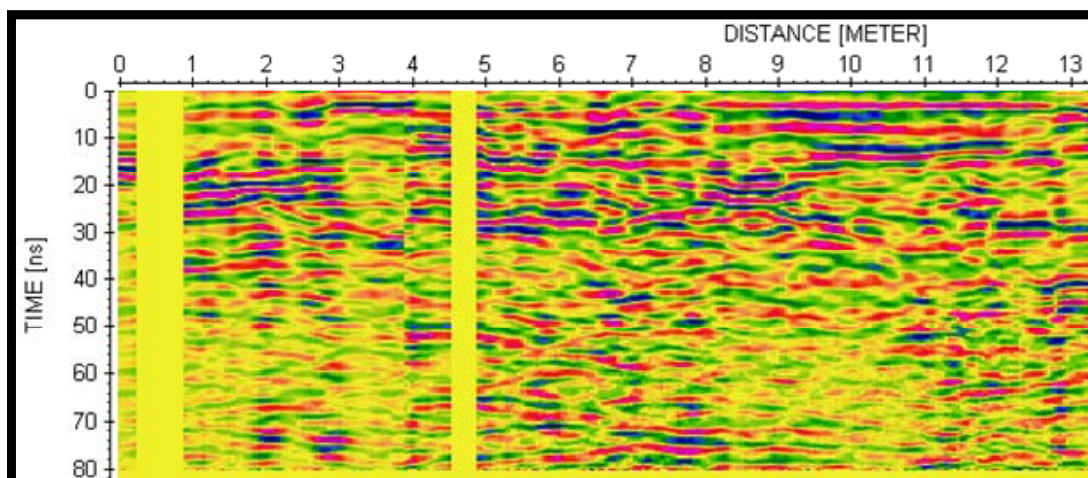


Figure B.14 Project 5: Line 4 across north plaza.

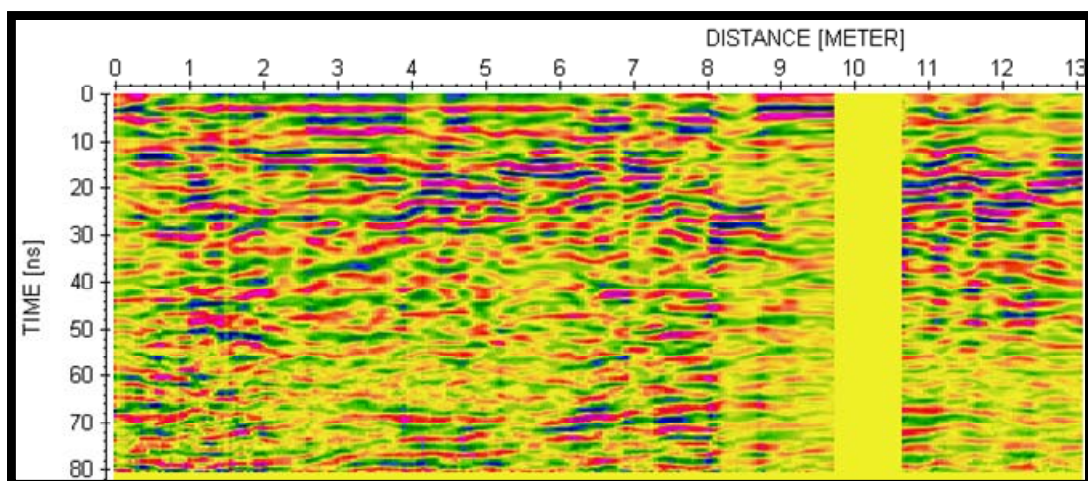


Figure B.15 Project 5: Line 5 across north plaza.

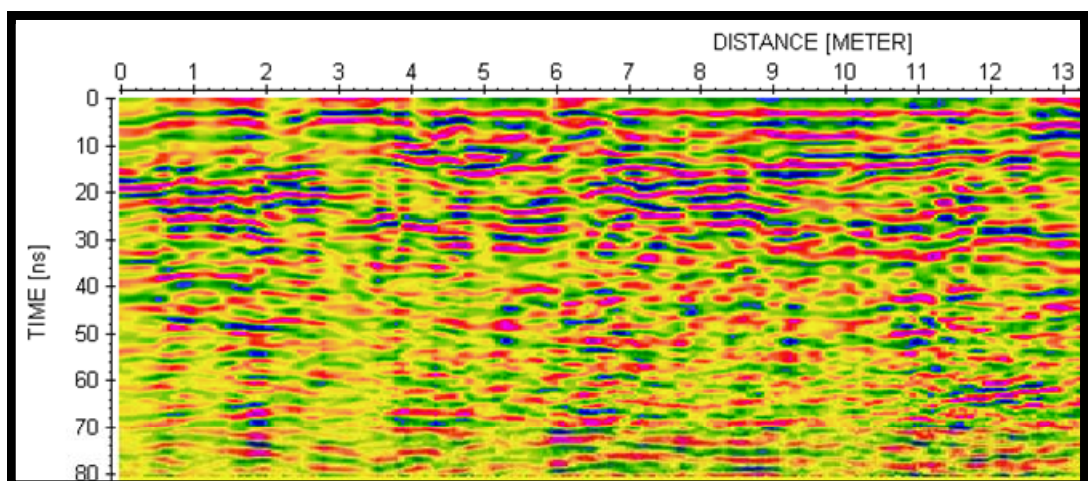


Figure B.16 Project 5: Line 6 across north plaza.

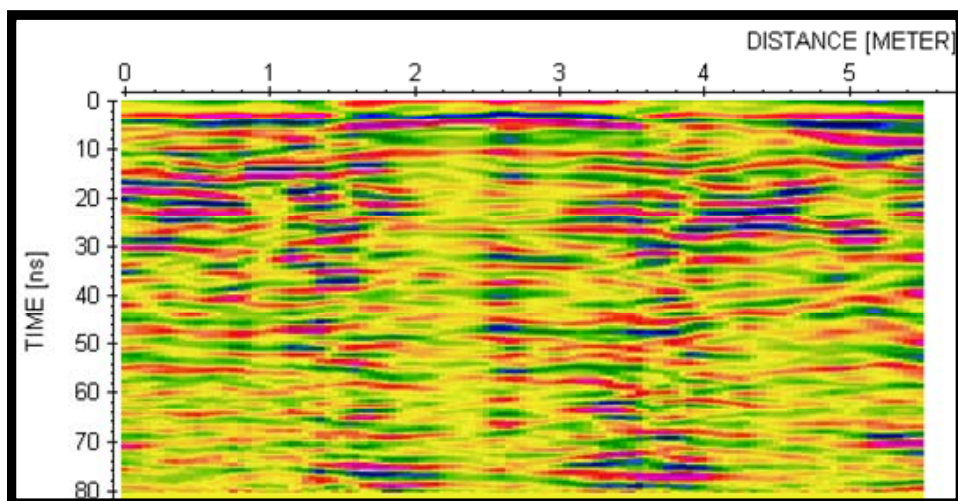


Figure B.17 Project 5: Line 7 across north plaza.

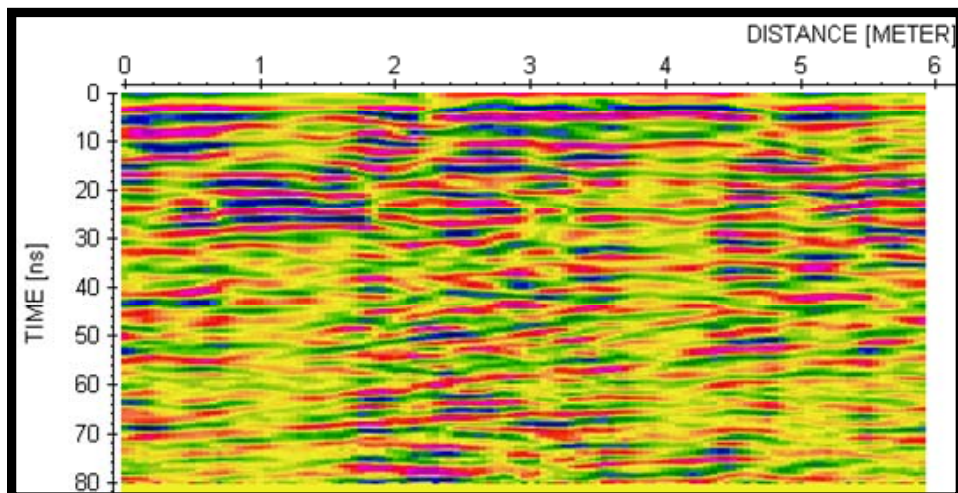


Figure B.18 Project 5: Line 8 across north plaza.

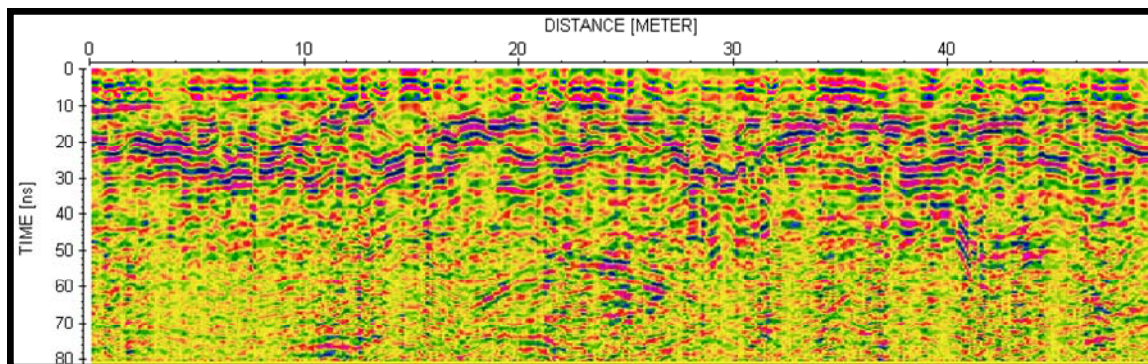


Figure B.19 Project 5: Line 9 across north plaza.

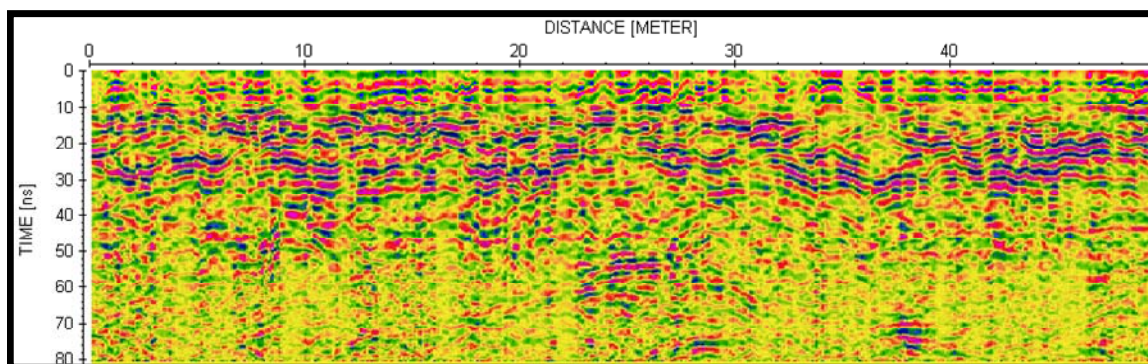


Figure B.20 Project 5: Line 10 across north plaza.

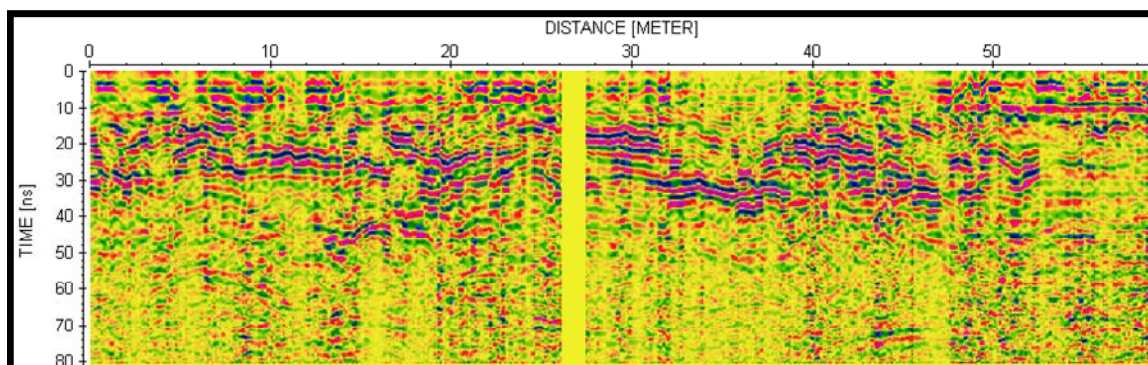


Figure B.21 Project 5: Line 11 across north plaza.

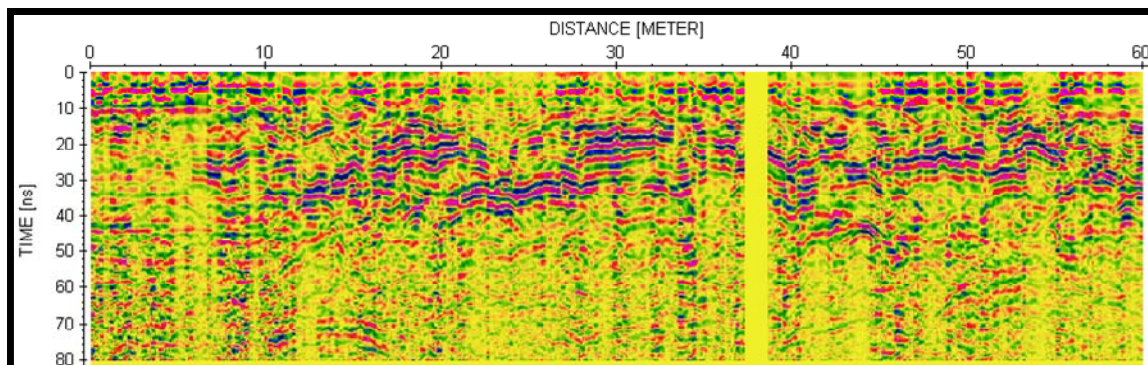


Figure B.22 Project 5: Line 12 across north plaza.

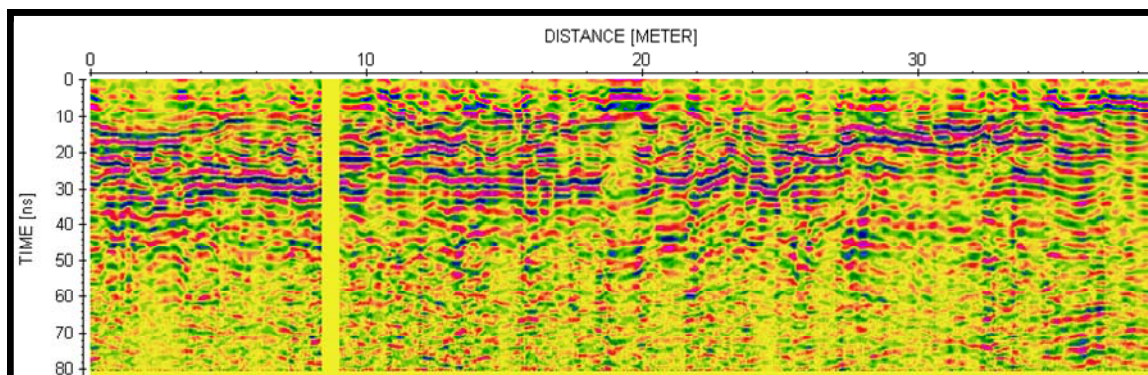


Figure B.23 Project 5: Line 13 across north plaza.

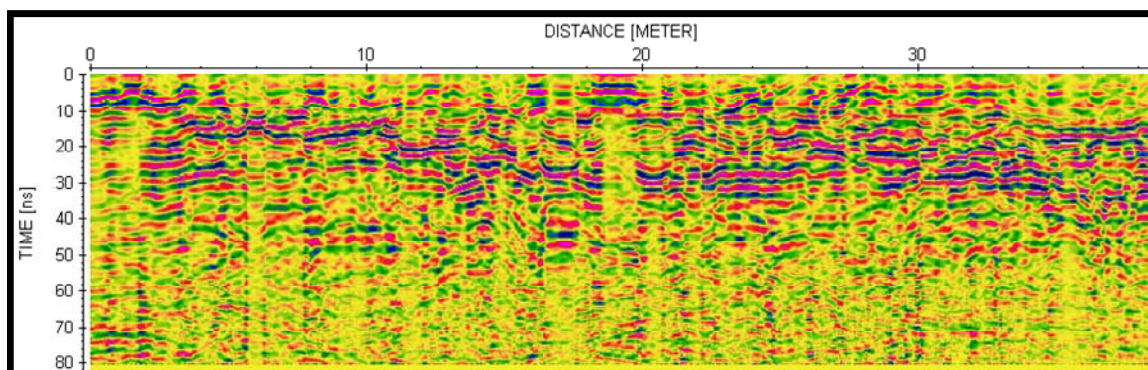


Figure B.24 Project 5: Line 14 across north plaza.

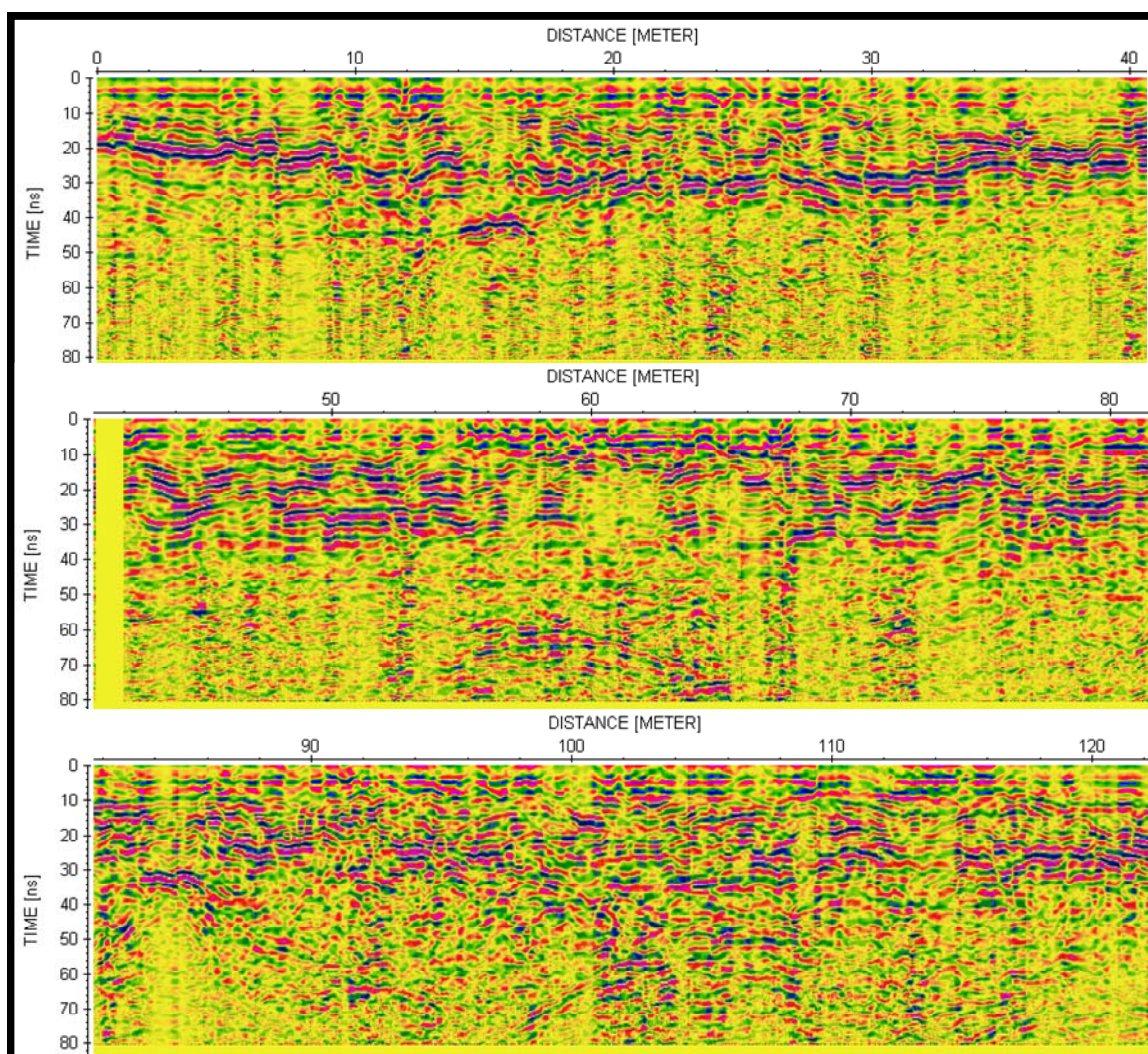


Figure B.25 Project 6: Line 0 across plaza.

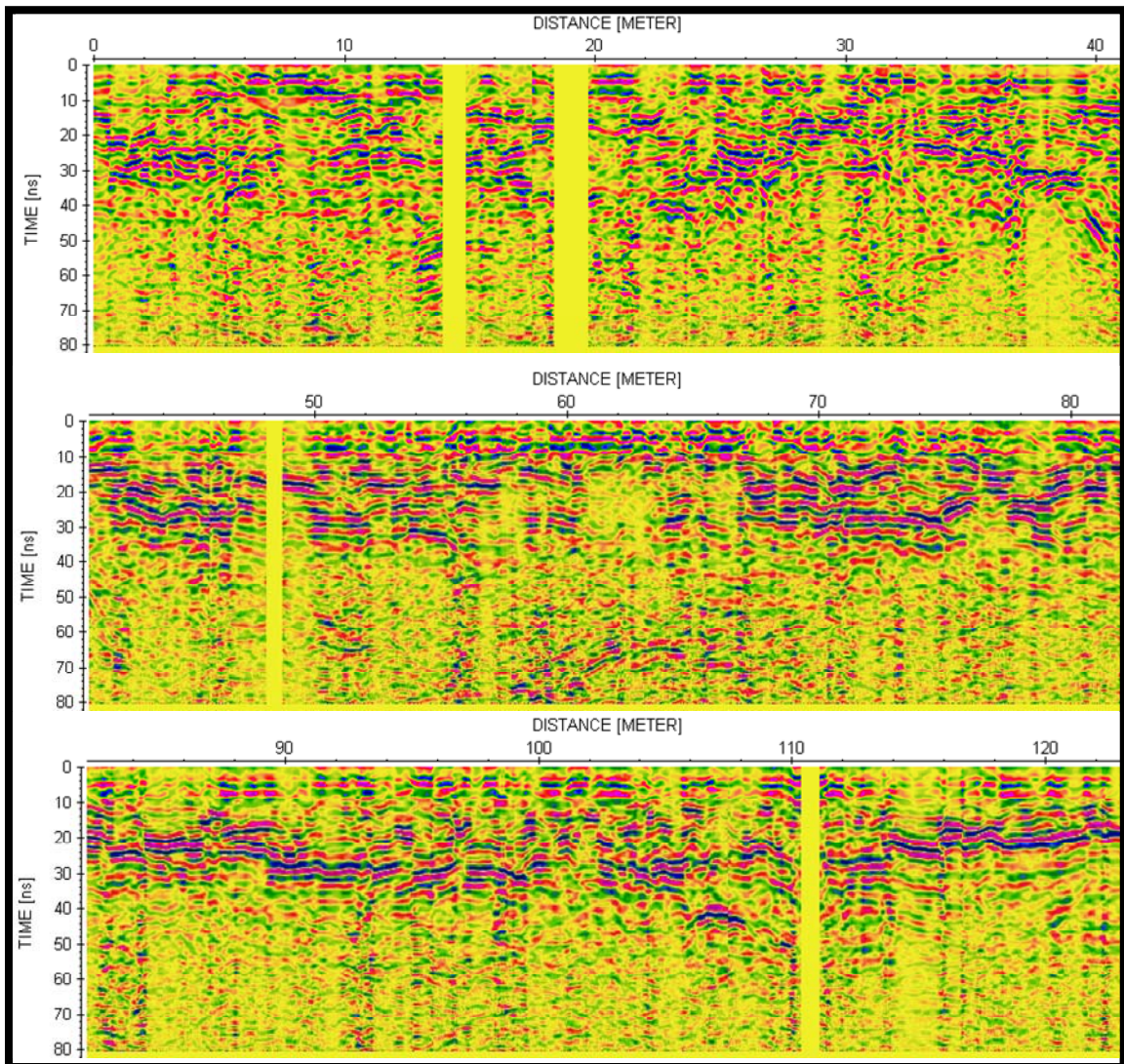


Figure B.26 Project 6: Line 1 across western part of north plaza; reverse to Line 0.

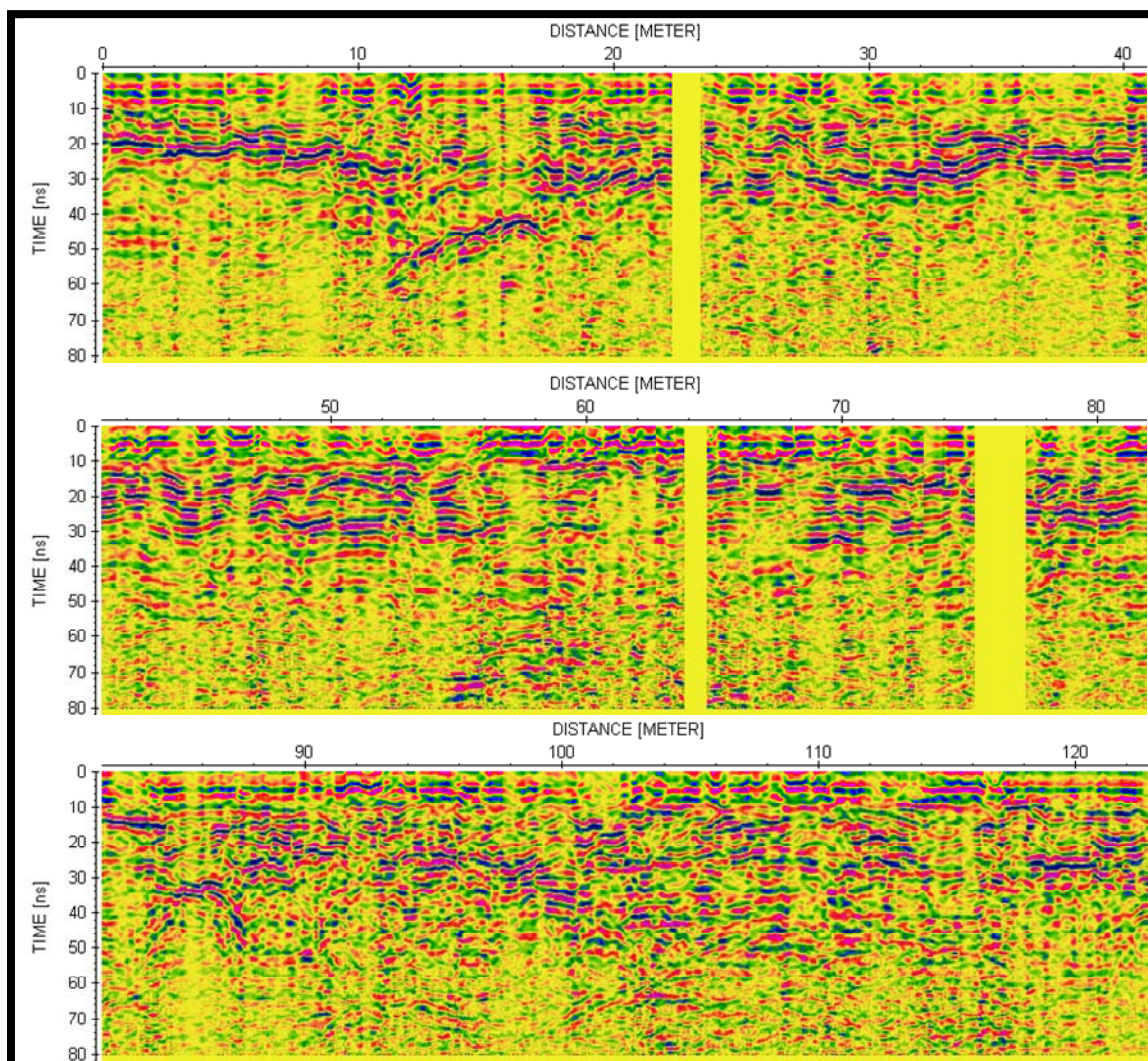


Figure B.27 Project 6: Line 2 across plaza.

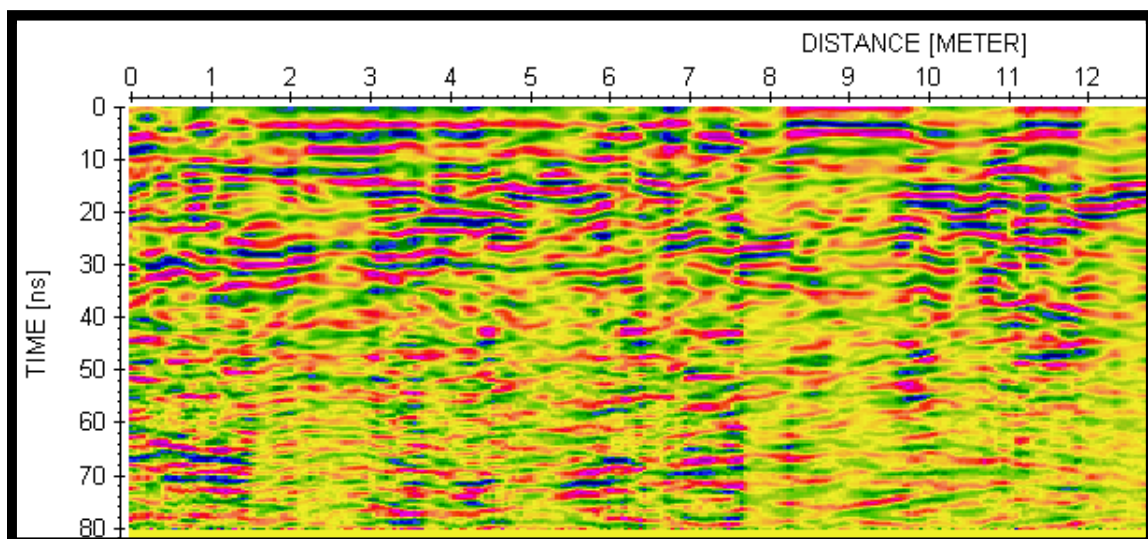


Figure B.28 Project 6: Line 3 across north plaza.

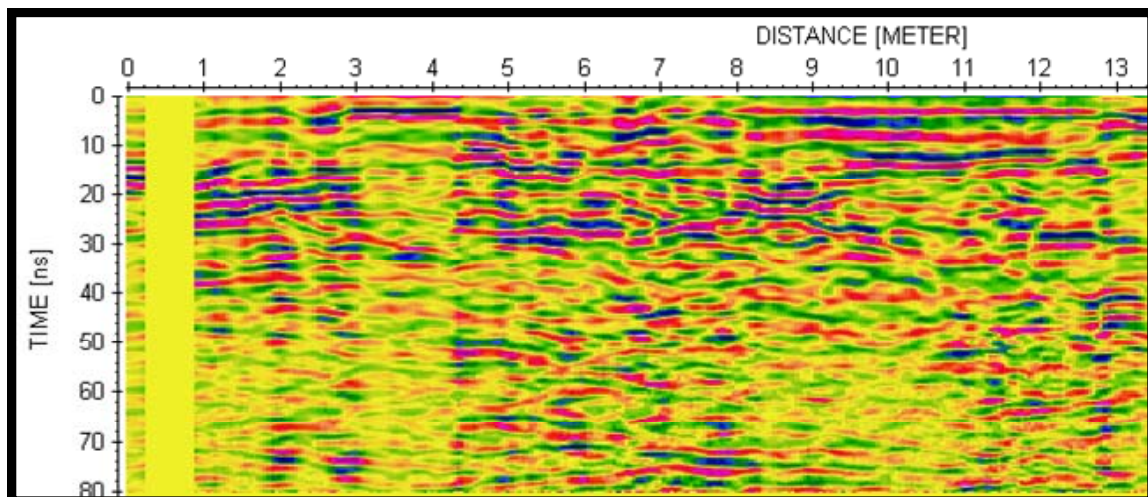


Figure B.29 Project 6: Line 4 across north plaza.

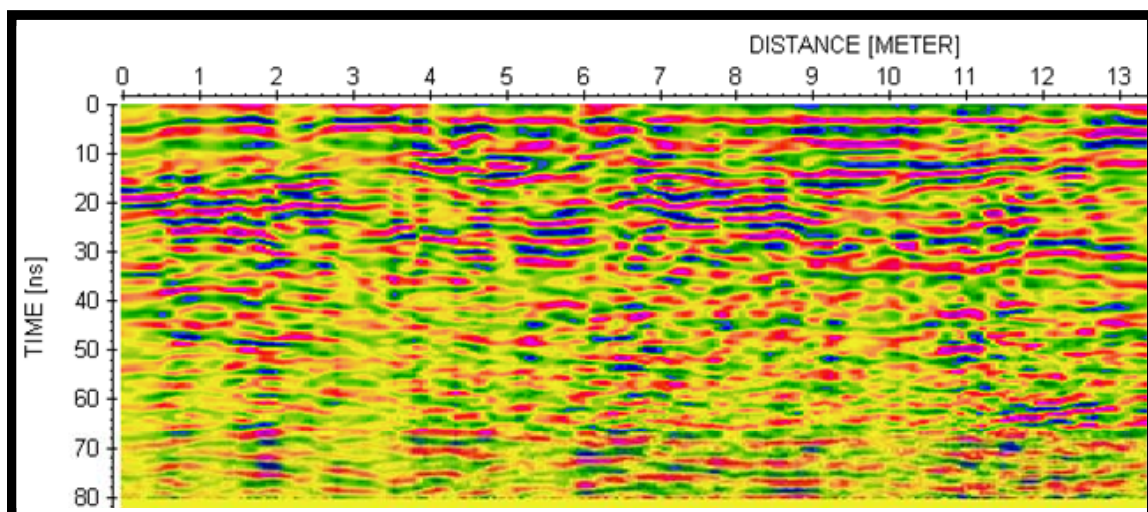


Figure B.30 Project 6: Line 5 across north plaza.

B.4. 2008 GPR data:

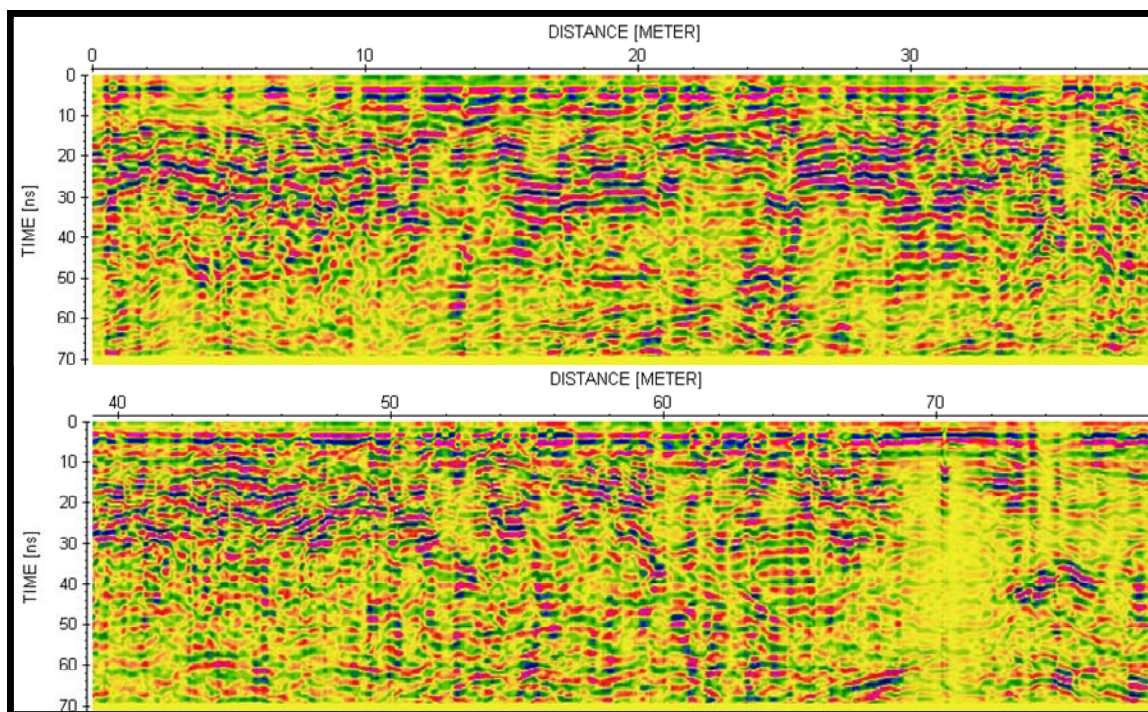


Figure B.31 Line 0 acquired east to west across eastern part of north plaza.

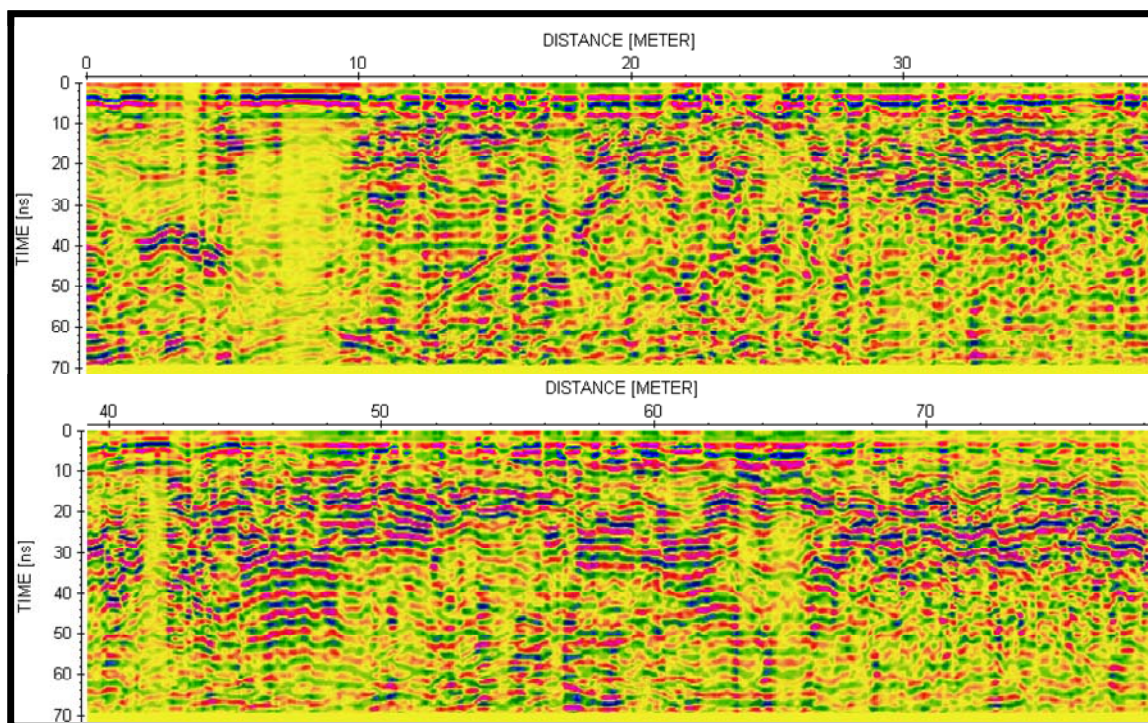


Figure B.32 Line 1 acquired west to east across eastern part of north plaza.

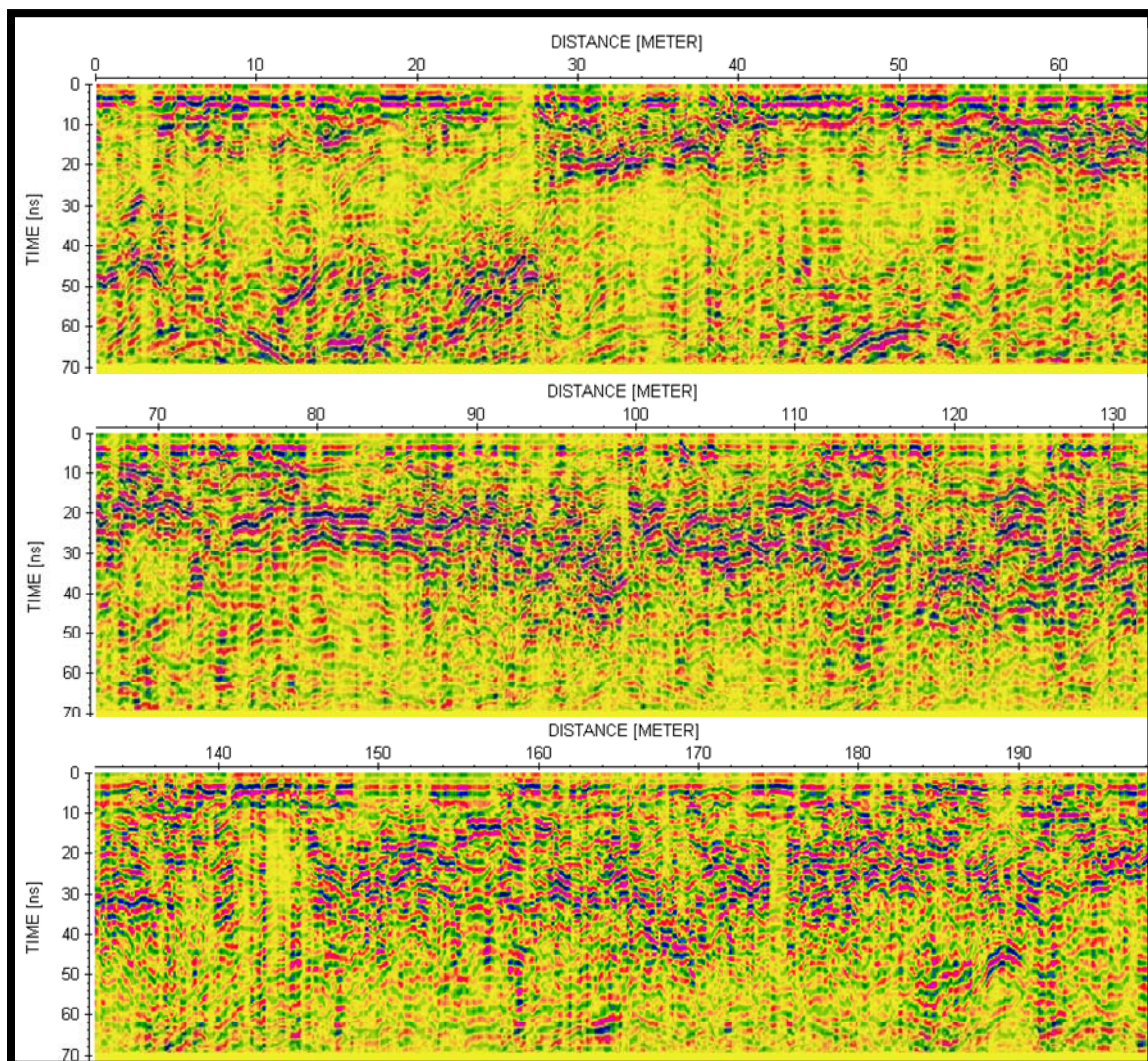


Figure B.33 Line 2 acquired north to south across eastern part of north plaza.

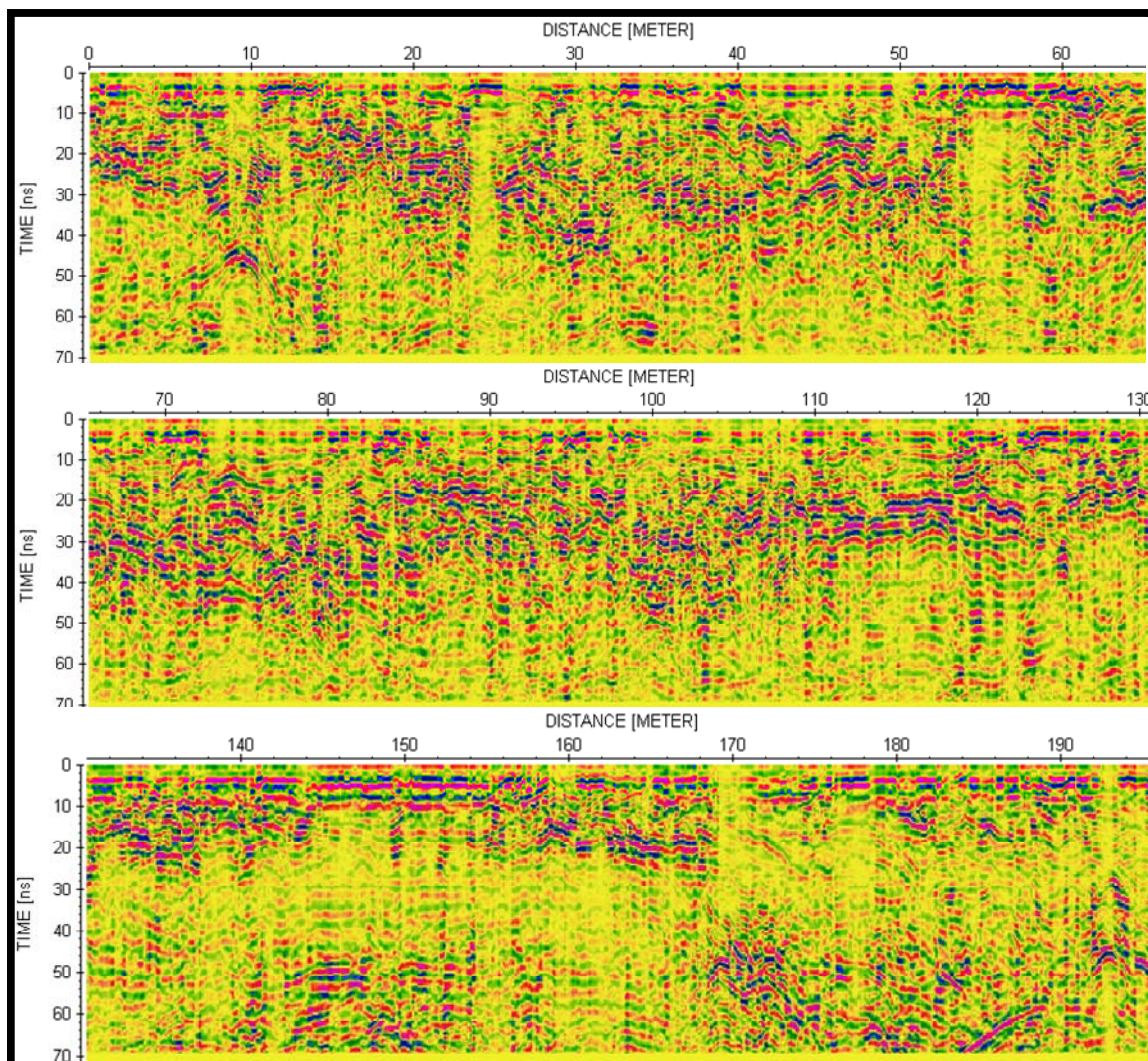


Figure B.34 Line 3 oriented south to north across eastern part of north plaza.

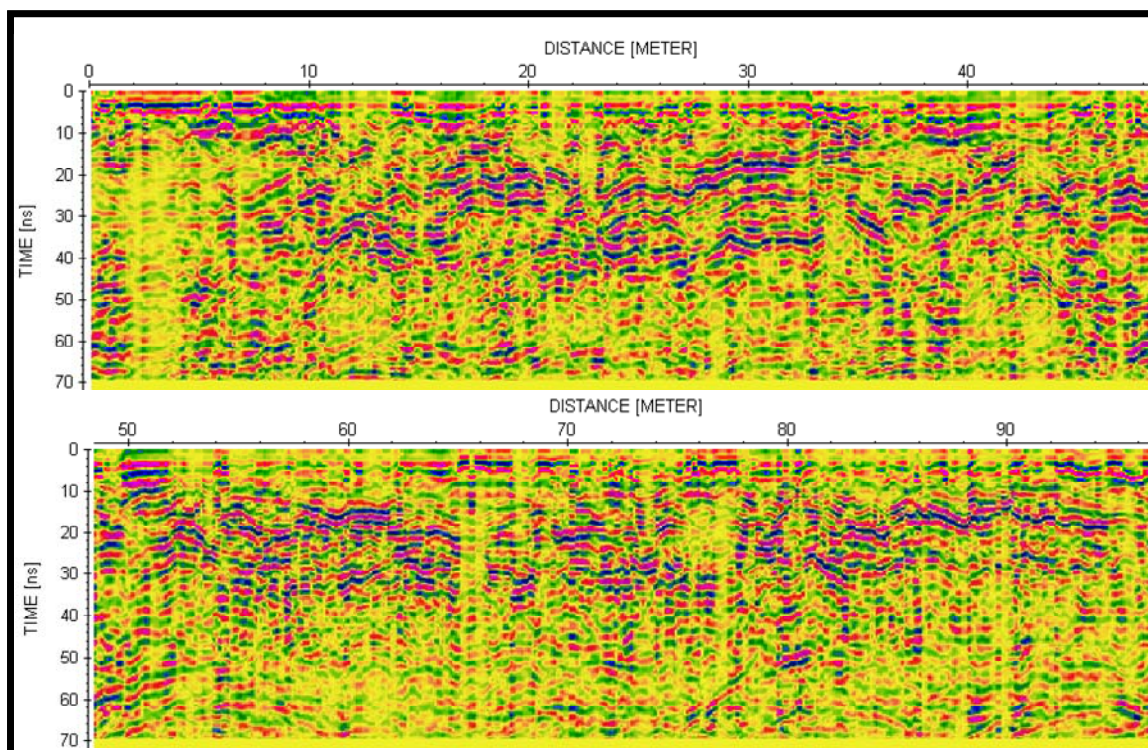


Figure B.35 Line 4 oriented north-south across western part of north plaza.

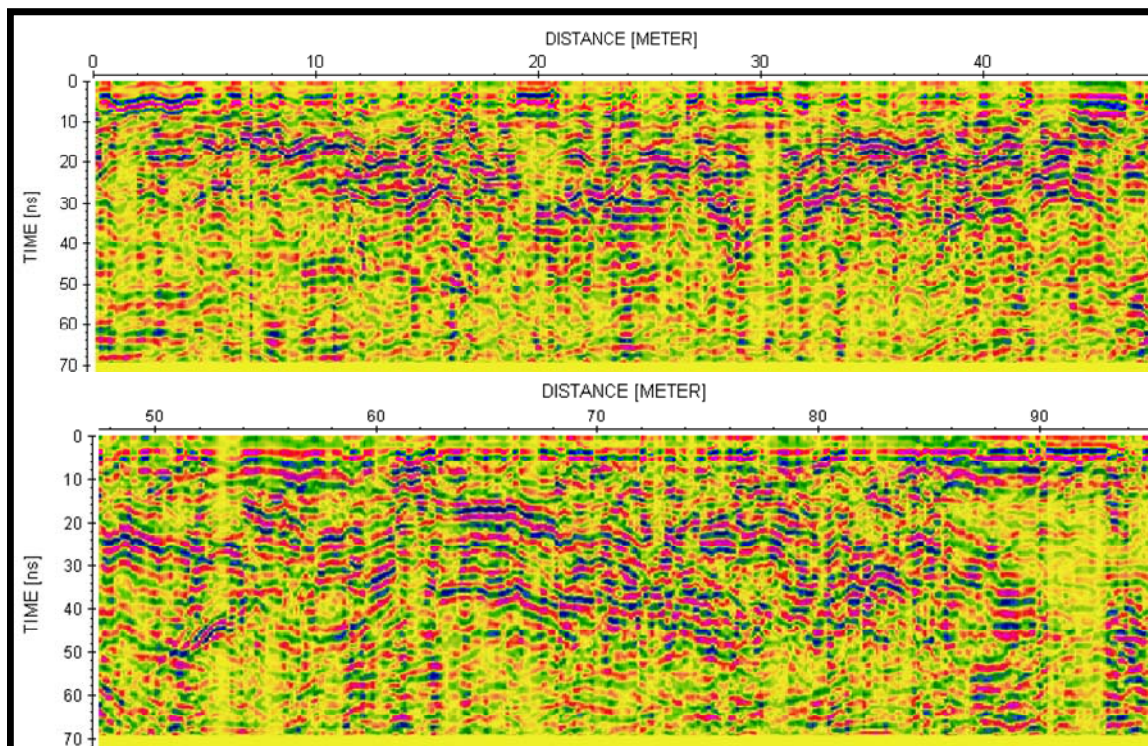


Figure B.36 Line 5 oriented south to north across western part of north plaza.

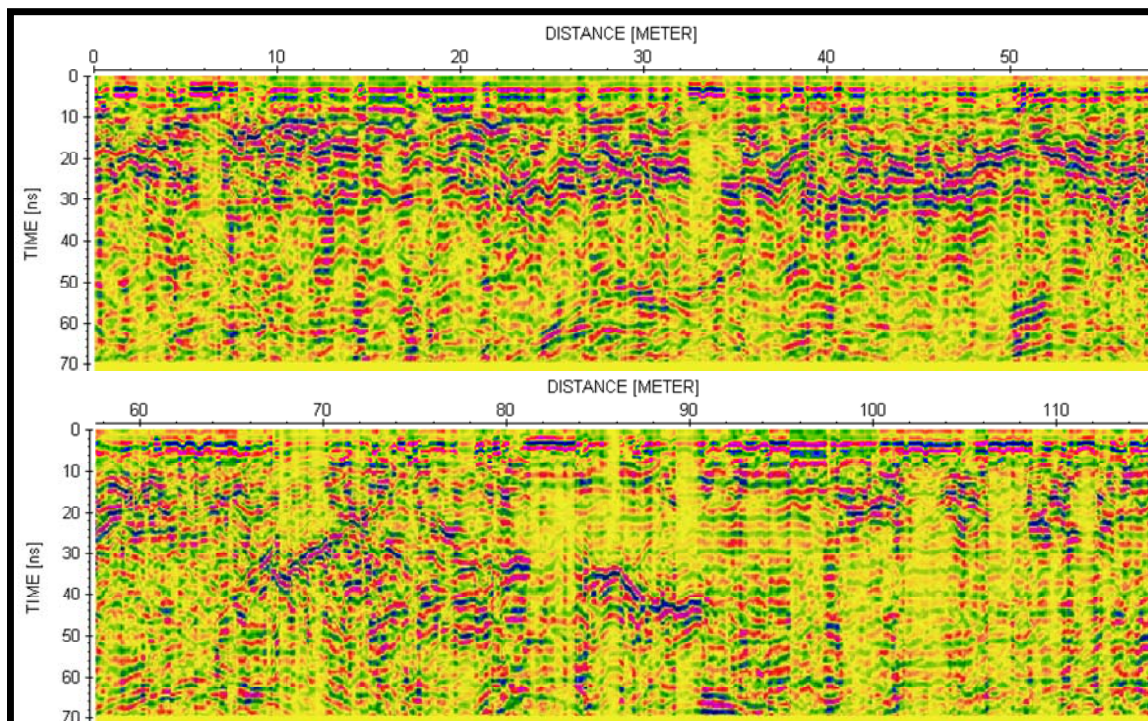


Figure B.37 Line 6 oriented west to east across western part of north plaza.

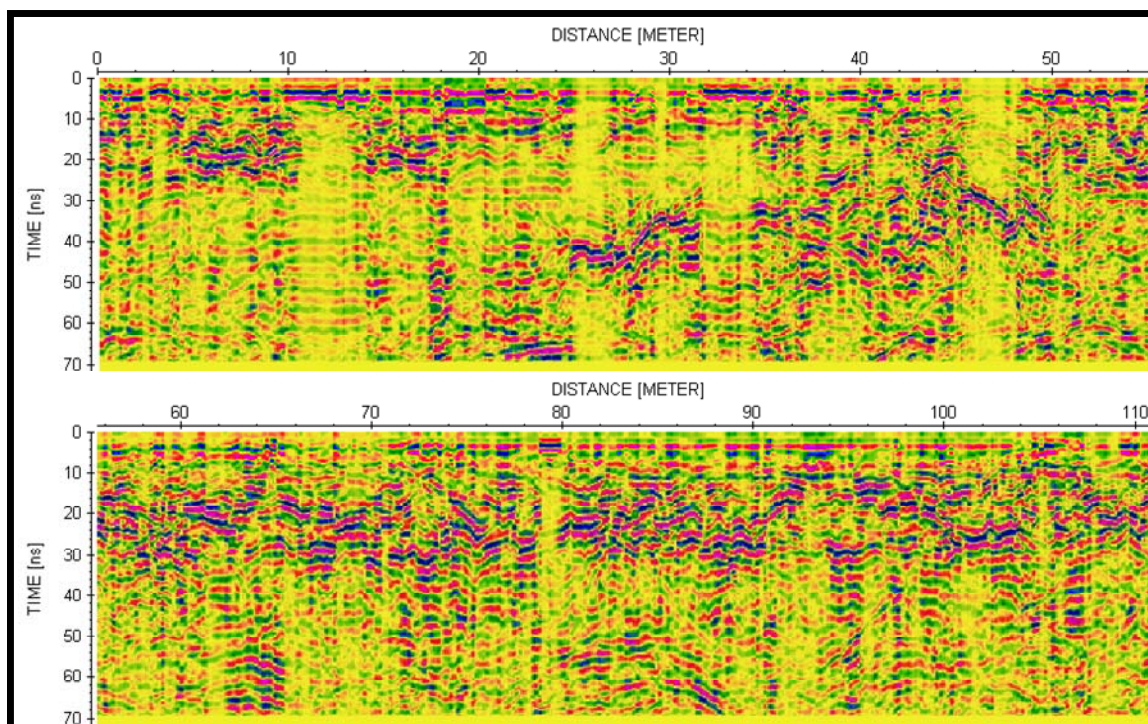


Figure B.38 Line 7 oriented east to west across western part of north plaza.

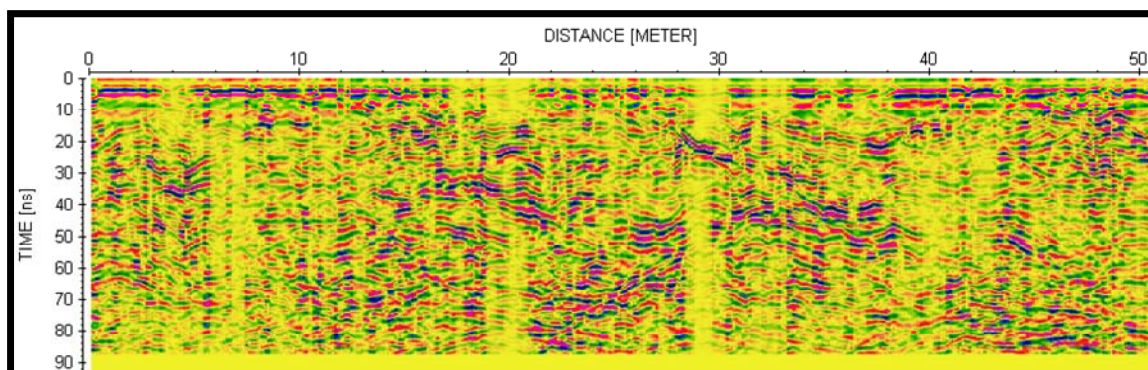


Figure B.39 Line 8 oriented west to east across ramp of north structure.

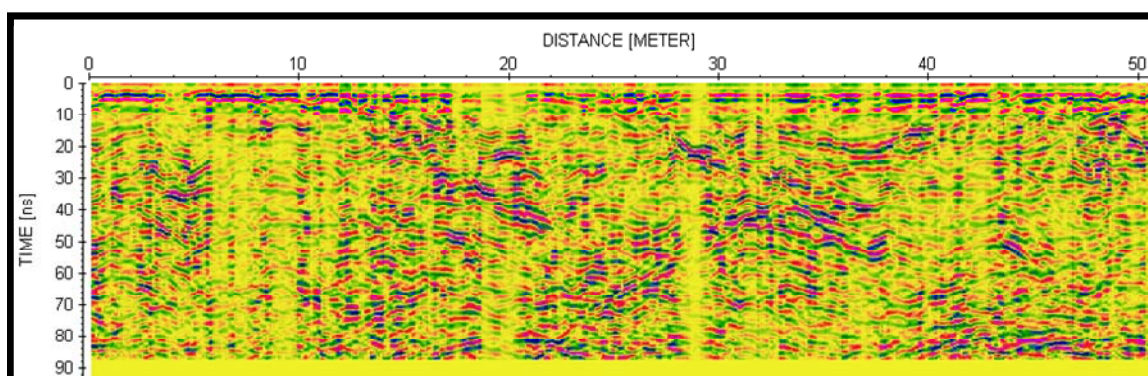


Figure B.40 Line 10 acquired across ramp - repeat of Line 8 due to skipped traces.

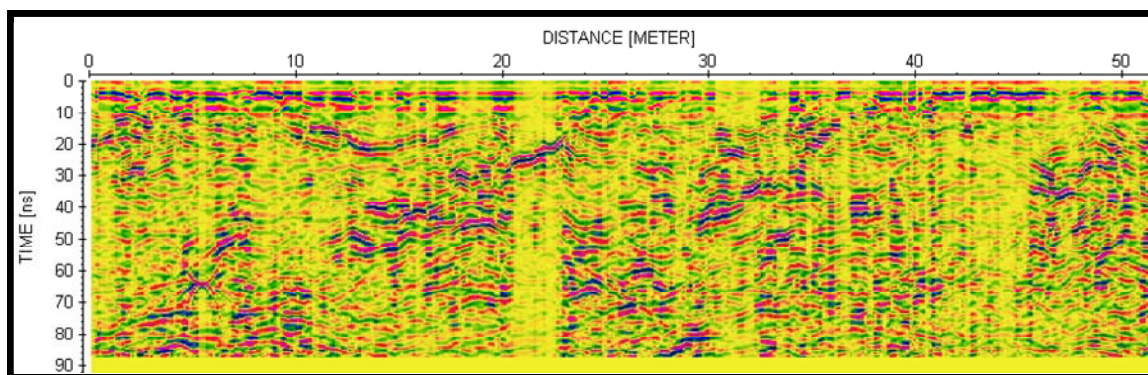


Figure B.41 Line 9 oriented east to west along ramp; reverse direction to Lines 8/10.

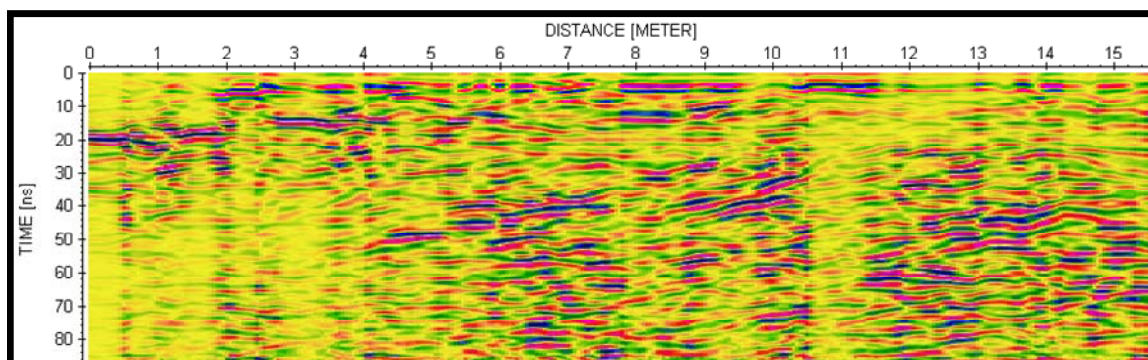


Figure B.42 Line 11 acquired north to south perpendicular to ramp; no topographic correction applied.

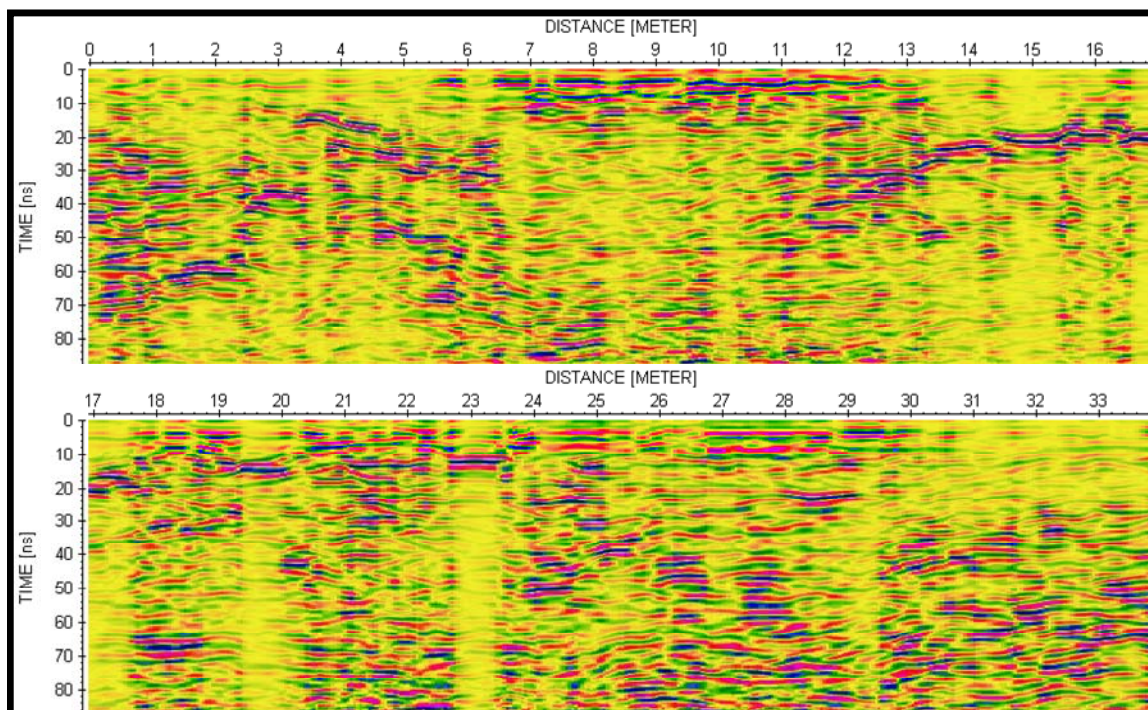


Figure B.43 Line 12: second line acquired north to south perpendicular to terrace; no topographic correction has been applied.

APPENDIX C: ANALYSIS AND OPTIMIZATION OF GROUND PENETRATING RADAR ACQUISITION PARAMETERS

In the fall of 2005, a small GPR survey was undertaken across a septic field located on an acreage south of Calgary, Alberta. Two sewer pipes were noted across the survey at an approximate depth of 0.50 metres. Two 3-D grids, in X and Y orientations, were acquired at a line separation of 0.20 m using the Sensors and Software Noggin Smart-Cart with an antenna frequency of 250 MHz. In-line trace spacing was set at 0.05 m with temporal sampling at 0.40 ns. Velocities measured in the field using hyperbolic curve fitting were calculated at 0.06 m/ns. A GPS survey was also conducted at the site to define survey coordinates and establish topographic measurements. The objective of the survey was to determine optimal parameter selection to achieve the best subsurface imaging, and to test whether the direction of acquisition affected the results. A comparison of the time slices created from the different acquisition directions contain noticeable differences in amplitude between X and Y grids but similar general patterns. This may be due to the fact the acquisition was done on different days with some precipitation noted during that period. Comparisons of decimated datasets show a decrease in resolution. The results serve to emphasize the importance in optimizing acquisition parameters before initiating field work and acquiring the surveys at the same time if possible.

C.1. Introduction

Near-surface geophysical surveying often has the constraints of limited time and budget, which may be compounded by unexpected and challenging site conditions. Thus, the GPR surveys might be acquired quickly with parameter selection set to default values. Even though the results of this work can be encouraging, is it possible to do better?

This project was undertaken to vary GPR parameters, and answer some of the questions that have arisen once processing and analysis of the GPR sections has been completed. Questions for consideration included: What is the optimal spacing for the GPR lines? How does the resolution respond to increased line spacing? and are the interpolated/non-interpolated time slices identical for different acquisition orientations and profile directions?

C.2. Survey Site

The survey site is located within a horse paddock on an acreage west of Fish Creek Park and south of Calgary, Alberta. At the end of the Pleistocene, approximately 33,000 BCE, the area around Calgary and Fish Creek Park was covered in glaciers. The retreat of the glaciers produced a number of valley systems and rivers, and a more hospitable environment for human occupation.

The park is believed to have been home to generations of native peoples and the first Europeans to settle in this region. Earliest occupation is estimated to have been around 6500 BCE. Fish Creek Provincial Park officially opened in 1975, and is considered to be an important archaeological site. Artifacts that have been unearthed include native weaponry such as spear points, and ancient cooking utensils.

This particular site was chosen with the hope of finding some archaeological features on the property, but a more detailed reconnaissance proved that the septic field area provided the best results in terms of resolving subsurface features. The septic field was located approximately 50 metres east of a house with two sewer pipes buried in the subsurface at an approximate depth of about 0.5 metres.

The survey site is within a grassy horse paddock, the greenest part located directly over the septic field. The surface proved to be irregular with rocks and small surficial depressions evident. Small topographic changes were detected by the GPS survey. The near-surface was composed of black organic rich soil, likely topsoil, overlain with grass.

C.3. GPR Survey

The GPR equipment consisted of a Noggin® 250 and Smart Cart® system manufactured by Sensors and Software Limited. The antenna frequency was 250 MHz. A trace interval of 0.05 m was selected for all the GPR lines, triggered by a wheel odometer. The sample rate was set at 0.40 ns. As the transmitter and receiver antenna are housed in the same unit, at a separation of 0.28 m, velocity information was garnered by the hyperbolic fitting of curves to point diffractors. A series of closely spaced 2-D lines were obtained consecutively in opposite directions for two orthogonal grid orientations. For example, for each of the thirty seven survey lines in the X grid, a forward and reverse profile was acquired. A similar procedure was employed two days later for the Y grid. Lines were spaced 0.20 m apart, approaching a practical survey limit given by the width of the NOGGIN unit itself. Instead of acquiring three separate surveys, this type of procedure allowed for three combinations of acquisition directions, created by simple file manipulation, as outlined in Figure C.1.

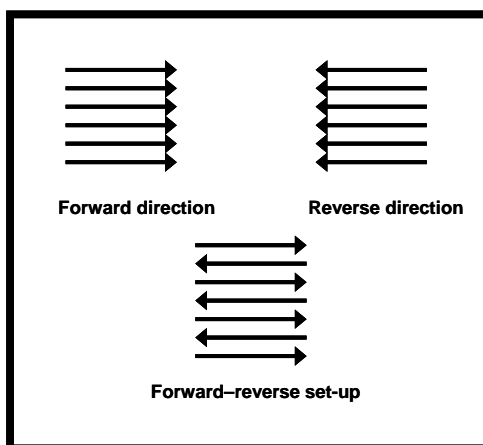


Figure C.1 Different acquisition directions.

To define the geometry of the survey, the 7.2 m x 7.2 m grid was measured and pegged at every 0.20 m. Using chaining tape and twine, the grid was roped off every 0.40 m in both the X and Y orientations. This allowed for a more effective GPS survey to be conducted at each of the pegs around the perimeter of the survey and at the intersection of the strings. The GPR lines were acquired by centering the unit, and either walking along each of the strings, or between them. This methodology proved very efficient.

A number of diffractors in the survey area indicated a near-surface velocity of 0.06 m/ns.

C.4. Processing of the GPR data

After the survey data was collected, it was necessary to create the various acquisition configurations which represented a forward direction, a reverse direction, and a forward-reverse set-up. Due to the internal numbering convention within the software employed (ReflexW), it was also necessary to rename the various lines in order to ensure the correct placement in the grid. This was done in both orthogonal orientations for a total of 6 acquisition directions.

Processing of the GPR data was accomplished using the ReflexW software specifically modified for application to ground-penetrating radar (Sandmeier, 2004). The processing flow consists of a static time shift, setting equidistant traces, application of a “dewow” or low-cut filter with and without a running average spatial filter, followed by the application of a Butterworth filter. As electromagnetic energy is both dispersed and attenuated as it radiates into the ground, the application of an energy decay curve was also necessary (Goodman and Conyers, 1997).

C.5. GPS Survey

The GPS grid consisted of a 7.2 m x 7.2 m grid with 0.40 m spacing. The GPS survey was conducted to account for elevation corrections and to accurately set the coordinates of the GPR survey. The GPS grid was surveyed at every intersection of the grid using a Sokkia GSR2650LB base/rover pair. Each point was occupied for a single epoch, and the antenna was mounted on a 2 m pole. The grid consisting of 361 points was completed in less than 2 hours using the GIS-CE software from Carlson. In Figure C.2, the squares are exactly 0.40 m x 0.40 m (the grid spacing). The surveyed points should (ideally) fall in the centre of each square. While the circular error probability (estimated mean error) was typically reported at 0.15 m, most of the observable error can be attributed to the accuracy of the layout and the ability to keep the rod levelled (Bland, 2005). The elevation accurately portrays the ground undulations at the field site with a high in the centre trending to the upper right and a low in the upper left corner.

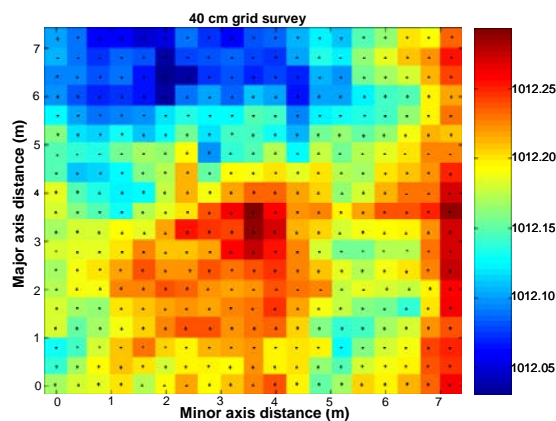


Figure C.2 GPS Survey topographic map.

C.6. Septic Field

The septic field is located within a horse paddock on the property. A schematic of a septic field which likely represents the set up at the acreage is shown in Figure C.3.

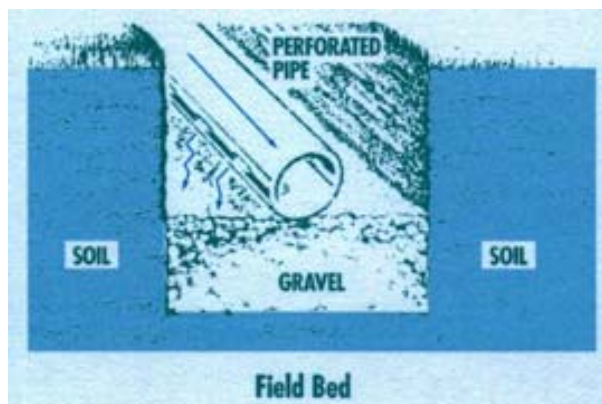


Figure C.3 A likely septic field configuration at site (courtesy of A1 Sewage Services).

The pipes from the house feed directly to a septic tank which collects and breaks down the solid waste. Two baked clay pipes spread the wastewater to a septic field. The pit containing the pipes was lined with gravel, filled in with the excavated material, and topped with a layer of topsoil and grass. This was confirmed by digging a small hole approximately 6 inches wide and 6 inches deep into the center of the grid where we encountered black, rich, organic soil.

The GPR response to buried items on a radar image is a hyperbolic shape (Jol and DeChaine). Thus, the sewer pipes can be clearly recognized on Profile line Y132, acquired in a direction perpendicular to the trajectory of the pipes. On this particular line, the spatial filter was omitted in the processing flow. Two distinct diffraction patterns are evident in Figure C.4 at 2 m and 6.3 m respectively and using a velocity of 0.060 m/ns are located at a depth of 0.42 m and 0.54 m. The pipe on the left has a stronger reflection which may suggest that it is liquid filled (Sensor and Software Inc., 2003).

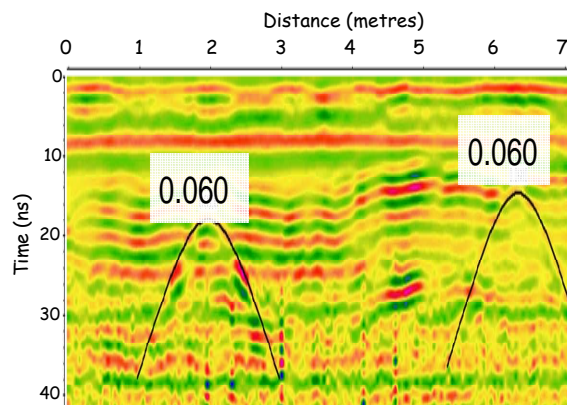


Figure C.4 Profile line Y132 showing the location of sewer pipes.

C.7. Results

Comparing the displays generated from the different orientations and directions, has led to some interesting results. Each of the displays was processed with the same processing flow, with close attention to the gain function and any process that might affect the amplitude of the data. The range of colour bar values was consistent for all the displays.

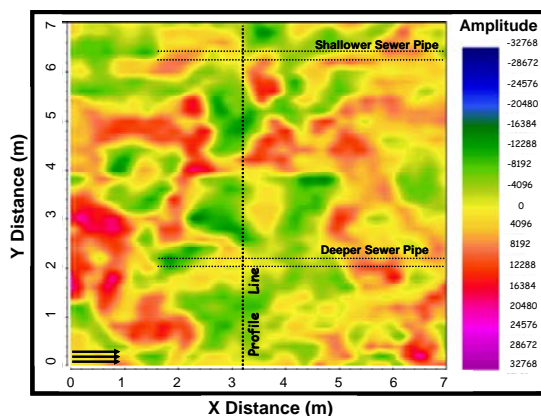


Figure C.5 Time slice of X grid forward pattern.

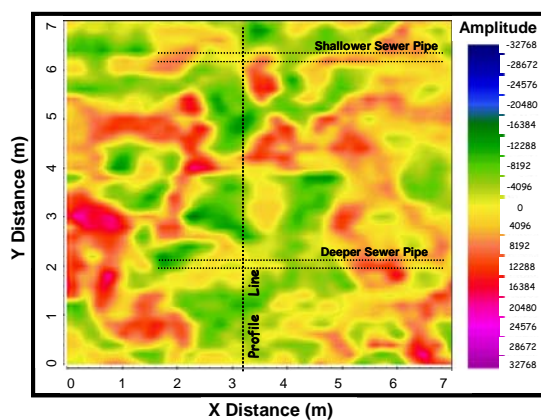


Figure C.6 Time slice of X grid reverse pattern.

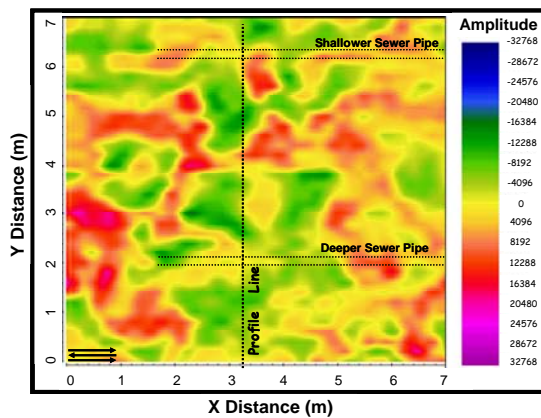


Figure C.7 Time slice of X grid forward-reverse set-up.

Figures C.5 through C.7 represent time slices created at an arbitrary time of 15.95 ns from the X grid in forward, reverse, and forward-reverse directions. On close inspection, the amplitude and character of the time slices is consistent for all three plots. It appears

that in this case, one can be reasonably confident in choosing any acquisition direction for subsequent surveys. This however may not be indicative of every survey as the success of GPR is dependent on the composition of near-surface material, antenna frequency, and conditions such as the clay content and saturation levels of the soil. Plots from the orthogonal orientation, Grid Y, showed similar results between the forward, reverse and forward-reverse directions.

Figures C.8 and C.9 represent the GPR time slices in the forward direction of the X grid and the Y grid. The interpreted location of the sewer pipe, based on the position of the diffraction apex, is superimposed onto the latter figure. Note that the linear trend representing the sewer pipe does not continue to the edge of the survey. The amplitude within the area of the pipe changes too, which may indicate a change in the saturation level of the soil in the immediate area. As one might expect, the trend is much more apparent on the Y grid since those lines intersect the pipe at a right angle.

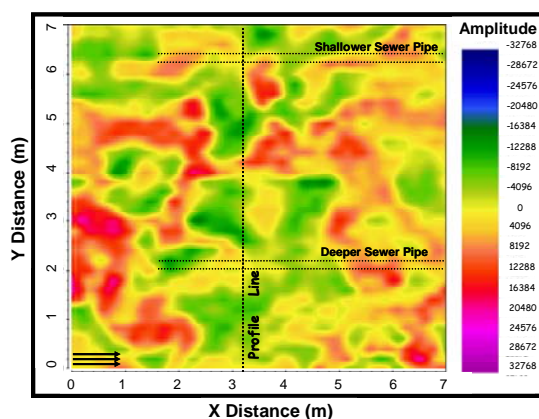


Figure C.8. Time slice of X grid forward pattern.

Although subtle differences in character exist between the two, there is quite a distinct difference between the orthogonal grids in terms of amplitude. The GPR surveys were completed two days apart. The temperature on both days was consistent at about 10 degrees Celsius with overcast skies. Although there was no precipitation on the acquisition days, precipitation of approximately 1 mm was noted in the period between. This may have been enough to trigger the differences. Other explanations for the amplitude differences may be due to strong amplitudes recovered in the areas of the grid where there was no overlap between the X and Y profiles and the subsequent normalization of those amplitudes, or with the calibration of the instrument before initiation of the survey.

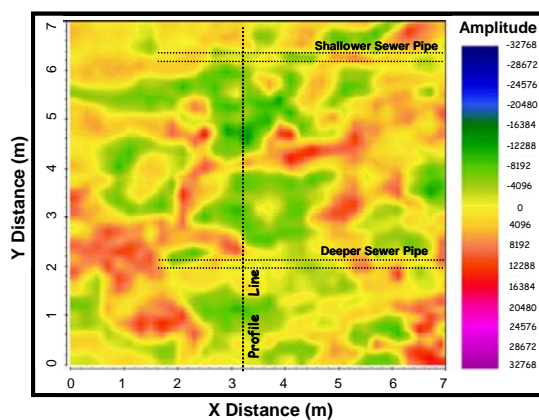


Figure C.9 Time slice of Y grid forward pattern.

Even though the GPR surveys were conducted with the same instrument along the same profile, direction does appear to affect the acquired GPR image to some degree. The plots shown on the previous page were collected using fine grid parameters, specifically a 0.20 m line separation. What would happen if the dataset was decimated to include every other line only? What would happen to the resolution and amplitude of the time slice?

Comparing the X grid reverse pattern using all the lines (Figure C.6), with the X grid reverse pattern decimated every second line (Figure C.10), small changes are evident in character but both show similar trends. This outcome is sufficient for situations in which buried features are fairly large, as in the case of detecting sewer pipes. In the case of archaeology, however, where artifacts may be small and resolution is critical to any detailed interpretation, there is an essential need for smaller line separation.

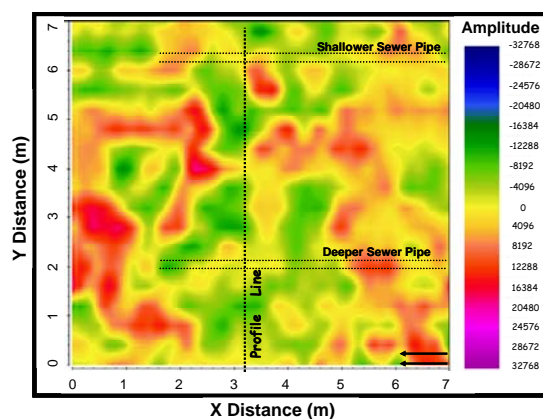


Figure C.10 Time slice of X grid reverse pattern decimated every second line.

C.8. Conclusions

In analyzing the different acquisition directions within each grid, one can feel reasonably confident that the images from the forward, reverse and forward-reverse time slices are almost identical in terms of the detail, character and amplitude. For this particular case, one can proceed to acquire in any one direction within the grid.

Comparing the individual X and Y grids does bring to light differences in amplitude but only a minimal change in the general character of the dataset. The amplitude differences may be due to soil saturation or amplitude calibration issues. The fact that the X and Y grids are not identical however does raise a red flag in terms of attempting to merge the two orientations. The fact remains that each survey grid is unique and merging the two would entail a smearing of the data or more specifically a smearing of the amplitude. The authors are reluctant to do so until we can reasonably explain our findings.

As expected, the finer the grid parameters, the better the resolution of the GPR image. Based on the results of this study, all subsequent surveys searching for small features or anomalies should have a finer line separation. Orthogonal surveys should be acquired at the same time if possible to minimize any possible amplitude variations.

C.9. Acknowledgements

The authors wish to acknowledge the support of the members of the CREWES Project especially Henry Bland, A1 Sewage Services (1989) Ltd, Jeff Berquist for allowing us to acquire the survey on his property, and Bill Cameron for his invaluable assistance with the project.